Interior and Orbital Dynamics at the Innermost and Outermost Reaches of Planetary Systems

Thesis by
Elizabeth Bailey

In Partial Fulfillment of the Requirements for the
Degree of
Doctor of Philosophy in Planetary Science

CALIFORNIA INSTITUTE OF TECHNOLOGY
Pasadena, California

2020
Defended June 22, 2020

Elizabeth Bailey
ORCID: 0000-0002-4769-8253

ACKNOWLEDGEMENTS

First, I would like to thank my thesis advisors Konstantin Batygin and Dave Stevenson for helping me learn to navigate the terrain of scientific research and writing.

Konstantin's advice and support over the years have been completely invaluable in my journey to completing the PhD program at Caltech, as well as my recent navigation of the postdoctoral job search. I especially appreciate that Konstantin helped me to recognize my own strengths and to provide encouragement when I needed it. His advisorship has equipped me with the skills necessary to succeed as a scientist, and I am very fortunate for that.

I am also extremely lucky to have had the opportunity to work with Dave. As an incoming graduate student, I was compelled to work with him after encountering his "modest proposal" to send a mission to the center of the Earth (Stevenson 2003). I was correct to infer that the scientific discussions to be had with someone who suggests such things, would certainly be interesting. Dave's mentorship has played an absolutely critical role in my scientific growth, and I would like to thank him for his intellectual guidance and support over the years.

Next, I would like to thank Mike Brown for allowing me to join in on his group meetings throughout my time at Caltech. Mike's mentorship, and his penchant for skepticism, have played a very important role in my growth as a scientist. In his group meetings, Mike and his research group (including but not limited to Ian Wong, Patrick Fischer, Sam Trumbo, James Keane, Katherine de Kleer, Madeline Schemel, Anna Simpson, William Denman, Alya Al-Kibbi, and Ryleigh Fitzpatrick) fostered some of the most interesting scientific discourse I experienced during graduate school, which I am extremely fortunate to have experienced.

Moreover, the Division of Geological and Planetary Science at Caltech contains so many people who have provided crucial, much needed guidance throughout the course of my PhD years. I am especially indebted to those who provided tutelage in field settings (including but not limited to Joe Kirschvink, Bethany Ehlmann, Claire Bucholz, Paul Asimow, and Brian Wernicke), so that I was able to actually learn something about how the Earth is understood. This is a learning experience I have absolutely cherished, despite focusing entirely on giant and hypothesized planets for the purposes of my thesis. I would also like to thank the rest of the Planetary Science faculty for their guidance over the years. I am particularly grateful to

Heather Knutson for agreeing to be on my defense committee and for fostering many interesting discussions throughout my time at Caltech.

I would also like to thank Smadar Naoz at UCLA for her mentorship and encouragement in the past few years.

Special thanks go to the folks in the Planetary Science office–Ruth Loisel, Margaret Carlos, Irma Black, Loreta Young, Ulrika Terrones, as well as other people elsewhere such as Julie Lee and Julia Zuckerman in the main division office, Mark Garcia, and probably some people I am failing to mention, who have done a ton of work to support my activities and research efforts during graduate school. Many thanks also go to Naveed Near-Ansari, Scott Dungan, Michael Black, and Tricia Ewald, who expertly managed various computing resources so I could be spared many headaches.

I should also mention that, before showing up at Caltech, several folks in the Earth, Atmospheric and Planetary Science (EAPS) department at MIT were extremely helpful sources of guidance and encouragement in my decision to become a planetary scientist. Taylor Perron and Mike Sori were my very first research mentors in the field, and really got me started on the right foot learning how research is done and encouraging me forward. I would also like to thank Ben Weiss, Sonia M. Tikoo, Claire Bucholz, Oli Jagoutz, and Leigh Royden for their mentorship during the course of my undergraduate senior thesis addressing the paleomagnetism of the India-Asia collision, and, notably, our guide Dorjay who expertly protected our lives during the associated travel. I would also like to thank the numerous students, postdocs, and faculty in EAPS whose time there overlapped with mine, who have provided so much continued guidance and friendship.

Special thanks go to my officemates throughout graduate school. I am grateful to Coco Zhang, Nancy Thomas, Ana Lobo, Siteng Fan, Joe G. O'Rourke, Sam Trumbo, Eva Scheller, Chris Spalding, and Danica Adams for their cameraderie, scientific discussions, and collegiality over the years. Overall, while there is not space to name you all (or even if there is, I would inevitably forget someone), I am extremely grateful to all the people whose time in the division overlapped with mine. The scientific discourse, friendship, support, and experience of learning together have been precious to me.

Extra-special thanks go to my partner Alex, for his vast love and support in the past year and a half.

Definitely not least of all, I would like to thank my wonderful, majestic, orange, fluffy, talkative, clever little kitty cat Venus for being my best friend of all time. I have been very lucky to have been graced with her friendship and support over the past several years. I love you, Veenie Beanie!! ♡

Finally, on a far more somber note, I would like to thank all the people who are continuing to help keep the world running during the COVID-19 pandemic. The last few months of my thesis would not have been possible without the warehouse and transportation workers who have provided me with necessary goods, and the people who are continuing to grow and process the coffee and food that made this thesis possible. While this document is in partial fulfillment of the requirements for me to become a doctor of planetary science, I would especially like to thank the *medical* doctors and other medical professionals who are currently risking their lives for us all.

ABSTRACT

In contrast to the canonical planets of our solar system, with semimajor axes in the familiar range of $\sim$ 0.3–30 au, exoplanets have been detected at considerably shorter and longer distances from their host stars. These planets, at the innermost and outermost reaches of planetary systems, have challenged many hitherto foundational ideas of planetary formation and evolution that were based solely on knowledge of our own solar system. This thesis addresses some of the emergent puzzles posed by the orbital and interior dynamics of planets orbiting very close and far away from their stars.

Chapters II-III consider the origins of planets on very short-period orbits. Two and a half decades ago, the discovery of the first hot Jupiter marked the dawn of exoplanet detections around sunlike stars. The existence of these extremely irradiated Jovian planets (orbital periods $\lesssim$ 5 days) runs in stark contrast to the utter absence of material orbiting interior to Mercury in our own solar system. This striking discrepancy between the close-in planetary content of observed systems and our own—together with the notion that, interior to the "snow lines" of stars at stellocentric radii of several au, water ice is not available to contribute to the accretion of the several Earth-mass cores necessary for runaway core accretion—has led to many works aiming to explain how Jovian-mass ($\gtrsim 0.1 M_{\rm J}$) planets can migrate inward to become hot Jupiters after forming beyond the snow lines of their stars. One such migration mechanism, known as high-eccentricity migration, occurs when a Jovian planet is excited to extremely high eccentricity such that it experiences significant tidal dissipation at perihelion passage, promoting orbital decay to a short-period orbit. For cases such as the massive ($\sim 9 M_{\rm J}$), eccentric ($e \sim 0.5$) hot Jupiter HAT-P-2b—for which the exterior perturber is characterized—the eccentric orbital state encodes information about the tidal history of the planet. In Chapter II, I outline a method for constraining the tidal dissipation rate in eccentric hot Jupiters such as HAT-P-2b and its analogues. In Chapter III, I consider the opposite limit of possibilities: local conglomeration. While observations of highly eccentric, tidally unstable hot Jupiters imply some hot Jupiters must form through high-eccentricity migration, I present a $-2/7$ power law prediction which naturally follows from a basic picture of viscous accretion and inner magnetic truncation of protoplanetary disks. This power law, combined with simple tidal corrections, agrees well with the observed period-mass distribution of hot Jupiters, possibly lending new credence

to the hypothesis that hot Jupiters predominantly form in situ, near their observed close-in positions.

Next, with Chapter IV, we move on from the inner regions of planetary systems to address the interior dynamics of our furthest observed solar system planets, Uranus and Neptune. The so-called "ice giants" present a major challenge to interior modeling efforts due not only to a relative lack of spacecraft coverage compared to other solar system planets, but also because of a compositional degeneracy which inherently arises from their intermediate densities. An especially confounding issue surrounding these planets has been the extremely low heat flux of Uranus compared to Neptune. Chapter IV addresses these challenges with the application of novel thermodynamic constraints that follow in the case where hydrogen and water are taken to be immiscible major constituents. As discussed in Chapter IV, this model framework can satisfy the observed masses, radii, and gravitational harmonics of these planets—without being at odds with observations of the magnetic fields. Importantly, as Chapter IV shows, hydrogen-water immiscibility in the deep interiors of Uranus and Neptune can offer a natural explanation for the disparate heat fluxes—but characteristically similar magnetic fields—of Uranus and Neptune.

Following this discussion of the outermost directly observed planets in our solar system, Chapters V-VI delve into the orbital dynamics of planets on extremely wide (hundred-au) orbits, with a specific emphasis on the hypothesized Planet Nine. In our own solar system, the existence of a massive planet on such a wide orbit, with considerable eccentricity ($e \gtrsim 0.1$) and inclination ($i \sim 20°$), has been proposed to explain several dynamical features of the outer solar system. In Chapter V, I describe how this very distant planet could affect the dynamics down to the innermost reaches of the solar system, through secular modulation of the so-called "invariable" plane of the canonical planets, relative to the solar spin axis. Next, in Chapter VI, I numerically derive a prior distribution for the relative occupation of individual mean-motion resonances with this planet by eccentric small bodies, showing that assumption of low-order resonances with observed objects is not a viable means to determine the current true anomaly of Planet Nine.

Finally, in Chapter VII, concluding remarks are given, and the findings of this work are discussed in relation to the ongoing exploration of related topics in planetary system dynamics.

PUBLISHED CONTENT AND CONTRIBUTIONS

Bailey, E., S. Naoz, and K. Batygin. "Long-term tidal evolution of the extremely eccentric hot Jupiter HAT-P-2b". *The Astronomical Journal, in review*.
E.B. contributed to the conception of the project, performed simulations and analysis to generate results, and led the writing of the manuscript. This work was adapted to constitute Chapter II.

Bailey, E., and D. J. Stevenson. "Thermodynamically Governed Interior Models of Uranus and Neptune". *The Planetary Science Journal, in review*.
E.B. contributed to the determination of the project's direction; performed modeling, calculations, and analysis to generate results; and led the writing of the manuscript. This work was adapted to constitute Chapter IV.

Bailey, E., and K. Batygin. 2018. "The hot Jupiter period-mass distribution as a signature of in situ formation". *The Astrophysical Journal Letters* 866 (1). doi:10.3847/2041-8213/aade90.
E.B. conceived of the project's primary objective, performed calculations and analysis to generate results, and led the writing of the manuscript. This work was adapted to constitute Chapter III.

Bailey, E., M. E. Brown, and K. Batygin. 2018. "Feasibility of a Resonance-Based Planet Nine Search". *The Astronomical Journal* 156 (74). doi:10.3847/1538-3881/aaccf4.
E.B. contributed to the conceptual evaluation of the project's goals, performed numerical simulations (Excluding the simulations referred to in Figure 7) and led analysis (of all simulations) to generate results, and led the writing of the manuscript. This work was adapted to constitute Chapter VI.

Bailey, E., K. Batygin, and M. E. Brown. 2016. "Solar obliquity induced by Planet Nine". *The Astronomical Journal* 152 (5). doi:10.3847/0004-6256/152/5/126.
E.B. contributed to the conceptual evaluation of the project's goals, performed calculations to generate results, and participated in writing the manuscript. This work was adapted to constitute Chapter V.

TABLE OF CONTENTS

LIST OF ILLUSTRATIONS

Number *Page*

LIST OF TABLES

Chapter 1

INTRODUCTION

In discussions of the history of scientific progress, it is widely regarded that anthropocentrism, in various forms, is one of the most pervasive fallacies of our species. Indeed, we humans have historically held a tendency to believe that: (1) we occupy a central role in everything, (2) that the situations in which we find ourselves are quintessential, and (3) that our limited observations offer complete representations of the universe. The first of these fallacies is most commonly illustrated with the famous example of the Copernican revolution. In retrospect, it is easy to feel vicarious embarrassment on behalf of those who actually believed the planets were orbiting the Earth on epicycles. It is also tempting to dismiss this problematic way of thinking as simply the result of humanity's lack of advancement several centuries ago; certainly we must have progressed considerably since then. However, in recent decades, other breakthroughs in planetary astronomy have offered shocking challenges to fallacies (2) and (3). While these recent advances may not be as fundamentally revolutionary as the realization that the Earth is not the central body of the solar system, they have served as a humbling reminder that we still have a long way to go in understanding our place in the cosmos.

Prior to observations of other planetary systems, it was natural to suspect that our solar system might be a quintessential case. Perhaps the discovery of planets orbiting a pulsar (Wolszczan and Frail 1992) should have served as a forewarning that planetary systems are often extremely unlike our own. However, as planet formation theory had, at that point, focused primarily on processes around sunlike stars, the main shock to the understanding of how planetary systems originate was felt when the discovery was announced (Mayor and Queloz 1995) of a gas giant planet around a sunlike star. While similar to our own Jupiter in mass and radius; this planet, 51 Pegasi b, was found to orbit its star with a period of less than 5 days—well within the orbital distance of Mercury, where nothing (not even a belt of asteroids) is known to orbit in our own system—and further detections of similar short-period giant planets followed thereafter. Prior to the discovery of these so-called *hot Jupiters*, the arrangement of planets in the solar system seemed to be neatly accounted for in the framework of the core accretion model, which holds that giant planets are nucleated by massive ($\sim$ 10-15$M_{\rm Earth}$) cores of condensed material that

accumulate in protoplanetary disks. Inside the *snow line*, the stello-centric distance in the disk at which volatiles (particularly water) condense, it was originally expected that suitably massive cores to form giant planets should not be available. After all, in our own planetary system, Jupiter resides just past the approximate distance of the snow line, with the modest-sized terrestrial planets positioned on closer orbits. However, with the first detection of a planet around a sunlike star presenting a stark counterexample to this expected outward ordering of terrestrial to giant planets, the entire understanding of planet formation—which previously seemed to neatly account for our solar system's arrangement of worlds—was suddenly jolted out of its seeming alignment with observations.

Accordingly, the predominant initial response to this challenge was to find ways to explain how planetary systems, initially forming with a structure similar to our own, could then proceed to evolve to produce this completely unfamiliar orbital configuration. In particular, a vast body of work has been produced over the subsequent decades to understand in detail how a planet similar to Jupiter could form at Jupiter-like orbital separations of several au, and migrate inward to a short-period orbit to become a hot Jupiter. One such long-range migration mechanism, in which the planet is perturbed by a massive companion onto a high-eccentricity orbit, so that it experiences tides which cause its orbit to shrink and circularize, is explored in Chapter II. As evidence for the occurrence of this particular migratory process, several highly eccentric ($e \gtrsim 0.1$) hot Jupiters have been observed residing on tidally unstable orbits. Chapter II addresses a particularly interesting case, for which the exterior companion, presumably responsible for perturbing the hot Jupiter to its eccentric state, is partially characterized. As will be discussed in Chapter II, characterization of the exterior perturber in this system and its analogues can allow for the obtainment of detailed constraints on tidal dissipation in hot Jupiters, using a novel method that will be discussed therein.

While it is known that hot Jupiters do form via the process of so-called high-eccentricity migration, in recent years, another formation mechanism, first proposed by Bodenheimer, Hubickyj, and Lissauer 2000a, has gained serious consideration as a possible predominant process by which hot Jupiters can form. In particular, the idea that hot Jupiters can form *in situ*—at or near their present-day observed orbital distances—presents an alternative to the migratory origin hypothesis. More recently, Batygin, Bodenheimer, and Laughlin 2016a have highlighted the theoretical feasibility of this formation scenario, demonstrating that conditions at the inner

regions of protoplanetary disks do not pose a hindrance to successful giant planet formation via core accretion—provided a suitably massive ($\sim$ 10-20$M_{\rm Earth}$) core is available. In fact, it is now understood that there is no shortage of such cores. In particular, the *Kepler* space telescope, built to detect transiting planets passing in front of their stars, has demonstrated that close-in (period $\lesssim$ 400 days) super-Earths reside around $\sim$ 30% of sun-like stars (Zhu et al. 2018). These massive, "*Kepler*-like" planets frequently occur on the several-day orbits typical of hot Jupiters; hot Jupiters, by comparison, are quite rare (albeit highly detectable), occuring around merely 1% of sun-like stars (Howard et al. 2010; Gould et al. 2006; Wright et al. 2012). The view of planetary systems offered by *Kepler* seems to indicate giant planet accretion at close-in orbital distances does not need to be particularly efficient to account for the entire hot Jupiter population, suggesting in situ formation—contrary to what was once widely believed based solely on the architecture of our own system—could potentially serve as a viable means to produce the majority of hot Jupiters. As in situ formation has attained recent credence as a possible predominant formation mechanism, a renewed discussion has emerged, two decades after the initial discovery of these seemingly exotic planets, about how they most often tend to originate. In Chapter III, I present a contribution to this debate—namely, I discuss how a $-2/7$ power law, which naturally arises from a simple model of in situ core accretion of hot Jupiters, taking into account the established understanding of magnetic star-disk interactions, can account for the evident sharp lower cutoff in the period-mass distribution of observed hot Jupiters.

On a related note, with the advent of their discovery, it was widely suspected that the highly irradiated, super-Earth to sub-Neptune planets found in abundance by *Kepler* might, in many cases, be inwardly migrated analogues to our local "ice giants" Uranus and Neptune. However, in the last few years, this view has become disfavored. More specifically, it is now understood that the radius gap (Fulton et al. 2017a) from (1.5-2.0$R_{\rm Earth}$) among close-in ($P < 100$ d) planets can be explained as resulting from evaporation of the primordial, hydrogen-rich envelopes of smaller planets (Fulton et al. 2017a; Owen and Wu 2017). These stripped cores are now understood to be primarily rocky in composition (Gupta and Schlichting 2019), suggesting the close-in, *Kepler*-like planets—despite often having masses and radii similar to Uranus and Neptune—are not likely to be inwardly-migrated ice giant analogues. Unlike the stripped rocky planets observed on short-period orbits around other stars, because Uranus and Neptune have not lost their overlying hydrogen-rich envelopes, their deep interior compositions are not directly

known. In fact, as discussed in Section IV, there is little direct information about the proportions of specific metals comprising Uranus and Neptune, although their observed atmospheric methane enrichments (Fegley et al. 1991; Baines et al. 1993), in conjunction with their intermediate densities and large present-day stello-centric distances, are highly suggestive of ice-rich interior compositions. In Section IV, I introduce models which apply novel thermodynamic constraints to the interior structure and composition of ice giants, treating hydrogen and water as the immiscible major constituents. Viewing Uranus and Neptune in this thermodynamically justified manner, I show how this new approach to interior modeling of these planets offers a natural explanation for the different heat flows of Uranus and Neptune (Fazio et al. 1976; Loewenstein et al. 1977; Loewenstein, Harper, and Moseley 1977; Hanel et al. 1986; Conrath et al. 1989; Pearl and Conrath 1991)—a longstanding mystery—and can simultaneously account for their different atmospheric ammonia abundances (Gulkis, Janssen, and Olsen 1978; de Pater, Romani, and Atreya 1991).

Until recently, Neptune was thought to be the solar system planet with the greatest heliocentric distance. However, several years ago, a challange to fallacy (3), as discussed earlier in this chapter, was posed when Batygin and Brown 2016a suggested that the anisotropic distribution (Brown 2017) of distant small objects with semimajor axes of hundreds of au could be explained as resulting from the influence of an unseen super-Earth on an eccentric, inclined ($i \sim 20°$) orbit. The Planet Nine hypothesis has generated much debate, and a number of alternative hypotheses (Madigan and McCourt 2016; Sefilian and Touma 2019; Scholtz and Unwin 2019) have additionally been put forth to account for the observed anisotropy of distant, eccentric small bodies beyond Neptune. Moreover, a few works have since questioned the anisotropy (Shankman et al. 2016; Bernardinelli et al. 2020), although these have referred to individual datasets with small numbers of detected objects (and have argued statistical consistency with an isotropic distribution, rather than inconsistency with an anisotropy). Indeed, without some perturbing influence in place to gravitationally shepherd the distant, eccentric objects into their observed configuration, the observed characteristic clustering would scramble on a timescale orders of magnitude shorter than the solar system's lifetime. Accordingly, the Planet Nine hypothesis remains actively considered, despite continued challenges to direct detection.

Chapter V addresses the effect a distant, eccentric, inclined, massive planet such as Planet Nine would have on the obliquity of the host star relative to the "invariable"

plane of the planets. A six-degree tilt of the sun relative to the planets was first observed by Sir Richard Carrington in the mid-nineteenth century (Carrington 1853-61). As Chapter V discusses, Planet Nine, with its preliminary proposed orbital parameters and mass, was initially thought to potentially account entirely for the observed solar obliquity, by inducing precession of the plane of the other planets relative to the sun. With current predictions for its mass and orbit, Planet Nine is no longer expected to account for the entire solar obliquity (Batygin et al. 2019). As mentioned further in Chapter V, numerous other processes inherent to planetary system formation can invoke the observed tilt. However, the dynamical construction presented in Chapter V remains generally relevant to exoplanetary systems, and it is included in this thesis with this caveat noted.

Finally, Chapter VI turns to address a major challenge inherent to the search for Planet Nine. While Le Verrier famously managed to predict the location of Neptune with a flourish of his writing utensil, no comparatively simple strategy has yet been found to locate Planet Nine. Orbital mean-motion resonances are currently expected to exist between Planet Nine and a subset of the observed small bodies crossing its path; at first glance, the existence of these resonances might seem to suggest a useful means exists by which to locate Planet Nine in the sky, as resonant dynamics are inherently dependent on the specific locations of objects along their orbits. However, in Chapter VI, I discuss how the eccentric dynamics of Planet Nine, and the associated predominance of high-order resonances—combined with the frequent chaotic transfer of objects between resonances—together pose an inherent statistical obstacle to the use of mean-motion resonances in determining Planet Nine's current location in the sky. As the dominating influences on the outermost reaches of the solar system remain to be fully accounted for, we are reminded that our very own planetary system remains to be more completely understood, in order to form a cohesive understanding of its place among exoplanetary systems. This discussion is followed by concluding remarks in Chapter VII.

Chapter 2

LONG-TERM TIDAL EVOLUTION OF THE HIGHLY ECCENTRIC HOT JUPITER HAT-P-2B

ABSTRACT

The massive ($M_b = 9M_J$), highly eccentric hot Jupiter HAT-P-2b (HD 147506b) ($e \sim 0.5, a \sim 0.07$) presents an intriguing opportunity to characterize long-term dynamical evolution of a short-period exoplanet. In contrast to the vast majority of hot Jupiters on circular orbits, the remarkable orbital state occupied by this planet encodes constraints on its tidal evolution. Furthermore, the inferred existence of an exterior dwarf perturber to HAT-P-2b (Lewis et al. 2013), having potential for follow-up, presents an opportunity for continued characterization of the long-term perturbations experienced by HAT-P-2b. Together, these features render the HAT-P-2 system—and similar analogues hosting highly eccentric, close-in planets—an effective probe of an exoplanet's tidal dissipation–parameterized by the viscous timescale t_v or alternatively, the present-day tidal quality factor Q. In this work, we derive an estimate of $Q \sim 10^4 - 10^5$ for HAT-P-2b based on its present-day orbital characteristics. Additionally, we present simulations of the planet's long-term (~Gyr) tidal evolution, facilitated by Lidov-Kozai evolution from an initially wide ($a > 1$ au) orbital separation from the star. We find that the system's current parameters can be produced over the system lifetime through long-range migration from a Jupiter-like orbit due to the eccentric Lidov-Kozai effect. Prospects for future follow-up of this system are discussed.

2.1 Introduction

When hot Jupiters came to be the first exoplanets discovered around sunlike stars (Mayor and Queloz 1995), it became necessary to explain how this class of gas giants—with masses comparable to Jupiter and Saturn—can exist at roughly a hundredth the distance from their stars. Today, the nature of hot Jupiter formation remains the oldest open problem of exoplanetary science. At first, it was proposed (Lin, Bodenheimer, and Richardson 1996) that these planets form on ~ 5 au orbits via core accretion—in the same manner as Jupiter—and subsequently, interactions with the remaining circumstellar disk (Kley and Nelson 2012) cause them to migrate inward. Then, another mechanism was suggested—high-eccentricity migration, during which the giant planet, again starting on a wide, several-au orbit, is excited to an extremely eccentric state (typically by a companion), leading to long-range tidal decay of the orbit (Rasio and Ford 1996; Wu and Murray 2003a; Fabrycky and Tremaine 2007a; Naoz et al. 2011a; Wu and Lithwick 2011; Beaugé and Nesvorn 2012; Petrovich 2015). More recently, in contrast to these long-range migration mechanisms, in situ formation via core accretion (Bodenheimer, Hubickyj, and Lissauer 2000a; Batygin, Bodenheimer, and Laughlin 2016b) has gained ground as a potentially viable means of formation.

Of the formation mechanisms listed above, a widespread consensus has not yet been reached on the relative importance of each. Although various sources of evidence might suggest that high-eccentricity migration may not be the main production line for hot Jupiters (a lack of highly eccentric hot Jupiters observed in the process of circularization; Dawson, Murray-Clay, and Johnson 2014a; an inadequate prevalence of companions capable of inducing migration; Knutson et al. 2014; Ngo et al. 2015; Ngo et al. 2016; Piskorz et al. 2015), hot Jupiters *have* been observed on eccentric orbits with inferred circularization timescales a mere fraction of their systems' ages—an apparent smoking gun to confirm that high-eccentricity migration does, in fact, occur. Moreover, the exotic nature of this process has, in its own right, justified extensive investigation over the past decade and a half. However, a major challenge in further characterizing high-eccentricity formation resides in the fact that most hot Jupiter orbits are circular, and thus lack a record of the timing of any previous circularization. In contrast to prototypical hot Jupiters on circular orbits, the orbital states of select, eccentric hot Jupiters encode their specific tidal histories. As a result, the individual examination of short-period giant planets observed on eccentric orbits (with the canonical example being HD 80606; Wu and Murray 2003a; Fabrycky and Tremaine 2007a) is essential to the study of high-eccentricity

migratory dynamics.

From a purely orbital point of view, an absolutely unique member of the hot Jupiter population is HAT-P-2b (HD 147506b). This highly massive hot Jupiter ($M_b = 9M_J$, $R_b = R_J$), discovered (Bakos et al. 2007) in observations from the HATNet transit detection survey (Bakos et al. 2002; Bakos et al. 2004), stands out due to a combination of unusual attributes. First, despite residing on a short-period orbit typical of close-in giants, this object is unusually eccentric ($e \sim 0.5$; Bakos et al. 2007; Loeillet et al. 2008; Lewis et al. 2013). This un-circularized, close-in ($a \sim 0.07$ au; Bakos et al. 2007; Winn et al. 2007; Loeillet et al. 2008; Pál et al. 2010; Lewis et al. 2013) configuration is intriguing in light of the advanced age of the system (2.6 ± 0.5 Gyr, Pál et al. 2010), appearing to suggest that this long-term unstable state may have been attained in the course of tidal circularization. Accordingly, the characterization of the evolution of this system has been addressed by numerous works (Jackson, Greenberg, and Barnes 2008; Fabrycky 2008; Matsumura, Takeda, and Rasio 2008; Baraffe, Chabrier, and Barman 2008).

Second, in addition to the eccentric and close-in present-day orbital state of HAT-P-2b, the uniqueness of this system is further elevated by the detection of a trend in the radial velocity data (Lewis et al. 2013). Based on this finding, in conjunction with non-detection of the companion in direct imaging, Lewis et al. 2013 suggested the existence of an additional, exterior object—an M/L/T/Y dwarf at 10 – 40 au separation. As Lewis et al. 2013 pointed out, the presence of this massive exterior perturber renders HAT-P-2b the quintessential candidate for migration through Lidov-Kozai cycles in conjunction with tidal friction (Referred to by numerous other works as KCTF) (Wu and Murray 2003a; Fabrycky and Tremaine 2007a; Naoz et al. 2011a). In the scenario of KCTF, HAT-P-2b would have initially formed at wide separation from the host star. Due to a substantial initial misalignment between the inner and outer orbits, repeated secular perturbations from the outer body would have produced eccentricity and inclination modulations in HAT-P-2b's orbit. As a result, during periodic excursions to high eccentricity, HAT-P-2b would have invaded the star's tidal zone and experienced tidal dissipation. After significant tidal shrinkage of its orbit, in accordance with the known characteristic behavior of this process, HAT-P-2b then would have decoupled from the long-period companion, and embarked on a final trek of circularization and inward migration.

To summarize, two features distinguish the HAT-P-2b system as especially useful for gathering tidal constraints. First, the planet's present-day eccentric state can po-

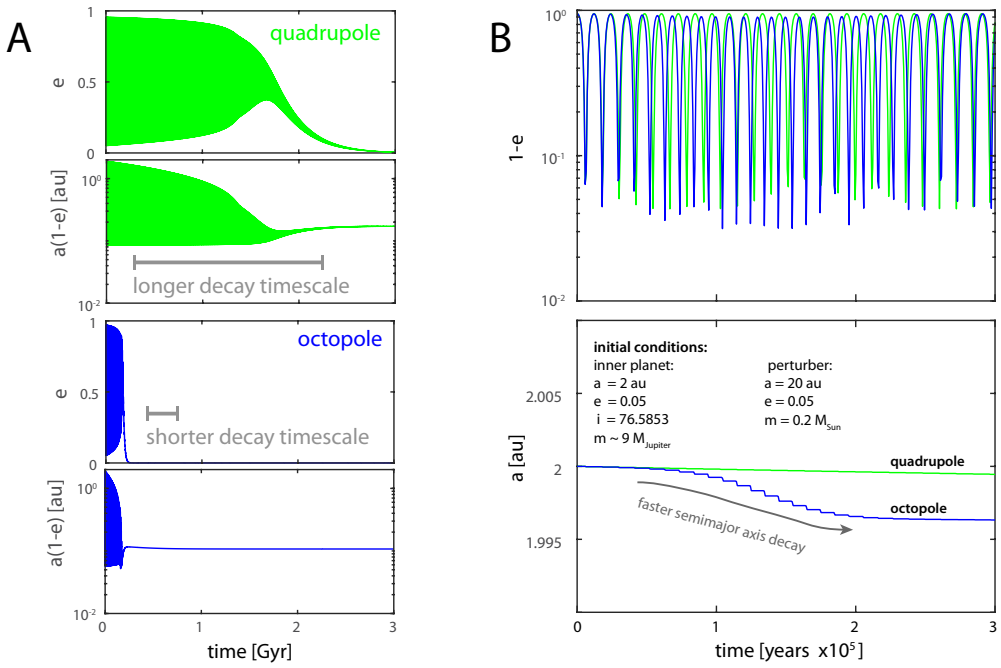

Figure 2.1: Side-by-side comparison of quadrupole- ($\mathcal{O}(\alpha^2)$) and octopole-level ($\mathcal{O}(\alpha^3)$) simulations of the orbital evolution of a super-Jovian Planet (mass $m = M_{\text{HAT-P-2b}} = 9M_{\text{Jupiter}}$ migrating inward due to the Lidov-Kozai effects induced by the influence of a massive outer perturber. The initial conditions (listed in the lower panel of column B) were one set of many chosen in the manner described in the text. The figures in column A show that these two levels of approximation produce qualitatively similar behavior, but a major disparity in evolution timescale between the quadrupole and octopole cases. In column B, the first several 10^5 years of the multi-Gyr simulations are shown in detail. While the behavior in both cases is qualitatively similar, it is apparent that the octopole-level dynamics allow for the Jovian planet to sometimes attain somewhat higher eccentricity than in the quadrupole case, which hastens the semimajor axis decay. This suggests that the octopole level must be taken into account when determining which long-term system evolutiofn scenarios are capable of producing HAT-P-2b on its present orbit over the system lifetime.

tentially encode its evolutionary history, unlike a planet on a circular orbit. Second, the opportunity exists for ongoing characterization of the outer companion and its associated secular effects on the planet, which, in conjunction with tidal effects, seem likely to have governed the system's long-term evolution. Accordingly, the primary goal of this study is to characterize high-eccentricity migration within this system from semi-analytic grounds, and to derive constraints on the dissipation in this giant planet from available data. In particular, we concern ourselves with the rate of tidal dissipation permitting the system's evolution to the observed present-day state over its multi-Gyr lifetime. As will be discussed shortly in more detail, the tidal dissipation rate can be parameterized in terms of the quality factors Q of the tidally interacting bodies, or equivalently, their viscous dissipation timescales t_V. While these parameters admittedly serve as a crude representation of tidal dissipation for the time being, we choose to neglect the detailed evolution thought to result from dynamical tides (e.g. Vick, Lai, and Anderson 2019). Such corrections to the tidal model may be considered in future work, when constraints are obtained in greater detail for the HAT-P-2 system and other highly eccentric hot Jupiter analogues with constrained perturbers.[1]

The remainder of the paper is organized as follows. In Section 6.2, we define the suite of calculations employed in characterizing HAT-P-2b's long-term tidal evolution, followed by the results and discussion in Section 6.3. Finally, conclusions about the orbital evolution and tidal dissipation of this highly unusual planet are presented in Section 5.4.

2.2 Methods

We employed the secular formulation of Naoz et al. 2011a; Naoz et al. 2013, constituted by an octupole-level expansion of the three-body Hamiltonian together with general relativistic corrections and tides, to derive the long-term evolution of the HAT-P-2 system. Secular theory is applicable (assuming the system was not initially near resonance) due to the significant discrepancy between the short period of HAT-P-2b and that of the outer perturber. The details of our simulations are discussed below.

[1]For circularized hot Jupiter orbits, tidal decay is expected to be dominated by tidal dissipation in the star (Penev and Sasselov 2011). In contrast, eccentric hot Jupiters offer information about dissipation rate in the planet, a quantity that is highly uncertain from first principles.

Octopole-level simulations

A widely-used formulation of the Lidov-Kozai mechanism is an expansion in semi-major axis ratio $\alpha = a_{\rm inner}/a_{\rm outer}$ of the disturbing function to quadrupole order $O(\alpha^2)$. In this framework, if one of the masses of the inner orbit of the hierarchical triple is a test particle and the outer orbit is circular (aka the test particle quadrupole approximation; see Naoz 2016 for a review), the component of the inner orbit's angular momentum parallel to the outer perturber's angular momentum, $L_z = \sqrt{(1-e^2)}\cos i$, is invariant. Hence, with L_z held fixed, the inner orbit experiences periodic exchanges of eccentricity and inclination. Overall, the widely used quadrupole-level Lidov-Kozai mechanism, assuming an inner test particle and axisymmetric outer orbit, is sufficient to reproduce accurate behavior in many systems. However, when the outer orbit has non-negligible eccentricity, or the inner object is unlike a test particle, behavior at the quadrupole level may differ significantly from higher-order results (Naoz et al. 2011a; Naoz et al. 2013; Naoz 2016). Typically, to characterize these scenarios, it is sufficient to carry out the expansion to the octupole level $O(\alpha^3)$. To this end, Naoz 2016 points out major differences arising in octupole-level simulations that are outlawed in the quadrupole case. In particular, because at this higher order, L_z is no longer fixed, the inner orbit's eccentricity can—in certain cases—approach unity. Remarkably, not even the *sign* of L_z is immune to variation, and the ability to produce retrograde inner orbits is a notable feature of the octupole-level expansion (Naoz et al. 2011a; Naoz et al. 2013; Li et al. 2014b).

In the octopole-level formulation, in which the Hamiltonian can be stated as $\mathcal{H} = \mathcal{H}_{\rm quadrupole} + \mathcal{H}_{\rm octopole}$, the octopole part $\mathcal{H}_{\rm octopole}$ scales as the parameter $\epsilon \equiv a_1 e_2/((1-e_2)a_2)$, where subscript 2 refers to the outer orbit of the hierarchical triple, and 1 to the inner orbit (Naoz et al. 2013). Indeed, it is known that the eccentricity of the outer perturber, which is likely to be significant if it was captured into a wide orbit around HAT-P-2 during a three-body interaction in the system's birth cluster, can considerably affect the maximum eccentricity reached by the inner orbit; in fact, either a high mutual starting inclination or a significant eccentricity of the outer perturber can lead the inner orbit to attain higher eccentricity (Teyssandier et al. 2013; Li et al. 2014b). However, for the time being, as the perturber's eccentricity lacks characterization, we opt to treat it as having low eccentricity ($e_2 = 0.05$). However, when the eccentricity of the outer orbit is better-known, the analysis can be revised, with an eye toward obtaining a more detailed description of the system's long-term evolution.

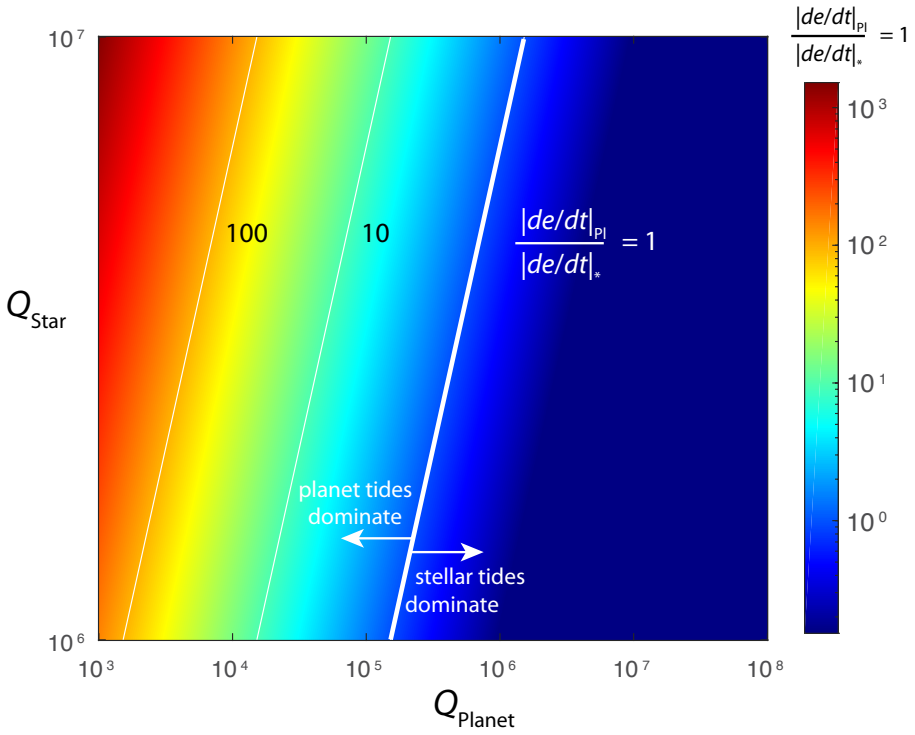

Figure 2.2: Contour plot showing, for a range of stellar and planetary quality factors Q given HAT-P-2b's presently observed orbital period, the relative importance of the tides raised on the planet versus tides raised on the star for governing the orbital circularization. In particular, the colors represent the ratio of $|de/dt|_{\text{Pl}}$ (the rate of eccentricity change due to tides raised on the planet) to $|de/dt|_{\text{S}}$ (the rate of change due to tides on the star), employing the formulation of Hut 1981 as described in the text. A large range of planetary Q is shown, while the stellar Q range shown is in agreement with the range found by Adams and Bloch 2015 for stars hosting planets in the *Kepler* dataset. The thick contour line corresponds to the place on the plot where the tidal effects of the star and planet are similar in magnitude, whereas tides raised on the planet dominate the circularization dynamics for $(Q_{\text{Planet}}, Q_{\text{Star}})$ to the left of the thick contour line.

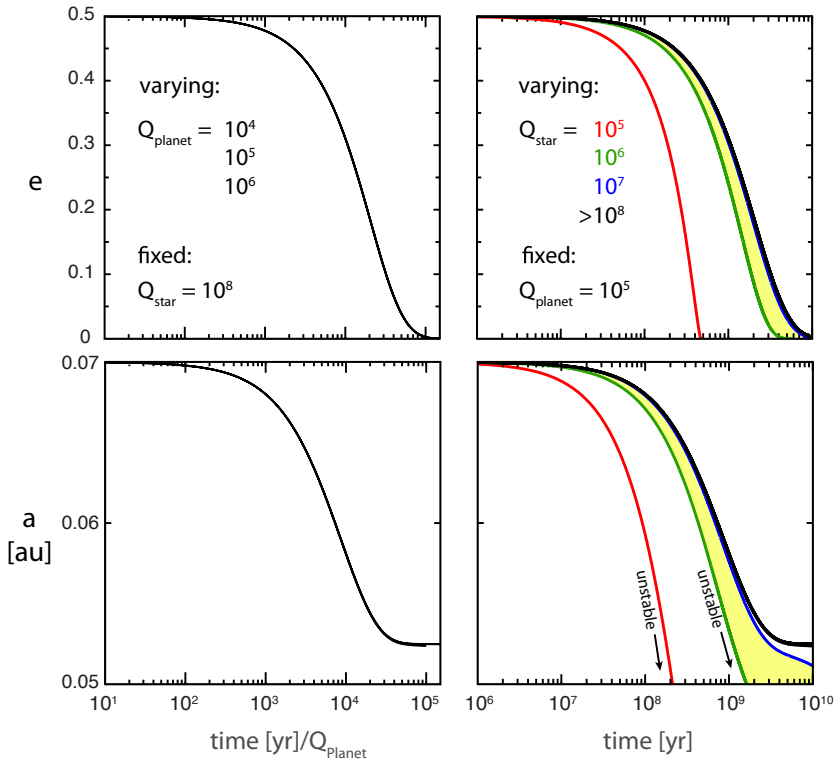

Figure 2.3: Tidal circularization of HAT-P-2b from its current state. *Left column:* Holding the stellar quality factor Q_{star} fixed, Q_{planet} was varied from 10^4 to 10^6. The time of each simulation was scaled by Q_{planet}, and the results stacked, demonstrating that the timescale of circularization in each case scales with Q, with the trajectories otherwise nearly identical. Given the observed system's ~Gyr evolution timescale, and taking into account that here it is shown that circularization timescale τ_{circ} is such that $\tau_{circ}/Q_{planet} \sim 10^4 - 10^5$, we infer an estimate $Q_{planet} \sim 10^4 - 10^5$. *Right column:* Informed by the aforementioned estimate, $Q_{planet} \sim 10^5$ was fixed and Q_{star} was varied from 10^5 to 10^{14}. Yellow shading shows the region corresponding to the $Q_{star} \sim 10^6 - 10^7$ estimate found by Adams and Bloch 2015.

Despite the aforementioned effect of the outer orbit's eccentricity on the strength of the octopole-level dynamics, it is still the case that, even where the outer perturber has negligible eccentricity, an important difference between the quadrupole and octopole cases can arise, shown in Figure (2.1). Specifically, for the HAT-P-2b system, we encountered a significant quantitative inaccuracy in the quadrupole-level simulations relative to the higher-order case: significant prolongation of the tidal circularization timescale. Employing a range of plausible initial conditions of the HAT-P-2 system, the system evolution timescale was, in some cases, an order of magnitude greater in the quadrupole case relative to the octopole-level examples. We attribute this effect to the tendency for slightly greater eccentricity to be permitted in the octopole- versus quadrupole-level simulations. Although the difference in trajectories arising in the two cases might appear minor at first glance, the compound effect is that the quadrupole-order evolution occurs more gradually relative to the higher-order case. Because a major aim of this work is to understand plausible initial conditions resulting in evolution to the system's observed parameters in agreement with the age of the system, we conclude that quadrupole-level simulations will ultimately be insufficient to fully characterize Lidov-Kozai migration for our purposes, and opt to employ the more computationally expensive octopole-level equations.

Hence, to ascertain the possible set of long-range evolution tracks of HAT-P-2b, we use the formulation of Naoz et al. 2011a; Naoz et al. 2013. General relativistic effects (first post-Newtonian expansion; Misner, Thorne, Wheeler, et al. 1973) are applied to the inner and outer orbits. The rotation rates for both bodies are initially set as 25 days, following Naoz and Fabrycky 2014. Setting the rotation rates to 4 days yields qualitatively identical results. The star is treated as a polytrope with $n = 3$, appropriate for a radiative body, while the planet is treated as a polytrope with $n = 1$ as a model for a Jupiter-class fully convective body (Stevenson 1982b); the associated apsidal motion constants k_2 assumed in the simulations are 0.014 and 0.25 respectively.

Parameterization of tidal dissipation

The notion of the quality factor Q for cyclic processes, defined as the ratio of stored to dissipated energy over one cycle, originated for the purposes of electrical engineering[2]. It was first employed by Johnson 1914 during his work for the

[2]In the more classic context of resonant RLC circuits, Q is inversely related to the bandwidth; in other words, circuits with greater Q resonate with minimal dissipation at a small frequency range, whereas those with lower Q resonate with greater dissipation at a wide frequency range.

American Western Electric Company (Smith 1986). From there, the use of Q has spread broadly across the physical sciences. In the astrophysical context, Goldreich and Soter 1966 introduced Q as a descriptor of tidal evolution; for a tidally distorted body, they defined it as the ratio of the energy lost during one orbit to the total energy stored in the tidal deformation.

Estimates for the Q of Jupiter, based on the present-day state of its satellites, originally ranged from approximately $6 \times 10^4 < Q_\mathrm{J} < 10^6$ (Goldreich and Soter 1966). Subsequently, (Yoder and Peale 1981) found that the tidal heating of Io can be accounted for only if Q_J resides at the lower end of the range obtained by (Goldreich and Soter 1966). Additionally, (Yoder and Peale 1981) pointed out that, while measurements of Io's heat flow (Matson, Ransford, and Johnson 1981; Sinton 1981; Morrison and . T.elesco 1980) implied that Q_J was as low as 4×10^4, no existing constant-Q model for the production of the present-day satellite resonances suggested such a low quality factor for Jupiter. However, by fitting a dynamical model to astrometric observations of the Jupiter system spanning over a century, Lainey et al. 2009 obtained a quality factor of Jupiter $Q = (3.56 \pm 0.66) \times 10^4$ — *specifically, at the present-day forcing frequency of Io* (assuming the conventional Love number value $k_2 = 0.379$; Gavrilov and Zharkov 1977). These discrepancies in understanding the value of Q highlight the challenges in understanding dissipative tidal processes in giant planets.

In practice, Q is merely a single parameter invoked to describe the effect of a range of possible interior dissipative processes. Giant planet interiors may experience time-varying effects that cause Q to vary (for example, a dilute suspension of one phase in another; Stevenson 1983); additionally, the specific fluid-mechanical processes responsible for tidal dissipation are thought to depend on the driving frequency (Ogilvie 2014; Greenberg 2009), which, for Jupiter, would have varied as the Jovian satellites migrated. As Greenberg 2009 points out, for a perfectly viscoelastic oscillator, it is reasonable to assume Q is directly proportional to the viscous dissipation timescale–or equivalently, that it exhibits inverse proportionality with respect to the time lag (e.g. Leconte et al. 2010). On the other hand, the extent to which planets are expected to resemble perfect viscoelastic oscillators is debatable, and the specific frequency dependence of Q remains an open question, highlighting the importance of having more examples of tidally evolving bodies with inferable Q.

In the original Goldreich and Soter 1966 formalism, Q is treated as a constant in

terms of an unchanging phase lag between the angle of the tidal bulge and the line connecting the centers of the interacting bodies. Alternatively, the quality factor is defined in terms of a constant lag time τ, such as the τ employed by Hut 1981—a classic formulation to which we refer in Section 6.3 as a comparison to our semi-analytic results. Rather than treating Q as a constant, this formalism treats Q as proportional to the period of the orbit. In the semi-analytic formalism used in this work to address the system's detailed evolution, Q is likewise treated as proportional to the period, but is also defined in terms of a constant dissipative timescale t_{V1} (Fabrycky and Tremaine 2007a; Hansen 2010; Naoz 2016)

$$Q_r = \frac{4}{3}\frac{k_1}{(1+2k_1)^2}\frac{Gm_r}{R_r^3}\frac{t_{Vr}}{n} \tag{2.1}$$

where k_1 is the classical apsidal motion constant, G is the universal gravitational constant, R_r is the body's radius, m_r is the body's mass, and the subscript r refers to the body on which tides are raised[3].

Choice of initial orbital parameters of HAT-P-2b

The initial orbital elements (a, e, i) are chosen by considering starting parameters for which the inner planet, in the course of its Lidov-Kozai orbital variations, attains perihelion distances within the tidal zone of the star. In this particular application, we resort to the test particle quadrupole (TPQ) approximation. Although the quadrupole level fails to reproduce accurate system lifetimes due to cumulative small differences in eccentricity, here we are merely concerned with dynamical evolution that unfolds on a timescale shorter than that associated with octupolar effects. Specifically, by uniformly randomly choosing initial a, e, and i from the ranges $a \in \{0.1, 5\}$ au, $e \in \{0, 1\}$, and $i \in \{0, 90\}$ deg and treating the angular momentum component $J_z = \sqrt{1-e^2}\cos(i)$ as fixed, we choose initial conditions for which the inner planet's initial minimum potentially attainable perihelion distance (agnostic to the argument of perihelion and longitude of ascending node) is less than 0.1 au and greater than a few times the Roche limit. This procedure thus serves as an approximate selection process for the initial (a, e, i) triplets of HAT-P-2b. The effects of varying the initial longitude of perihelion difference as well as the tidal dissipation rate of the planet are discussed in detail in the upcoming sections.

[3]Each body will, of course, have its own tides and its own value of Q. The question of whether the tidal dissipation of HAT-P-2b is dominated by the planet or the star is addressed in Section 6.3.

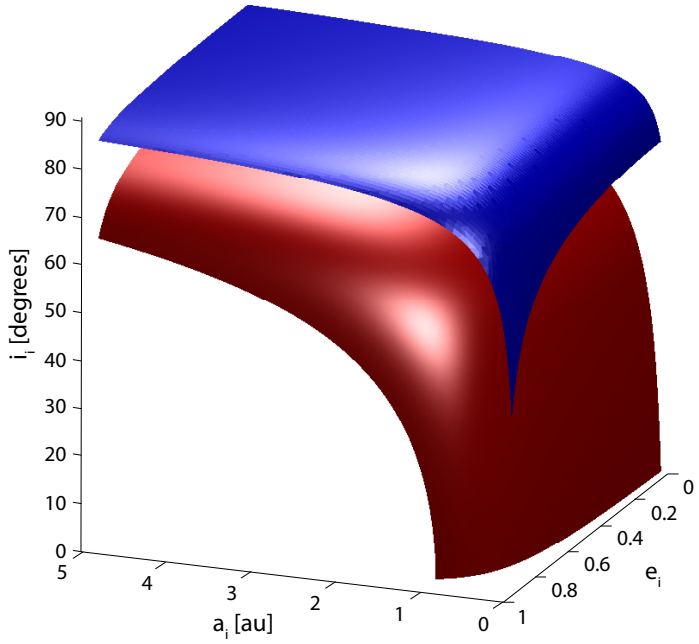

Figure 2.4: Approximate locus of suitable initial conditions for HAT-P-2b. The initial conditions allowing for tidal decay are expected to reside between the two isosurfaces of the inner orbit's approximate minimum perihelion distance. In the "test particle quadrupole" framework, in which L_z is conserved, the lower isosurface (red) represents orbits that initially come within 0.1 au of the star, in principle giving the planet an opportunity to experience significant tidal effects. The upper isosurface (blue) represents orbits that initially invade the Roche zone of the star. Orbits capable of producing long-term, long-range tidal migration of the planet are expected to reside between these two extremes.

2.3 Results

Beginning with the presently observed state of HAT-P-2b, and irrespective of the specific parameters of the exterior perturber, we can already obtain approximate tidal constraints on the system's evolution. The tidal evolution of HAT-P-2b's eccentricity depends on tides raised on both the star and the planet. Treating the inner two bodies of the system as a binary, and employing the weak friction model for close-in binaries developed by Hut 1981, the tidal evolution equation for the eccentricity due to tides raised on the *planet* is

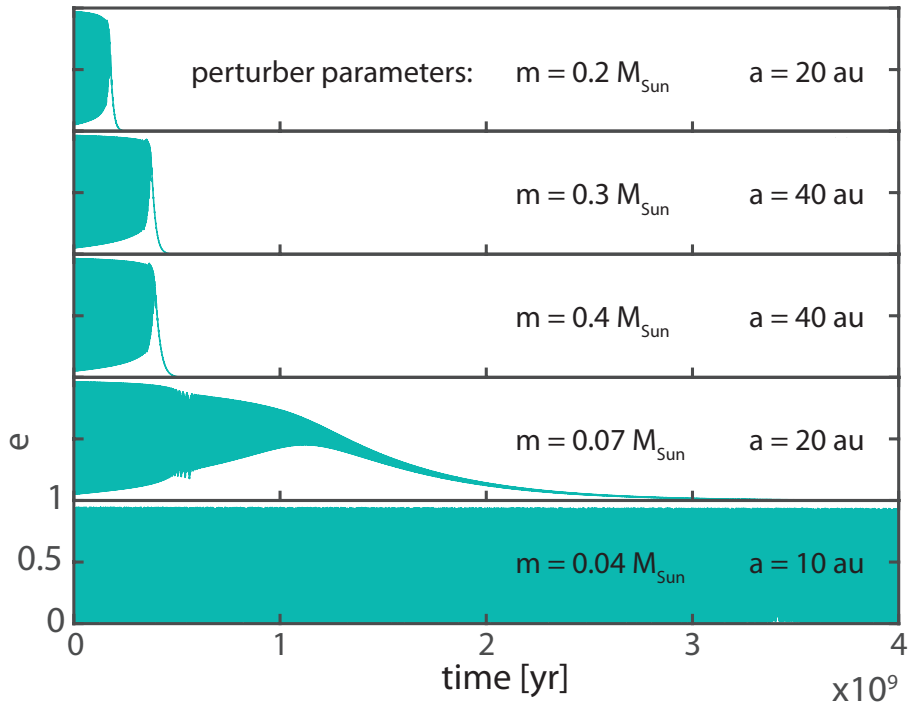

Figure 2.5: Side-by-side comparison of HAT-P-2b's eccentricity evolution where the perturber is varied. Starting conditions for the $m = 9M_{Jupiter}$ inner planet are $a = 2$ au, $e = 0.05$, $i = 76.5853$. The viscous timescales are $t_{V,1} = 100000$ yr and $t_{V,2} = 0.05$ yr for the star and planet, respectively.

$$\left[\frac{de}{dt}\right]_{\rm Pl} = -27\frac{k_{\rm Pl}}{T_{\rm Pl}}q_{\rm Pl}(1+q_{\rm Pl})\left(\frac{R_{\rm Pl}}{a}\right)^8 \frac{e}{(1-e^2)^{13/2}} \cdot \left\{f_3(e^2) - \frac{11}{18}(1-e^2)^{3/2}f_4(e^2)\frac{\Omega_{\rm Pl}}{n}\right\} \quad (2.2)$$

where $q_{\rm Pl} = m_\star/m_{\rm Pl} \gg 1$ is the mass ratio of star and planet, k_{Pl} is the planet's apsidal motion constant, Ω is the rotational angular velocity (assumed to be pseudosynchronous in the case of the planet), and $T_{\rm Pl} = R_{\rm Pl}^3/(Gm_{\rm Pl}\tau)$ is a typical tidal time scale, where G is the universal gravitational constant, $R_{\rm Pl}$ is the radius of the planet and τ is the constant small time lag, with $Q \sim \frac{1}{n\tau}$. Additionally, the functions $f_{3,4}(e^2)$ are polynomials which can be obtained in the original derivation. While the above expression describes the eccentricity evolution due to tides raised on the planet only, the effect due to tides raised on the star, $[de/dt]_\star$, is analogously given by the same expression, with the role of star and planet reversed.

Considering present-day parameters of the bodies and their orbits, we can employ the above formulation to carry out a precursory examination of the relative importance of dissipation in the planet versus the star. Assuming a stellar $Q \sim 10^6 - 10^7$ (the range which Adams and Bloch 2015 determined can best account for the survival of a sample of close-in *Kepler* planets having measured stellar rotation rates; McQuillan, Mazeh, and Aigrain 2013), the present-day ratio of $[de/dt]_{Pl}$ to $[de/dt]_\star$, obtained according to the above rationale, is shown in Figure (2.2). Upon examination, it is apparent that, for the assumed range of stellar Q, dissipation in the planet has an effect comparable or greater in magnitude, relative to dissipation in the star, for $Q_{Pl} \lesssim 10^5$. Furthermore, the timescale τ_e of eccentricity evolution can be approximated as

$$\tau_e \sim e/|de/dt|. \tag{2.3}$$

Equating τ_e to the age of the system, this expression provides a rough estimate of Q_{Planet}, i.e., $Q \sim 10^4 - 10^5$, remarkably close to the inferred Q of Jupiter itself.

Having obtained this precursory estimate, we proceed to numerically integrate the equations of motion for a more detailed analysis. Figure (3.1) shows the evolution of HAT-P-2b forward in time from its present-day orbital state, varying either the quality factor of the planet or the star. Taking into account the ~Gyr system age and the observation that the circularization timescale τ_{circ} scales as Q_{planet}, we again find that $Q_{\text{planet}} \sim 10^4 - 10^5$ corresponds to a circularization timescale comparable to the age of the system, a result which agrees with the analysis presented earlier in this section. Furthermore, we find that a stellar quality factor $Q_{\text{star}} \gtrsim 10^6$ produces evolution timescales that agree, to order of magnitude, with the behavior produced in the case of the aforementioned stellar constraint from Adams and Bloch 2015.

While HAT-P-2b is now essentially decoupled from the outer companion, its orbital state seems to indicate this was not always the case, as KCTF is the suspected mechanism behind its present-day eccentric orbit. Given the above precursory analysis, we now carry out a second analysis, this time accounting for the secular evolutionary history of HAT-P-2b. Specifically, we consider how the system evolution varies according to the specific mass and orbital radius of the perturber. The differences in timescale arising from varying the perturber within the rough range of likely parameters predicted by Lewis et al. 2013 is illustrated in Figure (2.5). When the perturber is better characterized, improved constraints will be attainable on the full

evolutionary history of HAT-P-2b.

Although additional constraints on the perturber will shed light on further details of HAT-P-2b's evolution, we do find that, for nominal perturber values in agreement with Lewis et al. 2013, Lidov-Kozai evolution can indeed successfully reproduce the system's present-day parameters over the system's age, from starting conditions beyond the approximate location of the "snow line." At the octopole level, we found examples of plausible evolutionary pathways. In these cases, HAT-P-2b initially possesses wide ($a > 1$ au) separation from the host star, and simultaneously attains the approximate observed eccentricity and semimajor axis of the planet. This occurs over a timescale comparable in order of magnitude to the system's lifetime of 2.6 ± 0.5 Gyr (Pál et al. 2010).

Method for deriving tidal dissipation rate

Because currently, the exterior perturber of HAT-P-2b is known only as a developing radial velocity trend, we are limited to a preliminary analysis of the system's evolution. Accordingly, we describe a generalizable method by which a hot Jupiter's viscous timescale t_V—and, by extension, its quality factor Q—may be refined based not only on the system age, but on the specific present-day a and e in conjunction with the system age.

First, to identify evolutionary pathways capable of producing the system's present-day orbit, we choose initial orbital parameters for HAT-P-2b uniformly at random from the locus of suitable initial conditions described in Section 2.2. For the purposes of this example, the viscous timescale of the star is taken to be great enough that tides from the planet dominate (e.g. $t_{V,1} = 1 \times 10^6$ yr) while the viscous timescale of the planet is chosen from a uniformly logarithmically random distribution, for example $\log_{10}(t_{V,2}, [\mathrm{yr}]) \in [-2, 1]$. In future cases where more detailed constraints render a more detailed analysis feasible, the viscous timescale of the star could also be varied. Sampling from this locus of plausible initial conditions and $t_{V,2}$, we evolve the system. To calculate the *extrapolated* viscous timescale $t'_{V,2}$ of HAT-P-2b, each simulation's evolutionary timescale is normalized to agree with the known system age. That is, for a $\tau_{\mathrm{obs}} \sim 10^9$ yr observed system age, if a simulated system required a time τ_{sim} to circularize with a planet viscous timescale $t_{V,2}$, we obtain the extrapolated viscous timescale $t'_{V,2} = (\tau_{\mathrm{obs}}/\tau_{\mathrm{sim}})t_{V,2}$.

The results obtained from this approach, for one nominal example of a perturber, are illustrated in Figure (2.7), showing semimajor axis $a_{f,e=0.5}$ when the planet crosses

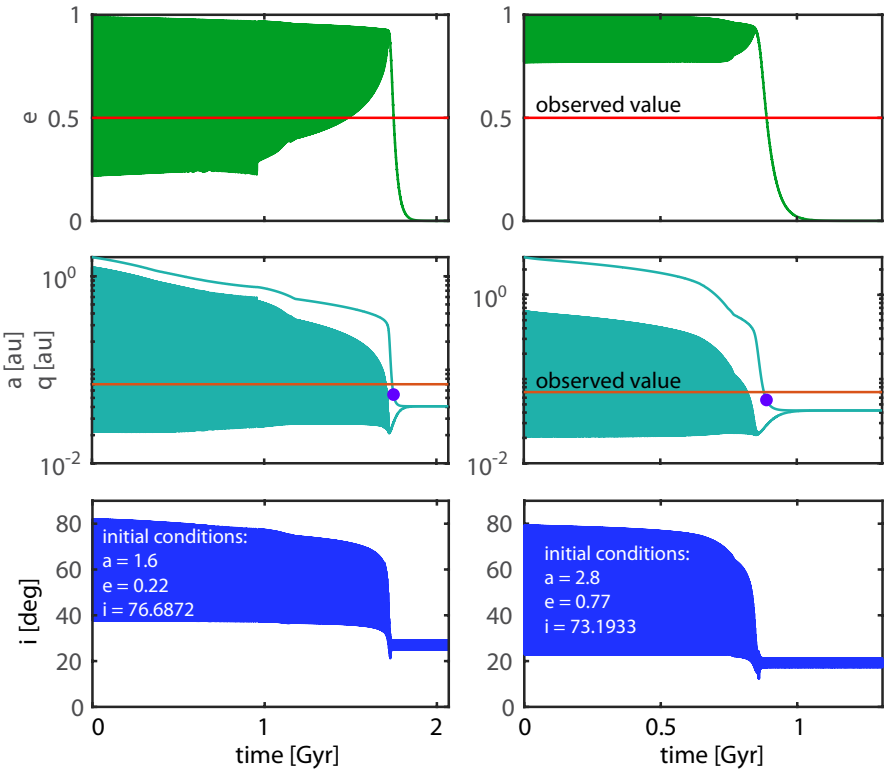

Figure 2.6: Two examples of octupole-level evolution pathways in which HAT-P-2b initially resides at several au from the star, and, under the influence of an exterior perturber, experiences circularization on a ~Gyr timescale comparable to the age of the system. Observed values of eccentricity and semimajor axis are illustrated with red lines, and the semimajor axis $a_{f,e=0.5}$ of HAT-P-2b occurring at the instant its orbit attains the observed eccentricity $e = 0.5$ during the final circularization pathway is shown represented by purple dots in the middle row, showing that the attained parameters agree roughly with observations. The viscous timescales $t_{V,1} = 100000$ and $t_{V,2} = 0.05$ yr for the star and planet, respectively.

through the observed eccentricity $e \sim 0.5$ in the course of its final circularization, as a function of *extrapolated* viscous timescale. Notably, this method does not merely account for the circularization timescale alone–*the specific parameter considered* is the semimajor axis at the moment of final circularization through the system's present-day eccentricity value ($e = 0.5$ in the case of HAT-P-2b). As shown in Figure 2.7, two cases were explored:

In the first suite of simulations (Figure 2.7, top plot), t_V was uniformly logarithmically randomly chosen from the plausible range $t_V \in \{10^{-2}, 10^{1}\}$ and initial longitude of perihelion difference $\Delta\varpi$ is zero for all simulations.

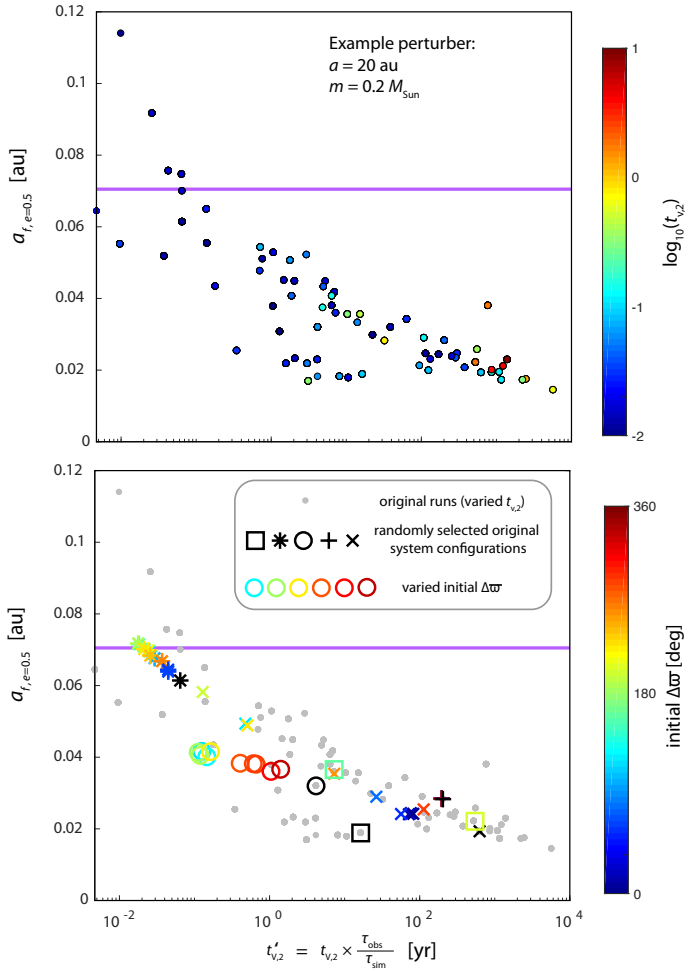

Figure 2.7: Example result from the method described in Section 2.3 for obtaining the viscous timescale $t'_{V,2}$ of HAT-P-2b, which is related to the period-dependent quality factor Q via Equation 2.1. Initial conditions were chosen according to the prescription outlined in Section 6.2, with simulated $t_{V,2}$ uniformly logarithmically randomly chosen. This plot shows the semimajor axis $a_{f,e=0.5}$ occurring when the planet executes its final traverse through the observed eccentricity value $e = 0.5$, as a function of *extrapolated* viscous timescale t'_V, obtained by multiplying the *simulated* t_V by a factor of $\tau_{\rm obs}/\tau_{\rm sim}$, where $\tau_{\rm obs}$ is the observed system lifetime and $\tau_{\rm sim}$ is the time it takes for each simulation to reach its final passage through $e = 0.5$ while circularizing. Notably, it is crucial to point out that in this case, $t'_{V,2}$ is the *extrapolated* viscous timescale derived by scaling according to the circularization timescale exhibited in the simulation for a chosen $t_{V,2}$. *Top:* the case where initial $\Delta\varpi$ is held fixed ($\Delta\varpi_i = 0$) and t_V is randomly chosen via the method described in the text. *Bottom:* the case where t_V is held fixed and initial $\Delta\varpi$ is uniformly randomly chosen. Grey points represent the simulations depicted in the $\Delta\varpi$-invariant case (top). Black symbols ($*, \circ, \square, \times, +$) mark each randomly chosen $\Delta\varpi = 0$ case that is re-run with uniformly randomly chosen initial $\Delta\varpi$, and the colors of symbols represent initial $\Delta\varpi$. The tendency for cases with varied $\Delta\varpi$ to follow the swath determined in the initial-$\Delta\varpi$-invariant case appears to suggest that the obtained mapping between inferred t_V and $a_{f,e=0.5}$ is robust to variation of initial $\Delta\varpi$.

In the second case (Figure 2.7, bottom plot), successfully circularizing initial conditions from the $\varpi_{initial} = 0$ case were chosen at random. From inspection of our simulations, there is an apparent trend that greater values of $\Delta\varpi$ lead to longer circularization timescales. In this second simulation suite, t_V was held fixed at $t_V = 10^{-2}$, the lower bound of the initial selection range. Using a fixed lower value of t_V allowed us to investigate the effect of varying initial $\Delta\varpi$ on the *extrapolated* viscous timescale t'_V, without sampling high-t_V cases with prohibitively long simulation timescales. Moreover, initial $\Delta\varpi$ was randomly varied, for several randomly chosen circularizing simulations from the constant $\Delta\varpi$ case.

In both cases, it is evident that the synthetic data obtained through this method form a particular swath across the plane, which appears to suggest a mapping of extrapolated viscous timescale $t'_{V,2}$ to the semimajor axis at the moment of final passage through a given eccentricity. In particular, for the given perturber, simulations producing a correspondent semimajor axis in agreement with observations are associated with a value of $t'_{V,2}$ between $\sim 10^{-2} - 10^{-1}$ yr, *for the example perturber used.* Moreover, it is necessary to emphasize that, because the circularization timescale is perturber-dependent, this method depends on characterization of the outer perturber.

As we have shown that wide variation arises in the system evolution timescale given different perturbers chosen within the parameter range allowed by Lewis et al. 2013, we do not consider this example to offer an actual constraint at this time. However, refinement of the perturber's parameters will allow for a more definitive analysis, and this procedure to use system lifetime in conjunction with the presently observed a, e to determine tidal dissipation rate in the planet may be applicable to additional systems in the future.

2.4 Discussion and Conclusion

Given the wide array of complexities inherent to the study of tidal dissipation in giant planets, hot Jupiters which encode tidal dissipation rates are highly valuable in that they offer a window into vastly more examples of dissipation in planetary interiors than the solar system can provide. Strides have already been made in this direction; as an example, Matsumura, Takeda, and Rasio 2008 have provided the estimate $10^5 \lesssim Q \lesssim 10^9$ for transiting planets. In this work, focus has been given to those hierarchical triples with a characterizable exterior perturber, as these systems can potentially allow for specific characterization of the system's orbital evolution.

This work provides an intriguing estimate of tidal dissipation within an exoplanet. In

addition to the approximate estimate of the present-day quality factor $Q \sim 10^4 - 10^5$ derived in this work from the hot Jupiter's present-day configuration, we have found that for eccentric hot Jupiter systems where an outer companion is characterized, more detailed constraints on tidal dissipation in the planet may be available. In particular, we have outlined a method to constrain the viscous timescale t_V for such systems. It is important to note that, in the formulation used in this work, the quality factor Q of the planet is a period-dependent function of t_V.

The hot Jupiter HAT-P-2b (HD 147506b) has presented an atypical opportunity to characterize the tidal dissipation occurring in a giant planet. Due to the highly eccentric present-day state of HAT-P-2b, combined with the preliminary characterization of its exterior companion (Lewis et al. 2013), HAT-P-2b encodes its tidal evolution history. Eccentric analogues to HAT-P-2b that also possess a characterized massive exterior companion (e.g. Rey et al. 2018) will provide similar contributions to an emerging perspective of the dissipation in tidally migrating exoplanets, particularly as the *Transiting Exoplanet Survey Satellite* (TESS) is expected to greatly increase the sampling of close-in exoplanets.

Given the presently observed conditions of HAT-P-2b, the estimate $Q_{\rm planet} \sim 10^4 - 10^5$ obtained (independent of the perturber's conditions) at the start of this work roughly agrees with existing estimates for giant planets, including that of Matsumura, Takeda, and Rasio 2008, as well as existing constraints on the value of Q for Jupiter and Saturn. Despite this agreement, it is prudent to remember that the formulation of tidal decay employed in this work neglects the inherently complicated nature of the processes underlying Q. When additional planets are discovered with similarly attainable Q values, this new set of examples may inform more detailed first-principles estimates of the dissipation.

We have confirmed that Lidov-Kozai evolution (Naoz et al. 2011a; Naoz et al. 2013) appears to be a feasible route for HAT-P-2b to have attained its present-day state. In particular, we have found that, in simulations with nominal perturber parameters in agreement with Lewis et al. 2013, the current a, e values of the system may offer constraints on planetary Q when characterization of the outer companion is further developed. In fact, for the nominal perturber parameters considered, we have found that a surprisingly tight bound on the planet's tidal dissipation may be attainable through simulation of the system's total secular evolution. Thus, as the exterior companion to HAT-P-2b is better characterized, we expect that it will be possible to derive improved constraints on the tidal dissipation in this highly exotic giant planet.

Furthermore, we reiterate that in the Lidov-Kozai formalism we have found that it can be necessary to consider the order of expansion of the disturbing function to ensure an accurate system evolution timescale is reproduced. Because at the octopole level $O(\alpha^3)$, the z-component of the angular momentum of the inner planet (where $\hat{z}$ is parallel to the system angular momentum) is not fixed, this effectively results in slightly higher eccentricities; the compounding effect of numerous slightly closer encounters with the star is for the orbit to decay at a significantly faster rate. Consideration of this effect is crucial in future studies of similar systems.

Historically, the understanding of tidal dissipation in planets has faced challenges from the lack of available examples. Although there are currently thousands of known exoplanets, the majority of close-in examples retain little information about their tidal histories. By considering eccentric planets with characterizable exterior massive companions, we conclude that it will be feasible to reconstruct tidal histories and obtain a broader understanding of planetary tidal dissipation.

Acknowledgments. We thank the anonymous reviewer for their useful comments. This work is based in part on work supported by NASA FINESST grant 19-PLANET19-0298. K.B. is grateful to the David and Lucile Packard Foundation and the Alfred P. Sloan Foundation for their generous support. S.N. acknowledges the partial support from the NSF through grant No. AST-1739160. S.N. also thanks Howard and Astrid Preston for their generous support. We also wish to thank Caltech High-Performance Computing for their assistance in managing the computer resources utilized in this work.

Chapter 3

THE HOT JUPITER PERIOD-MASS DISTRIBUTION AS A SIGNATURE OF IN SITU FORMATION

ABSTRACT

More than two decades after the widespread detection of Jovian-class planets on short-period orbits around other stars, their dynamical origins remain imperfectly understood. In the traditional narrative, these highly irradiated giant planets, like Jupiter and Saturn, are envisioned to have formed at large stello-centric distances and to have subsequently undergone large-scale orbital decay. Conversely, more recent models propose that a large fraction of hot Jupiters could have formed via rapid gas accretion in their current orbital neighborhood. In this study, we examine the period-mass distribution of close-in giant planets, and demonstrate that the inner boundary of this population conforms to the expectations of the in-situ formation scenario. Specifically, we show that if conglomeration unfolds close to the disk's inner edge, the semi-major axis-mass relation of the emergent planets should follow a power law $a \propto M^{-2/7}$ — a trend clearly reflected in the data. We further discuss corrections to this relationship due to tidal decay of planetary orbits. Although our findings do not discount orbital migration as an active physical process, they suggest that the characteristic range of orbital migration experienced by giant planets is limited.

3.1 Introduction

Speculation regarding the potential existence of giant planets that orbit their host stars in a matter of days dates back more than seven decades, to the proposed spectroscopic survey of Struve 1952. In retrospect, the remarkable lack of attention devoted to this possibility (in the forty years that followed its publication, Struve's manuscript received six citations) can almost certainly be attributed to the stark contrast between the imagined nature of such objects and the expansive orbital architecture of our solar system. Accordingly, the 1995 discovery of the first hot Jupiter, 51 Pegasi b (Mayor and Queloz 1995), proved to be an immediate challenge to the hitherto conventional theory of giant planet formation (Pollack et al. 1996), sparking considerable interest in reconciling the existence of Jupiter-like bodies on extremely close-in orbits with the theory of core-nucleated accretion. However, despite numerous efforts to conclusively resolve the problem of hot Jupiter formation, the origins of these remarkable objects remain imperfectly understood.

Generally speaking, the various formation pathways of Jovian-class planets at small orbital radii can be summarized into three broad categories: smooth migration, violent migration, and in-situ conglomeration. Within the framework of the first two scenarios, giant planet formation unfolds exclusively at large stello-centric distances (i.e. a few astronomical units) as originally imagined for the Solar System's giant planets (Bodenheimer and Pollack 1986). Subsequently, upon conclusion of the primary accretion phase, the planet's orbital radius undergoes large-scale decay, shrinking by a factor of $\sim 10^2$ (Lin, Bodenheimer, and Richardson 1996). In the smooth migration picture, this is accomplished by dissipative interactions between the planet and its natal disk (via the so-called type-II mode of gas-driven migration; Kley and Nelson 2012), while the violent picture entails a sequence of events wherein the planet first attains a nearly parabolic trajectory (as a consequence of planet-planet scattering or the Lidov-Kozai mechanism; Beaugé and Nesvorn 2012; Naoz et al. 2011b) and then gets tidally captured onto a close-in circular orbit.

The in-situ model of hot Jupiter conglomeration (Batygin, Bodenheimer, and Laughlin 2016a) is markedly different from the picture described above in that the extent of orbital migration is assumed to be limited, and the vast majority of the planetary mass is imagined to accrete onto the planet locally (i.e. at a radial separation of order ~ 0.1 au or smaller). Importantly, in this case, core-nucleated instability is envisioned to be triggered by massive super-Earth type planets[1], which are

[1]The fact that the process of core-nucleated accretion is relatively insensitive to the temperature

strictly disallowed within the context of the traditional Minimum Mass Solar Nebula (Weidenschilling 1977; Hayashi 1981) but are found in great abundance around Sun-like stars by photometric and spectroscopic surveys (Howard et al. 2010; Mayor et al. 2011; Batalha et al. 2013a; Dressing and Charbonneau 2013, 2015; Fressin et al. 2013; Petigura, Howard, and Marcy 2013; Mulders, Pascucci, and Apai 2015; Winn and Fabrycky 2015a). We note, however, that for the purpose of our study, we remain completely agnostic as to the origins of the high-metallicity cores themselves: whether they too form locally (Chiang and Laughlin 2013; Lee and Chiang 2016; Boley, Contreras, and Gladman 2016) or instead get delivered to short-period orbits by (type-I) planet-disk interactions (Fogg and Nelson 2007; Savvidou, Bitsch, and Lambrechts 2020) matters very little for the results that will follow.

In light of the relatively low occurrence rate of hot Jupiters ($\sim 1\%$ for Sun-like stars; Howard et al. 2010, Gould et al. 2006, Wright et al. 2012), it is not straightforward to determine which of the three aforementioned scenarios plays the dominant role in hot Jupiter generation. While observational signatures associated with each pathway have been widely discussed in the literature (see e.g. Winn and Fabrycky 2015a for a review), these predictions typically entail some level of degeneracy. To this end, Batygin, Bodenheimer, and Laughlin 2016a have shown that the in-situ model is characterized by a key observational consequence - namely that close-in Jovian planets should frequently be accompanied by (co-transiting as well as strongly inclined) super-Earth type companions. While circumstantial evidence has emerged for the existence of such companions (Becker et al. 2015; Huang, Wu, and Triaud 2016), Spalding and Batygin 2017 point out that the coexistence of hot Jupiters and low-mass planets is not strictly ruled out within the framework of the smooth migration paradigm, preventing a definitive distinction between the models. Furthermore, even spin-orbit misalignments, which were long touted as a marker of violent evolutionary histories (Fabrycky and Tremaine 2007b; Naoz et al. 2011b), have failed to conclusively inform the nature of hot Jupiter dynamical evolution, as numerous studies have shown that arbitrary stellar obliquities can naturally arise as a result of gravitational and magnetohydrodynamic disk-star interactions (Lai 1999; Bate, Lodato, and Pringle 2010a; Spalding and Batygin 2014a, 2015a).

With an eye towards resolving the ambiguity among the three categories of hot Jupiter formation models, here we examine the relationship between the masses of

and pressure of the nebula, and can therefore proceed anywhere in the disk, was first demonstrated by the analytic calculations of Stevenson 1982a. More realistic numerical simulations of hot Jupiter conglomeration at $r \sim 0.05$ au are presented in Batygin, Bodenheimer, and Laughlin 2016a.

close-in giant planets and the distribution of their orbital periods. In particular, we argue that the observations signal a strong consistency with the in-situ formation scenario, suggesting that the extent of orbital migration suffered by this population of planets is unlikely to be particularly large. The remainder of the paper is structured as follows. In Section 3.2, we show that the inner boundary of the period-mass distribution of locally forming hot Jupiters is expected to follow a well-defined power law, and demonstrate empirical agreement between this relation and the observations. From there, we proceed to discuss tidal evolution. We present our conclusions in Section 3.3.

3.2 Period-mass relation

The planetary mass as a function of the semimajor axis of the current observational census of extrasolar planets shown in Figure (3.1). Objects with confirmed (minimum) masses discovered via the radial velocity technique and transit observations are shown with blue and red points respectively. Transiting planets without direct mass measurements are shown as grey dots, and their masses are estimated using the mass-radius relationship of Chen and Kipping 2016.

The inner boundary

The inner edge of the $a - M$ diagram shown in Figure (3.1) has a rather well-defined profile, exhibiting a clear dependence on the planetary mass. Specifically, for planets less massive than $\sim 0.1 M_J$, the boundary has positive slope, while the converse is true for more massive planets (Mazeh, Holczer, and Faigler 2016). Given the four orders of magnitude spanned by the range of Figure (3.1), it is entirely plausible that the two dividing lines are carved by unrelated physical processes.

The distribution of sub-Jovian ($M < 0.1 M_J$) planets is almost certainly sculpted by photoevaporation (Owen and Wu 2013; Lopez and Fortney 2014). Recasting the period-mass diagram into an irradiation-radius diagram, Lundkvist et al. 2016 have argued that the region of parameter space that exhibits a strong paucity of planets (the so-called sub-Jovian desert) is fully consistent with the effects of atmospheric mass loss. Moreover, the recent determination that the radius distribution of sub-Jovian planets is strikingly bimodal (as predicted by the photo-evaporation models; Fulton et al. 2017b) adds further credence to the notion that the origin of the positively sloped boundary in Figure (3.1) is rooted in radiative stripping of planetary envelopes.

Intriguingly, the same process cannot be invoked to explain the orbital architecture

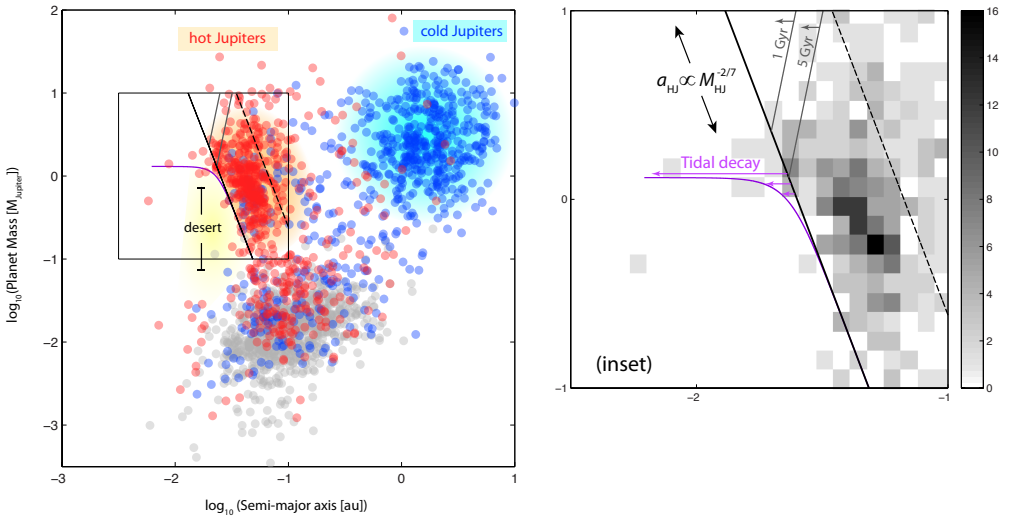

Figure 3.1: The $a \propto M^{-2/7}$ relation derived for in-situ hot Jupiter formation shows empirical agreement with the lower boundary of the observed giant planet population in the $a - M$ diagram. **Left panel:** The cold Jupiter (blue shading) and hot Jupiter (red shading) populations are shown in relation to the giant planet "desert" (yellow shading). *Blue points:* planets detected via the radial velocity technique, for which $M \sin i$ is plotted in lieu of M. *Red points:* transiting planets with directly determined masses. Transiting planets with masses inferred from a mass-radius relation are shown as grey points. **Right panel (inset):** A density histogram in the $\log a - \log M$ plane. The boundary of the hot Jupiter population is empirically well-described by a line with slope in agreement with the magnetically governed power law relation derived in the text. Adjusting the assumed T-Tauri parameters within the observed range yields lines traversing the hot Jupiter population, with a line corresponding to $R_\star \sim 2R$ bounding the approximate upper edge of the most populated region (dashed line). Divergence from this empirical best fit line at short orbital radii agree with the tidal decay curve (purple) showing the evolution from the best fit line expected after 5 Gyr of evolution. The grey lines illustrate the tidal decay isochrons described in the text.

of hot Jupiters as a population. Models of atmospheric mass loss from highly irradiated giant planets (Murray-Clay, Chiang, and Murray 2009; Adams 2011) suggest that over the main-sequence lifetimes of their host stars, typical hot Jupiters will only lose $\sim 1\%$ of their total mass, altering the period-mass distribution to a negligible degree. As a consequence, a separate mechanism is needed to establish the negatively sloped boundary in Figure (3.1). Let us now examine the possibility that the observed distribution is nothing other than a relic of giant planet conglomeration at short orbital periods.

in-situ formation of hot Juipiters

By now, it is generally accepted that the vast majority of hot Jupiters have formed via the core accretion pathway (Miller and Fortney 2011). Nevertheless, there is considerable uncertainty regarding the specific value of the critical core mass required to trigger runaway gas accretion at orbital radii smaller than ~ 0.1 au. In particular, 1D calculations of Ikoma, Emori, and Nakazawa 2001; Lee and Chiang 2015, 2016 yield $2-3$ and $2-8$ Earth masses respectively, while simulations of Bodenheimer, Hubickyj, and Lissauer 2000b; Batygin, Bodenheimer, and Laughlin 2016a suggest a value closer to $15M$. Adding further uncertainty to this estimate, 3D hydrodynamic models of Lambrechts and Lega 2017 draw attention to the importance of global circulation within the Hill sphere for the determination of the energetics of this problem.

The results of our study are largely insensitive to the specific characteristics of the high-metallicity core, as here we focus on the runaway accretion phase itself, during which the planet acquires most of its mass. Correspondingly, as a first step, it is worthwhile to consider the material budget of the inner disk. The amount of gas contained within $\xi = 0.1$ au of a Mestel 1961-type protoplanetary nebula with surface density profile $\Sigma = \Sigma_0(r_0/r)$ and $\Sigma_0 = 2000$ g cm^{-2} at $r_0 = 1$ au is

$$\oint \int_{r_{\rm in}}^{\xi} \Sigma r dr d\phi < 2\pi\Sigma_0 r_0 \xi \ll M_J, \tag{3.1}$$

where $r_{\rm in}$ denotes the inner edge of the disk.

This simple estimate alone is sufficient to conclude that upon entering the runaway accretion regime, a locally forming hot Jupiter does not attain its final mass on a comparatively short (e.g. $\sim 10^4$ year) timescale. Instead, the gas must be delivered to the growing proto-planet by viscous accretion. Therefore, it is sensible to crudely

express the hot Jupiter mass as

$$M_{\rm HJ} \sim \tau \dot{M} \tag{3.2}$$

where $\dot{M}$ is the gas accretion rate at the inner edge of the disk, and τ is some characteristic accretion timescale (generally, some fraction of the disk lifetime) governed by the efficiency by which material is accreted onto the hot Jupiter.

Within the framework of the in-situ model of hot Jupiter conglomeration, the smallest orbital radius where gas accretion can unfold is, roughly, the magnetospheric truncation radius of the disk. Importantly, like $M_{\rm HJ}$, the truncation radius is also determined by $\dot{M}$. The expression for this length scale is well-known and is written as (Ghosh and Lamb 1979; Koenigl 1991a; Shu et al. 1994)

$$R_t \sim \left(\frac{\mathcal{M}^2}{\dot{M}\sqrt{GM_\star}} \right)^{2/7} \tag{3.3}$$

where $\mathcal{M}$ is the stellar magnetic moment, $GM_\star$ is the star's standard gravitational parameter, and $\dot{M}$ is the disk accretion rate. Physically, R_t is a characteristic radius at which viscous spreading of disk material is balanced by stellar magnetospheric torque acting upon the gas.

Combining equations (3.2) and (3.3), we obtain the relation[2]

$$a \sim \left(\frac{\mathcal{M}^2 \tau}{M_{\rm HJ}\sqrt{GM_\star}} \right)^{2/7} \propto M_{\rm HJ}^{-2/7}. \tag{3.4}$$

In $\log(a) - \log(M)$ space, this power law relation manifests as a line with slope $-2/7$. Correspondingly, Figure (3.1) shows a line corresponding to the example T-Tauri parameters $M_\star \sim 1M$, and $\mathcal{M} \equiv B_\star R_\star^3$ ($B_\star \sim 1$ kG, $R_\star \sim 1.2R$), in excellent agreement with the lower boundary of the hot Jupiter population. This line corresponds, specifically, to the lower bound on the hot Jupiter cluster in the period-mass plane. Intriguingly, keeping the other parameters constant while setting $R_\star \sim 2R$, toward the somewhat higher end of observed T-Tauri radii Bouvier et al. 2007, yields an additional line which, together with the aforementioned lower bound, envelops the approximate region of the parameter space most densely populated with observed hot Jupiters.

[2]Serendipitously, Wisdom 1980, describing the onset of resonance overlap in the planar circular restricted three-body problem, *also* derives a $-2/7$ power law $s_{\rm overlap} \simeq \mu^{-2/7}$, where $s \simeq \sqrt{2/(3\Delta a)}$ and Δa is the approximate separation of resonances. However, the underlying physics in these two cases is unrelated.

In what now appears, potentially, to be a developing picture of in-situ hot Jupiter formation, the specific timing of planet accretion is a topic that will require extensive future study. Observationally derived estimates for $\dot{M}$ among T-Tauri stars of age $\sim$ 1 Myr have a median of $10^{-8} M_{\rm yr}^{-1}$ and intrinsic scatter an order of magnitude in each direction (Hartmann et al. 1998). If these values are well-representative of the conditions in which hot Jupiters form, then the median value of τ in relation (3.2) is roughly 10^5 yr. Due to the unknown accretion efficiency, the uncertain timing with which suitable cores appear, and the finding (Hartmann et al. 1998) that accretion declines with time, the characteristic accretion timescale will be left as a topic of future consideration. For now, these factors are absorbed into the constant tau.

Tidal evolution

At greater masses and shorter periods, the observations appear to diverge from the $a \propto M^{-2/7}$ trend. As a resolution to this apparent disparity, let us consider the role of tidal evolution in shaping the hot Jupiter population. In particular, we follow the formalism outlined in Murray and Dermott 1999a for the standard case of a planet moving on a circular, equatorial orbit with mean motion n, around a star rotating with angular speed Ω. For the case $\Omega < n$, the tidal bulge induced on the star by the planet lags behind the planet's orbit, leading to orbital energy loss and consequent decay of the semimajor axis.

The contraction of hot Jupiter semimajor axes is predicted by the well-established formula (Murray and Dermott 1999a):

$$\frac{da}{dt} = -\frac{3k_{2\star}}{Q_\star}\frac{M_{\rm HJ}}{M_\star}\left(\frac{C_\star}{a}\right)^5 an. \tag{3.5}$$

where $k_{2\star}$ is the tidal Love number of the star (equal to 0.01 for an $n = 3$ polytrope (Batygin and Adams 2013a), appropriate for a fully radiative body, and $Q_\star$ is the stellar quality factor, typically estimated to be roughly $\sim 10^5$ to 10^6 (Jackson, Greenberg, and Barnes 2008; Levrard, Winisdoerffer, and Chabrier 2009; Laughlin et al. 2009). The stellar mass is represented as $M_\star$, and the stellar radius is denoted as $C_\star$. Rearrangement of this equation and integration with respect to a and t yields an equation for the final semimajor axis a_f in terms of initial semimajor axis a_i and total evolution time t:

$$a_f = \left(a_i^{13/2} - t\frac{13}{2}\frac{3k_{2\star}}{Q_\star}\frac{M_{\rm HJ}}{M_\star}C_\star^5\sqrt{GM_\star}\right)^{2/13}. \tag{3.6}$$

Imagining orbital decay to unfold over a typical system lifetime of $\sim$ 5 Gyr, originating from initial values of (a, M) defined by the best-fit line found at the boundary of the hot Jupiter population, we obtain a tidally corrected inner boundary, which is shown in Figure (3.1) as a purple curve. Remarkably, tidal evolution appears to fully explain the bulk of trend-crossing hot Jupiters. The expected number of these tidally decaying planets is sensitively dependent on initial conditions. The Transiting Exoplanet Survey Satellite (TESS) mission is expected to further elucidate the initial conditions of the hot Jupiter swarm.

Finally, we consider the role of tides in shaping the hot Jupiter population at even greater masses. Specifically, by rearranging (3.6), we obtain, for a given time span, an expression for the initial radius from which a planet of given mass decays to the Roche limit. Examples of the resulting curves, for 1 and 5 Gyr, are shown in grey (Figure 3.1). Notably, these tidal decay isochrons agree with the approximate boundary of the hot Jupiter population for $M \gtrsim M_J$.

3.3 Conclusion

At the dawn of exoplanetary observations, the conceptual foundation of planet formation was built upon the lone case of the Solar System. Given the paltry mass of the terrestrial planets and the lack of material orbiting interior to Mercury, it was thought that planet formation was generally inactive at short orbital radii (Cameron 1988; Rafikov 2006). To alleviate the ostensible paradox brought about by the discovery of hot Jupiters, migration mechanisms were invoked to explain how giant planets could be delivered inward from distant, Jupiter-type orbits (Lin, Bodenheimer, and Richardson 1996).

Today, the landscape of exoplanet detections foretells a very different story (Laughlin and Lissauer 2015). It is observationally well-established that a generic outcome of the planet formation process is short-period super-Earths, the most massive of which can successfully trigger rapid gas accretion and become gas giants, if allowed to reside within their natal nebulae for $\sim$ 1 Myr (Bodenheimer, Hubickyj, and Lissauer 2000b; Batygin, Bodenheimer, and Laughlin 2016a). In fact, given the remarkable scarcity of close-in gas giants relative to sub-Jovian short-period planets, all that is needed to reproduce the vast majority of the hot Jupiter population in situ, is for $\sim$ 1% of young super-Earths to enter the runaway regime of conglomeration before dissipation of their protoplanetary nebulae.

In this work, we have explored the in-situ formation scenario of hot Jupiters further,

and demonstrated that a bounding relation $a \propto M_{\rm HJ}^{-2/7}$ is expected to manifest if a significant fraction of these objects formed locally. Intriguingly, we find that the slope of this power law is in excellent empirical agreement with the lower edge of the hot Jupiter population on the $a - M$ diagram, with corrections from tidal dissipation playing a secondary role (Figure 3.1). Accordingly, this finding yields further support to the hypothesis that in-situ formation accounts for a considerable fraction of hot Jupiters.

We note that, in addition to typical short-period Jovian planets that reside on nearly-circular orbits, there exist numerous instances of highly eccentric hot Jupiters with exterior companions, for which the most simple explanation is that they are undergoing the final circularization phase of violent (possibly Lidov-Kozai) migration (Wu and Murray 2003b; Fabrycky and Tremaine 2007b). While these objects certainly do not fit into the picture presented herein, Dawson, Murray-Clay, and Johnson 2014b have demonstrated that only a minority of hot Jupiters could have formed via this high-eccentricity pathway, weakening the case for this flavor of orbital transport as a dominant route for hot Jupiter production (see also Ngo et al. 2016). Moreover, unlike the upper boundary of the hot super-Earths in the $a - M$ diagram (which is adequately explained as resulting from photoevaporation; Owen and Wu 2013, Lopez and Fortney 2014), the mass-period relationship governing the sharp lower boundary of the hot Jupiters has so far evaded migratory explanations (Owen and Lai 2018).

Despite the aforementioned correspondence between the in-situ $a - M$ relation (3.4) and the data, it is clear that treating migration as utterly non-existent in planet formation theory is as extreme as demanding that migration must necessarily be long-range. To the contrary, there is no doubt that, at least to some extent, giant planet migration plays a role in shaping planetary systems. For example, mean motion resonances found in systems such as GJ 876 (Marcy et al. 2001) are almost certainly a product of convergent migration (Lee and Peale 2002). Moreover, our own solar system holds distinct markers of past giant planet migration, not least of all being the notion that the terrestrial planets are best reproduced in models that include successive inward and out-ward migration of Jupiter over several au (the so-called "Grand Tack;" Walsh et al. 2011, see also Batygin and Laughlin 2015). Importantly, however, systems that show evidence of migratory sculpting typically require only short-range orbital transport. Thus, our results cumulatively suggest that long-range migration of giant planets is likely to be the exception rather than

the rule.

Acknowledgments. We wish to thank Dan Fabrycky, Greg Laughlin, and Eugene Chiang for useful conversations, and the anonymous reviewer for useful comments. This research has utilized the NASA Exoplanet Archive, which is operated by the California Institute of Technology, under contract with the National Aeronautics and Space Administration under the Exoplanet Exploration Program.

Chapter 4

THERMODYNAMICALLY GOVERNED INTERIOR MODELS OF URANUS AND NEPTUNE

ABSTRACT

Interior models of Uranus and Neptune often assume discrete layers. However, sharply defined interfaces are expected only if major constituents are immiscible. Diffuse interfaces could arise if accretion favored a central concentration of the least volatile constituents (also incidentally the most dense); compositional gradients arising in such a structure would likely inhibit convection. Currently, two lines of evidence suggest possible hydrogen-water immiscibility in ice giant interiors. The first arises from crude extrapolation of the experimental H_2-H_2O critical curve to $\sim$ 3 GPa (Bali, Audétat, and Keppler 2013). The data are obtained for an impure system containing silicates, though Uranus and Neptune could also be "dirty." If this laboratory result pertains to the H_2-H_2O binary system, it disagrees with current *ab initio* models (Soubiran and Militzer 2015), though hydrogen and water are difficult to model from first-principles quantum mechanics with the necessary precision. The second argument for H_2-H_2O immiscibility in ice giants, outlined herein, invokes reasoning about the observed gravitational and magnetic fields. While a consensus remains lacking, in this work we examine the immiscible case. The interior composition is then governed by the H_2-H_2O coexistence curve. Applying this constraint, we find that to satisfy observations, Neptune models must contain an envelope water mole fraction $\chi'_{\rm env} \gtrsim 0.1$ relative to hydrogen. In contrast, Uranus models require $\chi'_{\rm env} \lesssim 0.01$. As cooling progresses, the layers approach a fully demixed state. We find enough total gravitational potential energy would be available from this process to supply Neptune's present-day heaflow for roughly ten solar system lifetimes. Hydrogen-water demixing could slow Neptune's cooling rate by an order of magnitude; different demixing states could account for the different heatflows.

4.1 Introduction

Currently, Uranus and Neptune are the only planets in the solar system that still await visitation by an orbiter mission. Due to this relative lack of spacecraft coverage, as well as challenges to ground-based work resulting from their greater distance, knowledge about the so-called ice giants[1] is limited compared to the other solar system planets. But despite the general dearth of detailed information for Uranus and Neptune, the *Voyager 2* flyby, as well as ongoing ground-based observations, have revealed a clear paradox for these two planets, to be addressed in this work. Specifically, while Uranus and Neptune possess qualitatively similar magnetic fields–suggesting similar interior convective geometries distinct from all other dynamo-generating solar system bodies–these two planets simultaneously exhibit distinctly different intrinsic heat fluxes. A cohesive narrative has not yet been agreed upon to explain these similarities and differences between Uranus and Neptune.

The intrinsic heat fluxes of Uranus and Neptune have been determined by ground-based observations (e.g. Fazio et al. 1976; Loewenstein et al. 1977; Loewenstein, Harper, and Moseley 1977), in conjunction with measurements from the infrared interferometer spectrometer (IRIS) on Voyager 2 (Hanel et al. 1986; Conrath et al. 1989; Pearl and Conrath 1991). These works have shown that, while Neptune's intrinsic heat flux might be consistent with standard adiabatic cooling models (Hubbard, Podolak, and Stevenson 1995), measurements of Uranus' heat flux seem anomalously low compared to the other giant planets, with measurements suggesting heatflow an order of magnitude lower than Neptune's (and consistent with the heat flux actually being zero). Proposed reasons for Uranus' low heat flux have invoked either a low initial formation temperature, or some mechanism that inhibits convection in the interior and prevents heat from escaping efficiently (e.g. Podolak, Hubbard, and Stevenson 1991; Nettelmann et al. 2016; Leconte and Chabrier 2012; Podolak, Helled, and Schubert 2019). Overall, a commonly considered possibility has been that Uranus' interior experiences a mechanism to block heat from leaving, and that Neptune is not subject to, or is less affected by, this mechanism. In light of

[1] This monicker assumes the intermediate density of these planets is due to a significant proportion of volatile species (i.e. "ices") in their interiors. However, as discussed in this work, there is actually no direct evidence that ices comprise a major proportion of these planets' mass. Observations of ices in the atmospheres do not necessarily inform the composition of the deep interiors, and the intermediate densities required to produce the mean densities and measured gravitational fields of these planets could, in principle, be produced in a scenario of mixed rock and hydrogen and no more methane than what is needed to explain the atmospheres.

our comments about uncertain composition, it is worth remembering that any statements about the heat content of these planets is necessarily uncertain because of the large differences in thermodynamic parameters for the constituents, especially the very high specific heat for hydrogen relative to ice or rock. Still, the simultaneous similarity of the observed magnetic fields of Uranus and Neptune appears to present a paradox to this natural assumption.

These similar magnetic fields are qualitatively different from all other dynamo-generating solar system bodies. In both planets, the magnetic dipolar component is offset from the planet center (0.3 R_U, 0.55 R_N), mathematically equivalent to the large quadrupolar moment of these bodies, and considerably inclined to the spin pole (Uranus: 60°, Neptune: 47°). This is in contrast to the dipole-dominated fields generated by all other solar system dynamos (Ness et al. 1986; Ness et al. 1989; Connerney, Acuna, and Ness 1987, 1991). The unusual field geometry of Uranus and Neptune has been reproduced with models in which the dynamo source region is a convecting thin shell surrounding a stably stratified fluid interior (Stanley and Bloxham 2004, 2006), as well as turbulent thick- and thin-shell models (Soderlund et al. 2013). Thin-shell dynamo models in particular seem to agree with the potential explanation of Uranus' low heat flux as resulting from heat entrapment in the deep interior of Uranus, due to inhibited convection beneath the convecting shell. However, if Uranus' low heat flux is the result of deep inhibited convection, it is then necessary to explain why Neptune has a significantly greater intrinsic heat flux than Uranus, despite exhibiting a similar magnetic field.

One proposed means to generate the key differences between Uranus and Neptune, is giant impacts. The origins of the significant obliquities of these planets remains an open question–especially the 98° spin axis tilt of Uranus, although Neptune's 30° misalignment is also non-negligible–and a collisional origin of tilting has long been proposed (Safronov 1966). A major problem with a collisional origin of the tilt has been the need to explain the equatorial orientation of the orbits of the Uranian moons and rings; however, Morbidelli et al. 2012 have found that a multiple-collision scenario allows for sufficiently gradual tilting that the proto-satellite disk can re-align with the planet. As an alternative explanation (Boué and Laskar 2010), Uranus gradually tilted as the result of a resonance between its orbit and precession of its spin axis. Recently, Reinhardt et al. 2020 have suggested that an oblique giant impact to Uranus and a head-on collision to Neptune could account for the planets' obliquities and the differences between their satellite systems. Furthermore, they

suggest that a head-on impact to Neptune could account for Neptune's less centrally condensed state relative to Uranus (inferred from rotation and gravity data), as well as the differences in heat flow between the planets. While the giant impact hypothesis represents an intriguing possible explanation for the differences in heat flow between the two planets, it is also worth considering other possible reasons for the origin of the disparity in heat flow between Uranus and Neptune.

Highlighting the importance of understanding the solar system's ice giants, it has often been suggested that Uranus and Neptune are possibly our best local analogues to the numerous observed exoplanets having masses and radii intermediate between those of terrestrial planets and gas giants. In fact, planets in an intermediate mass and radius range between gas giant planets and terrestrial planets are now understood to be an extremely common product of planet formation, at least at closer stellocentric distances (Batalha et al. 2013b). Although low detection sensitivity at host star separations beyond $\sim$ 10 au has ensured that no perfect exoplanetary analogues to the solar system's ice giants have yet been found, the presence of a significant proportion of both light and heavy constituents in Uranus and Neptune makes them our most readily accessible laboratories for investigating the interactions of planetary constituents within all intermediate-mass planets.

Moreover, it is often suggested that the intermediate sizes of Uranus and Neptune are due to their status as "cores" that failed to attain runaway accretion before the solar nebula dissipated, in the core accretion model for giant planet formation. However, despite the central role of Uranus and Neptune in understanding rates of planet formation in our own solar system, uncertainty about the composition and structure of their interiors remains a major obstacle to understanding the provenance and formation conditions of these planets– and accordingly, their position within the greater narrative of planet formation in our solar system. Compared to gas giants and small bodies composed entirely of ice and rock, intermediate-density planets such as Uranus and Neptune suffer from a degeneracy in composition (e.g. Podolak, Hubbard, and Stevenson 1991). From observations of the gravity fields of Uranus and Neptune, it is established that the heavier elements must be concentrated toward the center, and surrounded by an envelope dominated by hydrogen and helium. However, in lieu of additional constraints, there is not a unique compositional profile which satisfies the measured properties of these planets.

Over the span of decades, numerous models have been constructed that satisfy the mass and observed gravity harmonics (up to J_4) of Uranus and Neptune. A

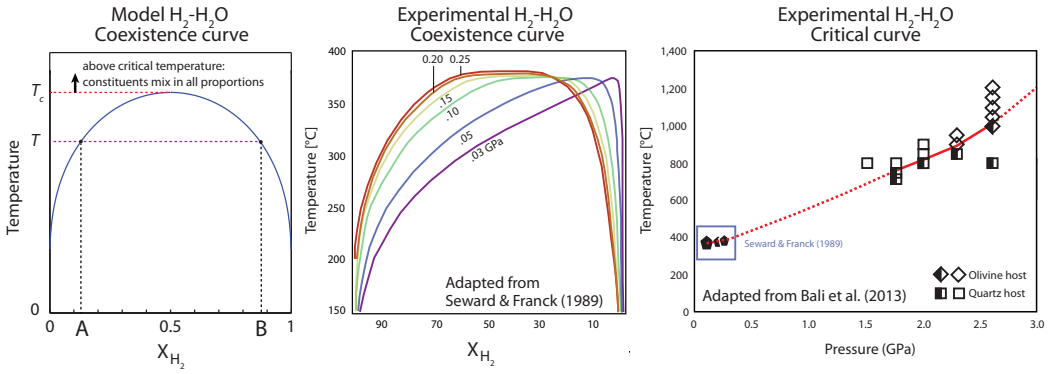

Figure 4.1: Experimental data for the H_2-H_2O system, and a diagram showing a model coexistence curve and its relationship to the critical temperature T_c. For the purposes of this work, the "critical curve" refers to the critical temperature as a function of pressure. *Left:* The peak of the coexistence curve occurs at the critical temperature T_c, above which the two species mix freely in any proportion. Below the critical temperature, the coexistence curve dictates the saturation compositions for coexisting phases. *Center:* The coexistence curves and critical temperature have been determined up to 0.25 GPa by Seward and Franck 1981, showing a trend toward increasing symmetry with pressure. *Right:* The critical curve has been experimentally derived up to $\sim$ 3 GPa by Bali, Audétat, and Keppler 2013, showing a roughly linear trend. The pentagonal markers show the critical temperature found by Seward and Franck 1981, while the square/diamond markers show the data found by Bali, Audétat, and Keppler 2013; black and white points indicate H_2-H_2O immiscibility.

traditional approach is to include several discrete, layers of uniform composition, with each layer typically composed primarily of "gas," "ices," and "rock." These three terms refer to composition rather than the phase in which these materials occur: "gas" refers to a solar-composition mixture, "ice" refers to volatile hydrides such as H_2O, NH_3, and CH_4, while "rock" generally refers to a combination of silicates and iron. In published works that invoke layers, their choice is not generally motivated by a specific physical rationale. Moreover, models which satisfy the inferred transition, from the hydrogen-dominated envelope to the denser mantle, using a substantial density gradient rather than discrete layers cannot satisfy the constraint that the dynamo magnetic fields require a well-mixed layer of sufficiently large radial extent. However, discrete interior layers (as opposed to a compositional gradient) are only expected to be stable when immiscible phases are present. In the case of terrestrial planets, formation of an iron core with a discrete core-mantle boundary occurs due to the immiscibility of iron in silicates at the relevant pressures and temperatures.

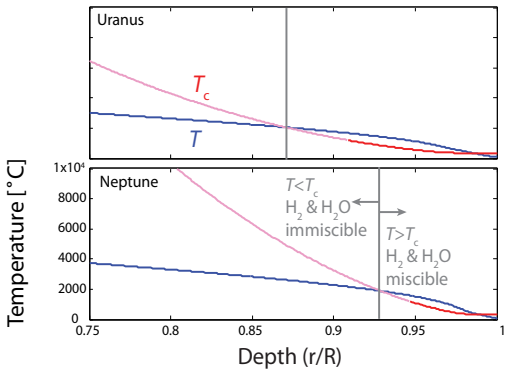

Figure 4.2: Comparison of the experimental critical temperature (red) derived by Bali, Audétat, and Keppler 2013 (Figure 4.1), and its approximate extrapolation (pink) linear in pressure to beyond the 3 GPa experimental limit, versus the adiabatic temperature profile (blue) in the outermost, hydrogen-dominant shell in models of Uranus and Neptune. A deep region of hydrogen-water immiscibility ($T < T_c$) is predicted in the deeper regions of this layer, indicating a plausible phase transition in the interiors of these planets, although further laboratory data is warranted. While these temperature profiles refer to the same best-fit Uranus and Neptune models discussed later in the text (see Figure 4.9), from this rough extrapolation, a deep interior region of immiscibility is suggested for all compositions of the H_2-dominant shell considered in this work.

In contrast, in the deep interiors of Jovian planets, it is expected (Wilson and Militzer 2012b, 2012a) that dissolution of ice and rock in metallic hydrogen is thermodynamically favorable; therefore, if a core is present today, it is widely expected to be in the process of dissolving (Wahl et al. 2017; Debras and Chabrier 2019). These are just a few examples of miscibility and immiscibility in planetary interiors. Another well-known example–helium immiscibility in giant planets–will be discussed in a later section. This work addresses the effects of inferred possible hydrogen-water immiscibility in the interiors of Uranus and Neptune.

In Uranus and Neptune, water is generally assumed to be the primary major constituent by mass. To satisfy the gravity harmonics, an underlying mantle with a density comparable to water, extending to $\sim$ 70 percent of the total planet radius, must be overlain by a hydrogen-rich envelope. Therefore, in this work, hydrogen and water are explored as possible dominant constituents whose mixing properties might dictate the state of ice giant interiors. As discussed herein, constraints on H_2-H_2O miscibility remain to be fully characterized. However, some advances have been made in understanding the hydrogen-water system at conditions relevant to the

interiors of ice giants, hence motivating this work. Figure 4.1 illustrates the existing experimental constraints for hydrogen-water mixing. In particular, two related thermodynamic curves that describe the mixing properties of hydrogen and water are the coexistence curve and critical curve. Figure 4.1 also shows a model coexistence curve for purposes of illustration.

Colloquially, it is often said that two immiscible species do not mix. However, immiscible species do mix to a limited extent–not freely, but in proportions specified by the coexistence curve, a curve which defines the compositions (typically in terms of mole fraction) at which minima of the Gibbs free energy of mixing occur, for given pressure and temperature. Experimental and theoretical examples of the coexistence curve are shown in Figure 1. The pressure-dependent critical temperature T_c is the maximum of the coexistence curve. At pressures and temperatures below the critical point of pure water (but above the critical point of pure hydrogen), hydrogen and water separate into two phases: a condensed phase of mostly water, and a gas containing a partial pressure of water in agreement with the vapor pressure of water. The H_2-H_2O coexistence curve has been determined to 0.25 GPa by Seward and Franck 1981. While their experimental work does not probe the deep interior conditions of the planet, for the purposes of this work, we employ a model coexistence curve, which will be discussed shortly in further detail.

While the H_2-H_2O coexistence curve has long been known at pressures relevant to giant planet atmospheres, more recently, Bali, Audétat, and Keppler 2013 have experimentally derived T_c for the H_2-H_2O binary system up to $\sim$ 3 GPa, a pressure range relevant to the deep interiors of Uranus and Neptune. Rough linear extrapolation of their result (Figure 4.2) appears to suggest that the temperature deep in the ice giants may be below the H_2-H_2O critical temperature at those pressures, appearing to suggest possible immiscibility of hydrogen and water, and hence separated phases. However, a few major caveats arise when making this rough linear extrapolation of the critical curve to higher pressures. First, while these experimental data suggest a roughly linear trend of the critical curve within the experimental range, there is no reason to expect the critical curve to continue linearly in pressure. In fact, to the contrary, as hydrogen approaches a more metallic state, the critical curve is expected to turn over (although the pressure at which this turnover begins, as well as its specific shape, are not known in detail). Indeed, Wilson and Militzer 2011 report solubility of water in hydrogen once 10-megabar pressures are reached. Moreover, Soubiran and Militzer 2015 reported results of *ab initio* simulations which appear

to possibly contradict H_2-H_2O immiscibility in the deep interiors of Uranus and Neptune. More specifically, they did not find evidence of concavity of the Gibbs free energy of mixing ΔG as a function of composition–in apparent contradiction to the experimental findings of Bali, Audétat, and Keppler 2013. In response to this discrepancy, Soubiran and Militzer 2015 argue that the experimental result may be due to contamination by the carrier silicates used in the experiment. On the other hand, an experiment contaminated by silicates may actually be more representative of the interiors of Uranus and Neptune than one that is not, as these planets likely include silicates as well. Clearly, more work is necessary to resolve the question of hydrogen-water miscibility in Uranus and Neptune. For the purposes of this work, we do not intend to make assertions about this question; however, we do explore the implications that hydrogen-water immiscibility would have for the interior states of these planets.

The discussion now turns from the critical curve to the specifics of the coexistence curve for hydrogen and water. While Bali, Audétat, and Keppler 2013 have experimentally determined the critical temperature as a function of pressure to 3 GPa, this finding does not inform the proportions at which hydrogen and water would be expected to mix. As mentioned previously, the specific compositions of coexisting (saturated) equilibrium phases are governed by the pressure-dependent coexistence curve, as was found by Seward and Franck 1981 at pressures relevant to the atmospheres of these planets. As is evident in Figure 4.1, at the lower pressures investigated in that work, the coexisting phases are asymmetric, trending toward symmetric with increasing pressure. The low-pressure asymmetry can be attributed to the significant repulsion experienced by a (nonpolar) H_2 molecule when inserted into water, whereas the analogous effect in the H_2-dominant phase is lacking due to the greater (i.e. gas-like) intermolecular spacing of H_2 at low pressures. With increasing pressure, the hydrogen-rich phase becomes more closely packed, and the coexistence curve becomes increasingly symmetric, as shown by the experimental curves of Seward and Franck 1981. This behavior of the symmetry of binary phase diagrams at high pressure is common, and can be described in terms of the following simple model for a two-component regular solution:

$$\Delta G = \chi(1-\chi)\Delta E + kT(\chi \ln \chi + (1-\chi)\ln(1-\chi)) \tag{4.1}$$

where ΔG is the Gibbs energy of mixing, ΔE is an interaction parameter, χ is the mole fraction of one of the components, k is Boltzmann's constant, and T is the

temperature. As the system will move toward the state with the lowest available Gibbs energy, the equilibrium composition(s) is/are associated with minima in ΔG. The critical temperature T_c, above which the two components mix in all proportions, is determined by the temperature above which $d^2\Delta G/dx^2$ is never negative. Below the critical temperature[2], there are two solutions symmetric about $\chi = 1/2$. At and above the critical temperature, they collapse to one solution $\chi = 1/2$, and phase separation does not occur for the case $T \geq T_c$. Taking this into account, for the binary system, it is possible to define the coexistence temperature $T_{\rm co}(P)$ as the temperature for a given pressure at which a phase containing a water mole fraction $\chi < 0.5$ of water coexists with a phase a water mole fraction $(1 - \chi)$:

$$\frac{T_{\rm co}(P)}{T_c(P)} = \frac{2(1-2\chi)}{\ln\left(\frac{1-\chi}{\chi}\right)}. \tag{4.2}$$

However, because only extrapolatory inference of T_c exists above 3 GPa, the equilibrium compositions deep in these planets is not known, and numerous pairs of complementary (symmetric) compositions are therefore considered in this work. We cannot be sure that the phase diagram is symmetric at high pressure, since the two species are not similar in size or behavior, but a more nearly symmetric behavior is often observed in systems of two condensed (i.e., fluid density) phases exhibiting immiscibility (Bernabe, Romero-Martinez, and Trejo 1988). Asymmetry can be due either to difference in size between the two species or to different spacings, as in the case of a liquid and a vapor (Damay and Leclercq 1991). The experimental curves of Seward and Franck 1981 show symmetry increasing with pressure, due to decreased difference in spacing between hydrogen versus water. However, the difference in molecular size between water and hydrogen suggests that a degree of asymmetry of the coexistence curve may be indicated at higher temperatures. We therefore allow coexisting equilibrium phase compositions to deviate from symmetric values by a factor of up to two.

Taking the symmetric rationale into account, we construct models of Uranus and Neptune, applying the constraint that models must be compatible with the coexisting equilibrium compositions implied by hydrogen-water coexistence diagram. In addition, the models must not be at odds with the observed magnetic fields of Uranus and Neptune; this rules out substantial compositional gradients in at least the outer $\sim$ 20% of the planets, as such gradients would preclude the large-scale

[2]Remember that T_c depends on pressure.

vertical motions necessary for a dynamo. Below the water cloud decks in Uranus and Neptune at tens or hundreds of bars, the thermodynamically permissible phases are thus either a water-rich ocean extending deep into the planet, or a hydrogen-dominant phase. Measurements of the gravitational moments, however, are at odds with the former, as they would imply too great a value of J_2. Therefore, we assume a hydrogen-dominant phase is present immediately below the water cloud decks of these planets. A schematic illustration of the thermodynamic constraint applied to this model, with the model critical curve described above, is shown in Figure 4.3. Because they introduce unphysical layering, most published layered models either violate these requirements, or are in danger of doing so.

The remainder of the chapter is outlined as follows. In Section 4.2, the method for constructing interior models is outlined. The results of this modeling effort are presented in Section 4.3, while the implications are discussed in Section 4.4, followed by some concluding remarks in Section 4.5.

4.2 Methods

Multiple approaches have been used to produce static models of ice giant interiors. In the most traditional approach (Podolak 1976; Hubbard and Macfarlane 1980; Podolak, Young, and Reynolds 1985; Hubbard, Podolak, and Stevenson 1995; Podolak, Hubbard, and Stevenson 1991; Podolak, Weizman, and Marley 1995), the number and composition of interior layers are initially defined, and a density profile is then derived using equations of state of the chosen layer constituents. In an alternative set of approaches developed for these planets, density profiles are generated to satisfy the gravity harmonics without any a priori assumption of the composition or equations of state (Marley, Gómez, and Podolak 1995; Podolak, Podolak, and Marley 2000; Helled, Anderson, and Schubert 2010). Although the latter approach circumvents the need to adopt equations of state at thermodynamic conditions that are a major challenge to statically produce in the laboratory, the generated density profiles are not guaranteed to represent any physical mixture of plausible planetary constituents. Because in this work, we aim to constrain the space of possible layer compositions of Uranus and Neptune, we take the more traditional approach, by pre-defining the layers and their compositions.

The models presented in this work are constructed and analyzed in three steps. First, layer compositions are chosen with χ and $(1 - \chi)$ roughly symmetric about 0.5, in agreement with the rationale discussed in Section 4.1. Next, taking into

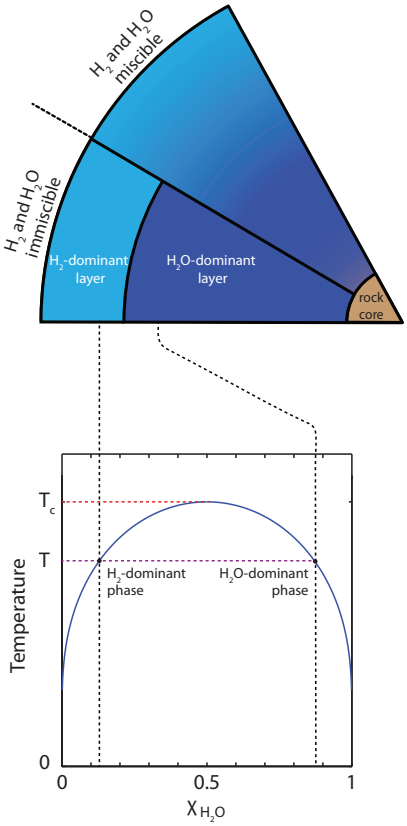

Figure 4.3: Schematic diagram showing the constraint imposed on the models in this work, that the compositions of the assumed H_2-dominant and H_2O-dominant layers should correspond to the coexisting phase compositions. A compositional discontinuity is thermodynamically favorable only if immiscibility of major constituents is implicated. The model critical curve shown is symmetric in accordance with Equation 4.1, although model critical curves deviating from symmetry by a factor of 2 were also considered, as discussed in the text.

account these chosen layer compositions, density profiles are derived that satisfy each planet's radius and mean density. Finally, we apply a theory-of-figures approach (concentric Maclaurin spheroids; Hubbard 2013) to derive the gravity harmonics for each density profile, comparing them to observational constraints on the gravity field. The relevant observational constraints for Uranus and Neptune are given in Table 4.1, and are discussed in further detail in the following sections.

Layer composition

We now discuss the range of layer compositions considered in our static models. Both two- and three-layer models were considered. In both cases, the outermost layer consisted primarily of hydrogen and helium, with the proportion of water varied,

and the proportion of atmospheric methane varied within observational bounds. The second layer consisted primarily of water, with ammonia and methane included in fixed amount relative to water, and the proportion of hydrogen included in this layer was varied. In the three-layer models, a separate core of silicates and iron was included. Two-layer models were constructed based on the three-layer models, by taking the proportion of rock in the cores of the three-layer models, assuming this rock is mixed with the overlying ices and hydrogen, and recalculating the model accordingly to find the effect on the gravitational harmonics.

In this work, following the thermodynamic rationale discussed in Section 4.1, complementary molar ratios of H_2O to H_2 were considered in the gas-rich and ice-rich layers. That is, for each model, the molar ratio $\chi'_{\text{env}} \equiv \chi_{H_2O}/(\chi_{H_2O} + \chi_{H_2})$ of H_2O to H_2 in the hydrogen-rich envelope was assumed to be equivalent to the molar ratio $\chi'_{\text{man}} \equiv \chi_{H_2}/(\chi_{H_2O} + \chi_{H_2})$ of H_2 to H_2O in the underlying water-rich mantle. Moreover, as discussed in the previous section, to account for the possibility of an asymmetric binodal curve, models were also constructed in which these two ratios varied from one another by a factor of 2. While the ratio of hydrogen and water in the adjacent layers is assumed to be thermodynamically governed, the fractions of other constituents, as well as small corrections to this assumption, are now discussed in detail.

In the gas-rich layer, in addition to water and hydrogen, additional constituents are expected to be present, most notably Helium, CH_4, and NH_3. A solar proportion of He relative to diatomic hydrogen was assumed. Ammonia abundances in the envelope were chosen according to the atmospheric values given in Lodders and Fegley 1994—however, especially as NH_3 is expected to be depleted by interaction with H_2S (de Pater, Romani, and Atreya 1991), these values might not represent ammonia abundances further down in the envelope. As discussed later in this work, due to its polar nature, ammonia may plausibly mix preferentially with water. It should be noted that, for the purposes of understanding the density profiles and gravity harmonics of these planets, ammonia and water are essentially interchangeable. For the purposes of this paper, we are motivated by the laboratory result of Bali, Audétat, and Keppler 2013 to focus on the possible effect of hydrogen-water demixing on ice giant structure and evolution, but the reader should keep in mind the uncertainty of the ammonia composition in the envelope and its potentially interchangeable role with water in the model framework put forth in this work.

Moreover, the observed atmospheric methane abundances of Uranus and Neptune,

relative to H_2 ($n/H_2 = 0.023 \pm 0.006$ and 0.029 ± 0.006 respectively; Fegley et al. 1991; Baines et al. 1993), also presented in Lodders and Fegley 1994, were assumed to extend deep into the envelope, and to disentangle the effect of methane on the result, models were constructed with methane abundances at the upper and lower reported error range. While this first-pass assumption may not accurately reflect reality, the main point of this work is to consider the role of water as a possible significant constituent in the envelopes of these planets. We acknowledge that the density contribution of water to the envelope assumed in this work could, in principle, be exchanged with that of ammonia and methane. Assumptions made for the atmosphere will be discussed in the next subsection. Below the assumed water cloud level, we assume for simplicity that the deeper water-rich region is well-mixed.

Moreover, in the ice-rich layer, the included constituents were H_2O, CH_4, NH_3, and varying amounts of H_2. The mole fraction of H_2 with respect to H_2O was defined as described above. Ammonia and methane were assumed to be present in solar proportion of N and C relative to the O of water, in accordance with Lodders 2010. The caveats of this assumption are discussed in Section 4.4. Finally, the rock core was taken to be comprised of the uniform mixture of SiO_2, MgO, FeS, and FeO assumed by Hubbard and Macfarlane 1980. The mantle and core were assumed to be chemically homogeneous.

Derivation of density profiles

Density profiles were derived beginning at the 1-bar pressure level (Lindal 1992; Lindal et al. 1987) and integrating to the center of the planet. Specifically, we start at the average 1-bar level $\bar{R}$ implied by the extrapolated equatorial and polar 1-bar radii from the Voyager 2 radio occultation data (Table 4.1).

We assume an adiabatic temperature gradient

$$T(z) = T_{\text{eff}}\left(\frac{P(z)}{P_e}\right)^{\Gamma}, \tag{4.3}$$

where z denotes depth, subscript e refers to values at the outer radius of the given region, and Γ is the Gruneisen parameter, ~ 0.3 for a solar hydrogen-helium mixture. This is only approximate.

The exception to this rule occurs in the atmosphere, where we account for the effect of water condensation on the temperature, in accordance with Kurosaki and Ikoma

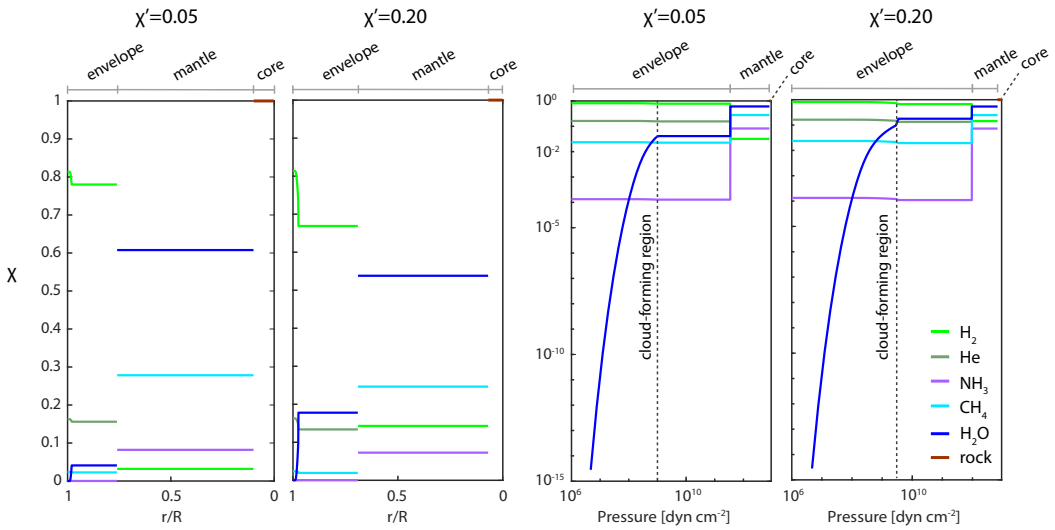

Figure 4.4: Example profiles of abundances of constituents, for $\chi'_{\rm env} = 0.05$ and 0.20, where $\chi'_{\rm env} \equiv \chi_{\rm H_2O}/(\chi_{\rm H_2O} + \chi_{\rm H_2})$ in the envelope. For these examples, a symmetric coexistence curve was assumed. Examples shown are for Neptune, but a similar scheme was used in Uranus. The left two plots show the mole fractions of constituents as a function of normalized planet radius, while the right two plots show mole fractions in the same models as a function of pressure. Water is taken to be present in the atmosphere at saturation vapor pressure until the cloud-forming region is reached. The cloud-forming region was assumed to occur either when the molar abundance reached the value chosen for the underlying homogeneously mixed region of the envelope (as in the $\chi' = 0.05$ case, or when the critical temperature of pure water was reached (as in the $\chi' = 0.20$ case), whichever came first. The abundances of homogeneously mixed regions were chosen according to the rationale described in the text.

2017, via Ingersoll 1969; Atreya 1986; Abe and Matsui 1988, by assuming a wet adiabatic temperature gradient:

$$\frac{d\ln T}{d\ln P} = \nabla_{\rm dry} \frac{1 + \frac{x}{1-x}\frac{d\ln p^*}{d\ln T}}{1 + \frac{R_g}{C_p}\frac{x}{1-x}\left(\frac{d\ln p^*}{d\ln T}\right)^2} \tag{4.4}$$

where the symbol $\nabla_{\rm dry}$ refers to the dry adiabatic gradient, while C_p is the mean heat capacity, x_i the mole fraction of water, and p_i^* the vapor pressure of water, which was calculated according to Nakajima, Hayashi, and Abe 1992. Water was assumed to be present at saturation vapor pressure until the chosen mole fraction of the lower region was reached (Figure 4.4). If the critical temperature of pure water (647 K) was reached before the chosen mole fraction of the lower well-mixed

region was attained, the 647 K temperature level was taken to be the cloud level, in accordance with Fegley and Prinn 1986. The density contribution of condensed water clouds was neglected, as was the density contribution of any other condensed species. Wet adiabaticity due to ammonia and methane was also ignored–this choice agrees with the finding of Guillot 1995 that a moist adiabat is not indicated by the deduced temperature gradient to $\sim$ 2 bar in Uranus and $\sim$ 4 bar in Neptune. While Guillot 1995 also notably finds that condensation of ammonia and methane inhibits convection around the $\sim$ 1 to 2 bar range, the temperature gradient evidently resumes a dry adiabat below these levels, and this and any analogous deeper effect of water condensation is ignored for the purposes of this work.

It should be noted that there is at present no consensus on the correct treatment of the temperature profile in a region where there is a compositional gradient arising from condensation alone. In the "wet adiabat" assumption described above, the latent heat effect can cause the temperature profile to be substantially *colder* than the dry adiabat. On the other hand, a sufficiently large compositional gradient (arising from the strong dependence of vapor pressure on temperature for a condensable such as water) may actually inhibit convection and cause the temperature gradient to be *hotter* (that is, superadiabatic) relative to a dry state (Leconte et al. 2017). Indeed, this effect is invoked in models for Jupiter's atmosphere based on microwave data (Li et al. 2020) and implies a hotter adiabat for Jupiter than the traditional one that ignores condensation.

Hydrostatic equilibrium is also assumed, taking into account the latitude-averaged centrifugal force (following Hubbard, Podolak, and Stevenson 1995):

$$\frac{dP}{dr} = -\Big[\frac{GM(r)}{r^2} - \frac{2\omega^2 r}{3}\Big]\rho(r), \tag{4.5}$$

where P denotes pressure, ρ denotes density, ω the angular velocity, and $M(r)$ the mass contained inside radius r. Given the pressure and temperature computed in this manner, and the temperature given by Equation (4.3) at each depth in the planet, the EOS for each constituent is used to determine the resultant density. In the outer few percent of the planet, the ideal gas equation of state (EOS) is assumed. Deeper in the planet we model the density contribution from each constituent with zero-temperature equations of state, with a thermal pressure correction taken into account in the envelope and mantle. The transition between the ideal gas to zero-temperature EOS is assumed several percent of the distance into the planet where the two equations of state cross.

Before describing our approach to the equations of state at great depth, we need first to make a philosophical point: It is not our goal to have the "best possible" descriptions of the constituent materials. We need only to have descriptions that are realistic enough to uncover the differences implied for the planets once our phase diagram assumptions are enforced. This approach is reasonable for Uranus and Neptune because of the large uncertainties in composition and because the inferred differences in the planets are large enough to affect the interpretation of their heat flows and atmospheres. It would be an unreasonable approach for Jupiter or even Saturn where there are very precisely known parameters and there is an obvious need to adopt very precise descriptions of hydrogen in particular.

For the zero-temperature equation of states of the assumed constituents, we use the polynomial approximations suggested by Hubbard, Podolak, and Stevenson 1995 and briefly summarized here. The equation of state for molecular hydrogen is taken to be the experimental result of Mao et al. 1988 up to pressures of $\sim 8 \times 10^{11}$ dynes cm^{-2}, above which we use the approximation for theoretically determined values of Zharkov, Tsarevsky, and Trubitsyn 1978. For helium, we use the approximation to the equation of state of Zharkov, Tsarevsky, and Trubitsyn 1978. For water, we use the polynomial approximation of the EOS determined by Ree 1976. Due to their smaller expected abundances, the accuracy for CH_4 and NH_3 is less crucial, and again, we use the polynomial approximations given by Hubbard, Podolak, and Stevenson 1995 for the shockwave CH_4 data determined by Nellis et al. 1981 as well as the approximation given by Hubbard, Podolak, and Stevenson 1995 for the zero-temperature CH_4 equation of state. Finally, to model the density of rock within the planets, we employ the EOS from Zharkov and Trubitsyn 1978 used by Hubbard and Macfarlane 1980 for the mixture of 38% SiO_2, 25% MgO, 25% FeS, and 12% FeO which we similarly take to approximately constitute "rock."

The approximations to the zero-temperature equations of state mentioned above all take on a form

$$P_0 = f(\rho), \tag{4.6}$$

where P_0 is the electron degeneracy pressure and f is a polynomial function. To account for the effect of thermal pressure in the planets, we apply a thermal correction to the zero-temperature equation of state, accounting for the thermal pressure P_t:

$$P_0 + P_t = f(\rho), \tag{4.7}$$

where, according to Debye theory, P_t is approximated to order of magnitude as

$$P_t = 3n\gamma kTD(\Theta/T) \tag{4.8}$$

where n is the number density of molecules, γ is the Gruneisen parameter, k is Boltzmann's constant, T is the temperature, D is the Debye function, and Θ is the Debye temperature.

Following Demarcus 1958; Peebles 1964, we use the linear mixing assumption for the EOS of a mixture of individual constituents:

$$\frac{1}{\rho(P,T)} = \sum_i \frac{m_i}{\rho_i(P,T)} \tag{4.9}$$

where i is iterated over all constituents present in the mixture, $\rho(P,T)$ denotes the density of the mixture at a given pressure and temperature, m_i and ρ_i are respectively the mass fraction and density of constituent i. Densities of ice mixtures derived using this standard assumption have been found to vary by $\sim 4\%$ from a real mixture of ices at conditions relevant to the interiors of ice giants (Bethkenhagen et al. 2017).

Construction of two-layer models

A range of water-hydrogen ratios for the envelope and hydrogen-water ratios for the mantle are tested. Three-layer models are constructed with a range of mantle-envelope transition levels. Specifically, for each set of chosen layer compositions, the range of mantle-envelope transition depths is found for which it is feasible to construct a model satisfying the planet radius and mean density. Every feasible mantle-envelope transition depth has an associated rock core extent which permits the model to satisfy these basic constraints.

Having constructed this suite of three-layer models, we then derive associated two-layer models with mixed rock-ice mantles, and lacking separate rock cores. The mantles in these models retain the same relative proportions of ices and hydrogen in the mantle, and the mantle is given an ice-rock ratio equivalent to the ratio collectively present in the mantle and core in the original three-layer model. The gravitational harmonics for the two-layer models are then derived in a manner analogous to the three-layer models, as discussed below.

Derivation of model gravity harmonics

After computing a range of models satisfying the planet mass and mean radius, with varied composition and extent of the layers, we then derived the implied gravity

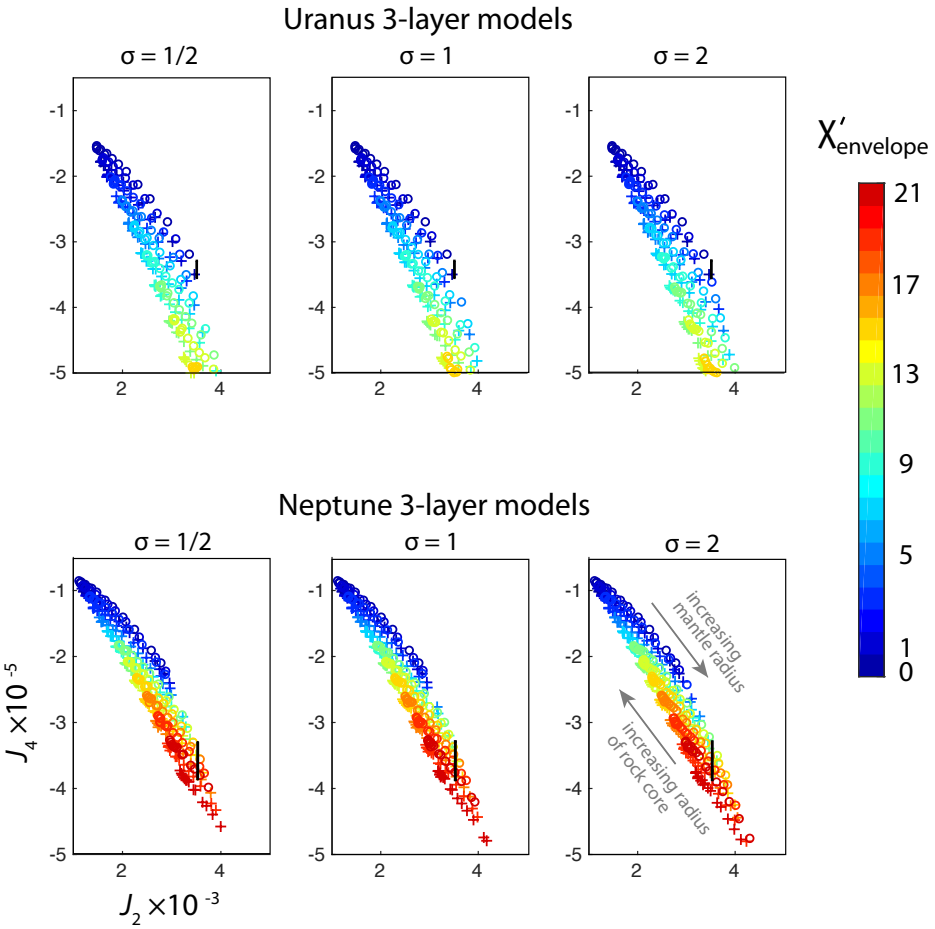

Figure 4.5: Gravitational harmonics derived for three-layer models. Observationally derived harmonics J_2 and J_4 for Uranus and Neptune (Jacobson 2014, 2009) are shown as black boxes (the boxes resemble line segments due to sufficiently tight constraints on J_2). Colors represent the mole fraction $\chi'_{\rm env} \equiv \chi_{\rm H_2O}/(\chi_{\rm H_2O} + \chi_{\rm H_2})$ in the envelope. Layer compositions were chosen in accordance with the rationale described in Figure 4.3 and in the text. The parameter σ describes the assumed asymmetry of the model critical curve and is defined such that $\chi_{\rm env} = \sigma\chi_{\rm man}$, where $\chi_{\rm man} \equiv \chi_{\rm H_2}/(\chi_{\rm H_2O} + \chi_{\rm H_2})$, the ratio in the mantle. For every set of layer compositions, a range of models was constructed to satisfy the mean density and radius of the planets, by varying the radius of the ice-rich mantle and rock core, as described in the text. As indicated by the arrows, models toward the lower right have comparatively larger icy mantles and smaller rock cores. The circle markers refer to gravity harmonics derived by taking the spheroid density to be the outer extent of each spheroid, while the plus-sign markers refer to the harmonics derived by taking the spheroid density to be that of the outer limit of the adjacent interior spheroid, in accordance with the rationale described in the text.

Table 4.1: Observational constraints used in this work.

	Uranus	Neptune
total planet mass [kg $\times 10^{25}$]	8.68[a]	10.241[a]
measured equatorial radius a at 1 bar [km]	25559[b]	24766[c]
measured polar radius b at 1 bar [km]	24973[b]	24342[c]
mean planet radius at 1 bar [km]	25362[d]	24624[d]
present-day effective temperature [K]	76(2)[b]	72(2)[c]
assumed solid-body rotation period [s]	59664[e]	62849[e]
quadrupole gravitational harmonic $J_2 \times 10^{-2}$	0.35107(7)[f]	0.35294(45)[g]
octopole gravitational harmonic $J_4 \times 10^{-4}$	−0.342(13)[f]	−0.358(29)[g]

[a] via JPL Horizons.
[b] Lindal et al. 1987.
[c] Lindal 1992.
[d] $\bar{R} \equiv \sqrt[3]{a^2 b}$
[e] Helled, Anderson, and Schubert 2010.
[f] Jacobson 2014.
[g] Based on Jacobson 2009; Lindal 1992 in the same manner as Helled, Anderson, and Schubert 2010; Nettelmann et al. 2013, for a reference radius of the 1-bar pressure level.

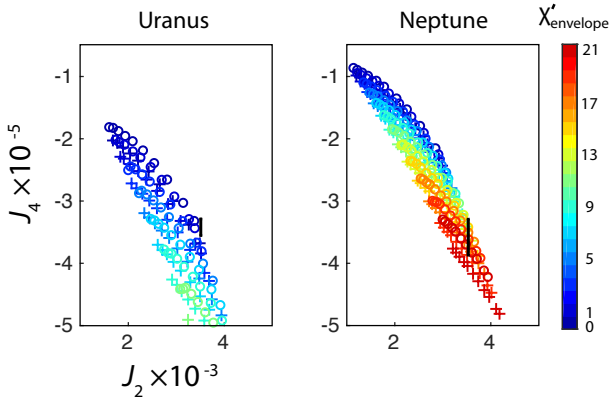

Figure 4.6: Gravitational harmonics for derived two-layer models, in a manner analogous to Figure 4.5.

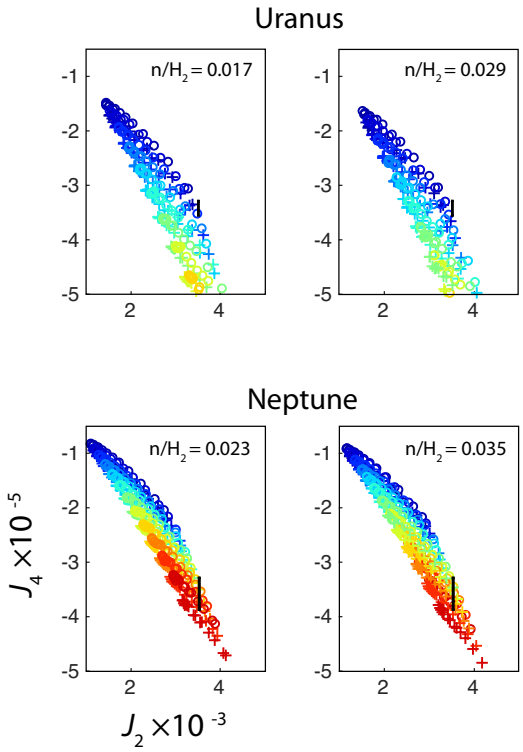

Figure 4.7: Models of Uranus and Neptune assuming a symmetric H_2-H_2O critical curve ($\sigma = 1$ case) with methane abundances n/H_2 relative to hydrogen chosen at the lower and upper observational bounds for each planet (Table 4.1).

harmonics and compared the result with observations. Due to the presumed presence of a density discontinuity in the outer region of these planets, the Radau-Darwin approximation is not robust (Gao and Stevenson 2013), and moreover the traditional approach to theory of figures (Zharkov and Trubitsyn 1978) is not ideal here. Instead, we use the concentric Maclaurin spheroids approach to theory of figures developed by Hubbard 2013, in which the planet is treated as a set of concentric spheroids with homogeneous densities. The shape of the jth spheroid is an equipotential surface found by iteratively solving for the balance of gravitational and rotational potentials. The CMS method was chosen in this work because it allows trivial inclusion of substantial density discontinuities, while permitting density gradients to be modeled with arbitrarily many concentric spheroids. A potential caveat resides in the assumption of solid-body rotation; however, Kaspi et al. 2013 have found that the gravity field can be explained by limiting the zonal winds to the outer 1% of the radii of Uranus and Neptune.

For both planets, 30 equally spaced spheroids, with an additional spheroid at the

location of each transition (i.e. the envelope-mantle transition, and the mantle-core transition in 3-layer models containing a separate rock core), and 15 iterations between the shape and gravity, were found to be more than sufficient to compute the gravitational harmonics to observational precision. It should be noted that one source of error inherent to the CMS method arises from the discretization of density gradients within the planet. To address this limitation, two versions of the CMS calculation were computed for each model, which can be considered as providing lower and upper bounds on the gravitational harmonics: one in which the density chosen for each spheroid was the (lower) density occurring at the outer bound of the next interior spheroid, and another calculation with the chosen density being the higher density present at the inner boundary of each spheroidal shell (i.e. the outer bound of the next interior spheroid). The results of these calculations are discussed in the next section. Another input to the determination of the gravity harmonics is the assumed solid-body rotation rate. In this work, we use the rotation rates determined by Helled, Anderson, and Schubert 2010 to minimize the dynamical heights of the 1-bar isobaric surfaces of Uranus and Neptune. While plausible (and compatible with our observational understanding of Jupiter and Saturn), accurate rotation rates must come from future missions.

4.3 Results

Figure 4.5 shows the derived gravitational harmonics J_2 and J_4 for three-layer models of Uranus and Neptune. For Uranus, the models that best fit the gravity data have a mole fraction in the envelope $\chi'_{\rm env} \lesssim 0.01$ of water relative to hydrogen. For Neptune, to fit the observed gravitational field, it appears that $\chi'_{\rm env} \gtrsim 0.10$ is necessary. This result holds for both symmetric and asymmetric assumed critical curves, as seen in Figure 4.5. Evidently, the envelope proportion of water relative to hydrogen dominates the gravity harmonics in these models. The qualitative robustness of this result to asymmetry in the phase diagram suggests that, for interior models of ice giants which take into account hydrogen-water mixing constraints, it is necessary to include a substantial proportion of metals in Neptune's envelope, compared to Uranus, which must be more centrally condensed. Evidently, this appears to point to the nature of a dichotomy between these two superficially similar planets, which may be related to their disparate heatflows, as we will discuss further in the next section. In particular, if hydrogen-water phase separation, as hypothesized in this work, does hold, and if Neptune is indeed in a less demixed state than Uranus, we find that an explanation naturally arises for the large heat flow of Neptune relative

to Uranus.

Next, we consider the dependence of this result on the number of assumed layers. While, as discussed in the prior section, the gravitational harmonics dictate that a transition must take place between a lighter, hydrogen-rich region to an intrinsically denser region, it is also warranted to quantify the possible effect of a separate rock core on the gravity field. As gravitational harmonics generally probe the density structure at levels above $\sim 0.5 R_{\rm planet}$, it might be expected that the inclusion of a separate rock core versus homogeneously mixed rock might not make a substantial difference to our result. To check that this expectation holds, Figure 4.5 shows the gravitational harmonics for the associated two-layer models–including rock mixed in the mantle, rather than in a separate core, as described in the previous section–for the case of a symmetric coexistence curve. Indeed, although slight variation is seen from the three-layer case, the resulting gravity harmonics are qualitatively similar overall.

Moreover, we took into account the effect on our result of the uncertainty for the abundance of methane in the envelopes of Uranus and Neptune. Models with methane abundances chosen at the upper and lower observational bounds for each planet (Table 4.1) are shown in Figure 4.7, again for the case of symmetric H_2-H_2O coexistence curve. Although the model gravity harmonics can vary by as much as several percent within the observational error range for methane abunance, the result is qualitatively similar at the upper and lower bounds of the measured concentrations.

Examples of density profiles of two- and three-layer models of Uranus and Neptune producing a close fit to the observed gravitational harmonics with the assumed solid-body rotation, are shown in Figure 4.8. While these models generally appear quite similar to many other published models of these planets that assume homogeneous layers, the key difference in this case is that our novel mixing constraint (Figure 3) has been imposed for the layer compositions of the envelope and mantle, removing a degree of freedom compared to traditional layered models.

We now turn to further discussion of these results. In particular, we consider in some detail the effect our hypothesized demixing scenario–and associated gravitational potential energy release–could have on he heatflow. We also relate these results to the observed atmospheric abundances of methane and ammonia.

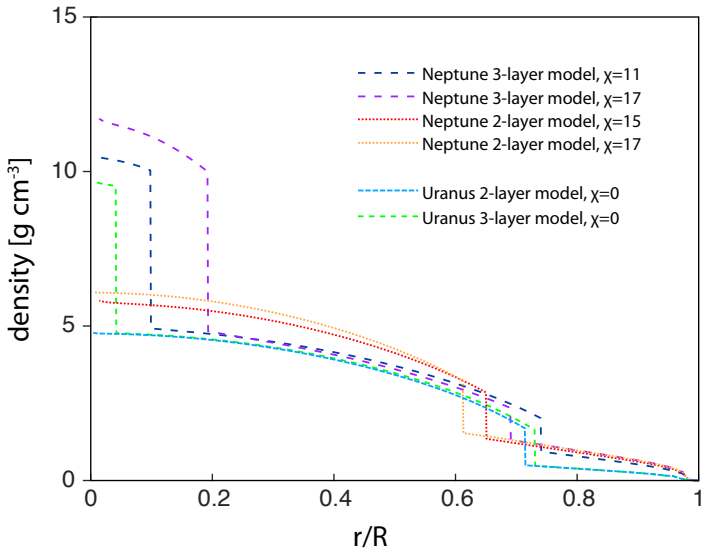

Figure 4.8: Examples of derived two- and three-layer density profiles for Uranus and Neptune which were found to approximately reproduce observed J_2 and J_4.

4.4 Discussion

Our finding that Neptune, in the model framework discussed in this work, would require substantial metallicity of its outer layer to account for the observed gravity harmonics, agrees with results of other layered models (e.g. Nettelmann et al. 2013) showing that Neptune can have substantial metal enrichment in its envelope compared to Uranus in models that satisfy the planets' gravity fields. From gravity and rotation data, Neptune is known to be less centrally condensed than Uranus–a difference that has alternatively been suggested by Reinhardt et al. 2020 to result from different giant impact histories of Uranus and Neptune. This work presents an alternative hypothesis for this dichotomy—namely, that both planets might contain demixed hydrogen and water as major constituents, and that Neptune is currently in a considerably less-demixed state than Uranus. To test this new hypothesis, it will be critical to resolve the disagreement between the experimental work of Bali, Audétat, and Keppler 2013 and the ab initio study of Soubiran and Militzer 2015 addressing the question of whether hydrogen and water are miscible in the deep interiors of ice giants. Moreover, if it is found that hydrogen-water immiscibility is in fact expected in Uranus and Neptune, the specific nature of the hydrogen-water critical and coexistence curves will be of utmost importance in constraining the interior states of these planets. As will now be discussed, the properties of the hydrogen-water system may also be crucial for understanding the disparate heat flows of Uranus and

Neptune.

In the model framework presented in this work, as Neptune cools, the equilibrium mole fraction χ'_{env} of water in the envelope should currently be decreasing with time. This process is expected to be associated with a change in gravitational potential energy in the planet. Our finding that Uranus may have considerably less water in its envelope than Neptune suggests that, unlike Neptune, hydrogen-water demixing in Uranus could be at or near completion, and no longer contributing to the heatflow. Accordingly, it may be worth considering the role of present-day gravitational energy release due to present-day hydrogen-water demixing in Neptune but not Uranus, as a potential major source of the observed heatflow in Neptune.

To test whether it is feasible for hydrogen-water separation to account for the present-day observed heatflow of Neptune, the available gravitational energy release from this process was estimated as follows. An approximate model of Neptune's interior was constructed by taking the masses of hydrogen and water present in the original best-fit $\chi = 0.11$ Neptune model (assuming a symmetric critical curve), and then recalculating an associated simplified present-day two-layer model, containing only hydrogen and water in the original proportions.[3] As in the previous, more detailed models, adiabaticity of the interior was assumed, with T_{eff} of the present-day model assumed to be the same value as before (76 K). The resulting present-day model of Neptune has a total radius $\sim 92\%$ that of the original, the same order of magnitude. Next, a model of Neptune's future demixed end state was constructed, with an envelope of pure hydrogen and a mantle of pure water, and the total masses of each constituent held fixed compared to the present-day model (Figure 4.9). The effective temperature of the end-state model was derived by equating the power absorbed to the power radiated,

$$T_{\text{eff}} = \sqrt[4]{\frac{L(1-a)}{16\pi\sigma D^2}} \sim 47 \text{ K}, \tag{4.10}$$

where the solar luminosity L and bond albedo of Neptune a (Pearl and Conrath 1991) are assumed not to deviate from present-day values, σ is the Stefan-Boltzmann constant, and D is orbital distance from the sun.

[3]The other constituents are neglected for the purposes of this first-pass model, but it is expected that the nonpolar species (e.g. He and CH_4) would be incorporated into the hydrogen, and the polar species (e.g. NH_3) with the water. Improved constraints on abundances of polar and nonpolar constituents relative to solar in the envelopes of these planets might eventually shed light on whether this mechanism is present, and may potentially even serve as an indirect test of hydrogen-water miscibility in these planets.

Due to reduced self-compression in the envelope, the total planetary radius in this model was found to increase by $\sim 4\%$ relative to the initial present-day simplified model. Moreover, the combined effects of intrinically greater mantle density (due to demixing of hydrogen from the mantle), but reduced compression from the overlying envelope, coincidentally produce a similar mantle extent compared to the present-day model, at least in this simplified example. Comparing the total gravitational potential energy in the two models, we find that the available total gravitational potential energy release from hydrogen-water demixing in Neptune is $\sim 2 \times 10^{40}$ erg, sufficient to supply Neptune's present-day heat flux of $\sim 3 \times 10^{22}$ erg/s (Podolak, Hubbard, and Stevenson 1991; Pearl and Conrath 1991) for roughly ten solar system lifetimes. This rough estimate of total available energy appears to suggest that gravitational potential energy release from hydrogen-water demixing could plausibly supply Neptune's entire present-day heat flux.

It is natural to compare the proposed process of hydrogen-water demixing in Uranus and Neptune with the well-known mechanism of helium rainout expected to occur in gas giants due to the immiscibility of helium in metallic hydrogen. This latter process has been proposed (Stevenson and Salpeter 1977b, 1977a) to account for the luminosity excess of Saturn, as well as atmospheric depletion of helium in Saturn (Stevenson 1980; Conrath et al. 1984). But while both helium rainout and the currently proposed mechanism of continued hydrogen-water demixing invoke potential energy release of separating constituents as a contributor to the planet's luminosity, the two processes are not perfectly analogous. A key difference exists– more specifically, helium rainout, as it is generally discussed, occurs when the cooling giant planet's adiabat crosses into a regime of immiscibility for helium and metallic hydrogen, causing the helium to become immiscible and rain out (bringing dissolved noble gases with it). In contrast, with the presently discussed mechanism of continued hydrogen-water demixing, it is assumed that hydrogen and water are *already* immiscible and separated into two phases in ice giant interiors. The gravitational potential energy release in Neptune is instead proposed to be due to variation of the equilibrium compositions of the already-separated phases, as the planet cools and approaches a state where hydrogen and water are completely demixed. The difference arises primarily because of the much lower pressure of relevance for the hydrogen-water system, though of course it is contingent on unknown aspects of the phase diagram at high pressure and can therefore only be viewed as a hypothesis.

We now proceed with a somewhat more detailed consideration of the effect of hydrogen-water demixing on Neptune's cooling rate, adapting the precedent set forth for helium rain in gas giants by Stevenson and Salpeter 1977a, to the hypothesized phase separation addressed at present for ice giants. As previously described in this section, the planet is treated as consisting of a compositionally homogeneous envelope comprised of the hydrogen-dominant phase, with a compositionally homogeneous mantle comprised of the water-dominant phase. The envelope is assumed to be adiabatic, in agreement with magnetic field observations. The phase separation of hydrogen and water dictates the existence of two simultaneous, opposing gravitational effects: the downward redistribution of water from the envelope to the mantle, and the upward redistribution of hydrogen from the mantle to the envelope. Assuming a critical curve roughly symmetric in mole fraction, as we have done in this work, the proportion of redistributed hydrogen is about an order of magnitude less than the distributed water by mass. Therefore, because the average vertical displacement is similar for both, the gravitational effect of rising hydrogen is neglected for the purposes of this work, and we focus on the effect of water redistributing from the envelope to the mantle. The mass of redistributed water necessary to change the mole fraction of water in the mantle from x to $x + dx$ is approximately

$$M_{H_2O} \approx \frac{9dxM_{\text{man}}}{(1-x)(1+8x)} \tag{4.11}$$

where M_{man} is the total mass of the mantle. The gravitational energy release is approximately

$$E_{\text{grav}} \approx M_{H_2O}gH \tag{4.12}$$

where $g \sim 1400$ cm s^{-2} is the typical gravitational acceleration in the planet and $H \sim 1.2 \times 10^9$ is the approximate vertical height between the centers of mass of the two layers. Moreover, the temperature T_b at the boundary between the envelope and mantle is related to the mole fraction x of water in the mantle by the hydrogen-water coexistence curve. Unfortunately, this curve is not yet known, so we resort to using our model critical curve as described earlier for a two-component regular solution, stretched so that the value $T_b \sim 3800$ K from our good fit $\chi \sim 0.11$ adiabatic Neptune model corresponds to an equilibrium saturation mol fraction of $\chi \sim 0.11$. The value of the critical temperature derived in this manner is then $T_c \sim 7000K$; comparing this value to Figure 2, this derived critical temperature is

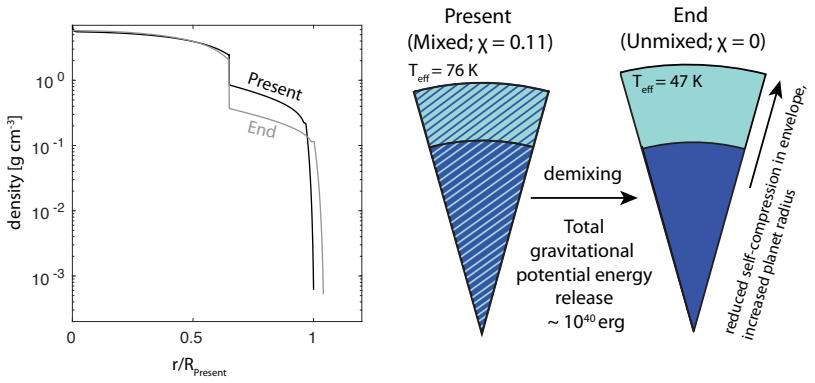

Figure 4.9: The estimated gravitational potential energy difference between Neptune's inferred present-day mixing state with the unmixed future evolutionary end-member is $\sim 10^{40}$ erg, sufficient to supply Neptune's present-day observed heat flux, 2×10^{22} erg (Podolak, Hubbard, and Stevenson 1991; Pearl and Conrath 1991), for roughly 10 solar system lifetimes.

indeed potentially suggestive of the aforementioned critical curve turnover expected in these planets.

The parameter $T_0 \equiv (dT_b/dx)_{\rm coex}$ is the temperature change of the envelope-mantle boundary as dictated by the coexistence curve. Specifically, T_0 can be viewed as the tangent slope to the scaled model coexistence curve (i.e., scaled such that $T_c \sim 7000$ K) at the present-day inferred mole fraction of $\chi \sim 0.11$ (i.e. $x = 0.89$ for the main constituent). While we again emphasize that the critical curve remains unknown, we employ our model critical curve for now, and estimate $T_0 \sim 8000$ K.

Then, treating the mantle as adiabatic[4], the thermal energy increase $E_{\rm th}$ of the mantle can be expressed (Stevenson and Salpeter 1977a) as

$$E_{\rm th} \equiv A C_v T_0 dx M_{\rm man} \tag{4.13}$$

where A is the ratio of typical internal temperature to T_b and is of order 2, $C_v \sim 2{\times}10^7$ erg g^{-1} K^{-1} is the specific heat of the mantle, and $M_{\rm man}$ is the mass of the mantle. (Note that this treatment assumes the mantle is where the thermal energy is deposited; as the extrapolated curvature of the critical curve relative to the adiabat suggests

[4]As discussed earlier in Section 4.1, the mantle may well not be adiabatic, but it is difficult to account for the observed magnetic fields if the outer $\sim$ 10% is not adiabatic. If heat transport is inhibited between an outer convecting region and inner stratified region, the thermal energy increase of the mantle may be less, making the ratio $E_{\rm th}/E_{\rm grav}$ (which we are about to discuss in the text) even smaller.

(Figure 4.2), the envelope may be undersaturated in the regions above the envelope-mantle boundary. It is the critical temperature at this boundary which we assume dictates the coexisting phase compositions of the envelope and mantle.) With the above parameterization, the ratio of thermal energy increase to gravitational energy release due to demixing water in Neptune can be approximated as

$$\frac{E_{\rm th}}{E_{\rm grav}} \approx \frac{AC_v T_0}{9gH} \approx 0.02 \tag{4.14}$$

This ratio is an upper bound, as discussed in footnote 4. In a similar vein as Stevenson and Salpeter 1977a, the small value of this ratio suggests most of the released gravitational energy is radiated. Therefore, we will proceed to estimate the change in effective temperature with time. We treat the envelope as adiabatic, such that

$$\frac{T_b}{T_e} \equiv \left(\frac{P_b}{P_e}\right)^{\Gamma} \tag{4.15}$$

where T_e is the effective temperature, P_e is the corresponding pressure, and $\Gamma \sim 0.3$ is the adiabatic index. Because the water content of the outer atmosphere is negligible due to the low vapor pressure of water at the relevant temperatures (Figure 4.4), demixing of water from the envelope should not affect P_e, so we treat it as roughly constant. Moreover, although P_b can decrease by a factor of several over the entire lifetime of the planet, due to the demixing of the water from the envelope and the associated diminishment of overpressure, P_b and Γ are treated as roughly constant in a time window surrounding the present day. Therefore $d \ln T_b/dt \approx d \ln T_e/dt$, and in a similar manner as Stevenson and Salpeter 1977a, the gravitational energy release over time can be expressed as

$$Q_{\rm grav} \approx \frac{9M_{\rm man}}{(1-x)(1+8x)T_0}\frac{dT_b}{dt}gH \tag{4.16}$$

and if $Q_{\rm grav}$ is equated with the present-day observed heat flux $\sim 3 \times 10^{22}$ erg s^{-1} of Neptune, for $M_{\rm man} \sim 8 \times 10^{28}$ g, $x \sim 0.89$, $T_0 \sim 8000$ K, $g \sim 1400$ g cm^{-2}, and $H \sim 1.2 \times 10^9$ cm, then, accounting for the logarithmic temperature relation between T_b and T_e, the cooling rate is estimated as $dT_e/dt \sim 0.1$ K Gyr^{-1}. Comparing this to the estimated present-day cooling rate of roughly ~ 2 K Gyr^{-1} found for standard adiabatic cooling models (e.g. Hubbard and Macfarlane 1980)

that do not account for gravitational energy release of phase separation, it is evident that the hypothesized demixing could indeed significantly prolong cooling.

Relationship of model to atmospheric abundances

We next turn to a discussion of our model as it relates to the observed abundances of minor constituents in the atmospheres of Uranus and Neptune. In the partially analogous case of helium rainout in gas giants discussed above, nonpolar neon is proposed to dissolve into the helium rain droplets, leading to atmospheric depletion of neon in gas giants when helium rainout occurs (Roulston and Stevenson 1995). The depletion of neon by an order of magnitude relative to solar observed by Galileo in Jupiter's atmosphere (Niemann et al. 1996) has been interpreted as possible evidence for the commencement of helium rainout in Jupiter (Wilson and Militzer 2010). In a somewhat analogous manner, in the potential framework for understanding Uranus and Neptune that has been discussed in this work, polar constituents (e.g. ammonia) may be expected to partition preferentially into the water-rich phase, while nonpolar constituents (e.g. methane) may be expected to partition preferentially into the hydrogen-rich phase. This partitioning will be progressive and grow as the demixing proceeds. Hence, if our framework of immiscibility is correct and if it is true that the demixing of Uranus is further advanced than Neptune, then there may exist the expectation of ammonia depletion in the atmosphere of Uranus relative to Neptune. Indeed, de Pater, Romani, and Atreya 1991 find that the Voyager radio occultation data (Lindal et al. 1990) are best in agreement with the presence of an ammonia ice cloud at the $\sim$ 5-bar level in Neptune. While the radio occultation data did not probe deep enough on Uranus to make an analogous determination, ground-based observations (Gulkis, Janssen, and Olsen 1978) indicate emission at short cm wavelengths from below the analogous level in Uranus, indicating that such an ammonia cloud appears to be absent on Uranus. The generally accepted explanation for the atmospheric ammonia discrepancy between the two planets invokes possible differences in atmospheric convection, which might allow some ammonia to bypass depleting reactions with H_2S in Neptune but not Uranus. While this explanation remains entirely plausible, the apparent atmospheric depletion of ammonia in Uranus relative to Neptune can also be explained as possible evidence for the more advanced demixing, relative to Neptune, of the atmosphere of Uranus.

In an analogous fashion to ammonia in the envelope, methane could otentially demix from the mantle phase, possibly leading to enrichment over time of methane in the atmosphere of Uranus compared to Neptune. The atmospheric methane

abundances of Uranus and Neptune, (n/H_2 = 0.023 ± 0.006 and 0.029 ± 0.006 respectively) from Voyager spectroscopic measurements (Fegley et al. 1991; Baines et al. 1993 via Lodders and Fegley 1994) do not indicate a clear discrepancy in atmospheric methane between the two planets, although the measurements are consistent with Uranus having up to 26% more methane in its atmosphere than Neptune. More work is needed to understand the mixing properties of methane and water at conditions relative to the interiors of these planets, to determine whether the methane abundances are consistent with the hypothesized relative demixing states of Uranus and Neptune.

Potential caveats of models

There exist several caveats inherent to the theoretical framework used in this work. Notably, the relevance of H_2-H_2O mixing properties are expected to diminish at depths in the planet where the hydrogen and water molecules become some other configuration of hydrogen and oxygen atoms. In particular, the occurrence of superioinic ice phases in the lower regions of the inferred ice mantle (e.g. Wilson, Wong, and Militzer 2013; Bethkenhagen et al. 2015) is expected to affect the relevant species interactions at those depths, as well as the densities. These effects are not relevant at the shallower depths ($\sim 0.7 R_{\text{planet}}$) at which the transition from a hydrogen-dominated envelope to heavier materials must occur to satisfy the planets' gravity fields. In our assumed model framework of hydrogen-water immiscibility, if it is assumed this density change is due to a phase transition between coexisting hydrogen- and water-rich phases, then the coexistence curve at the $P-T$ conditions of this transition zone would be expected to govern the layer compositions. Accordingly, the superionic behavior of ices at greater pressures would be expected to be irrelevant to the compositions of the envelope and upper mantle. It may be relevant to the presence or absence of a separate "rock" component. As shown by Figures 4.5 and 4.6, in our models, it is the composition of the envelope that appears to have the predominant effect on the gravitational harmonics.

Moreover, a related concern is that the ratios of ammonia, methane, and water chosen for the envelopes and mantles of our models may not correctly reflect what is really present. The compositional degeneracy inherent to these intermediate-mass planets ensures that the ice-like density inferred for their deep interiors could be satisfied by numerous combinations of ices, rocks, and hydrogen. While we assume the interiors of both planets contain mantles with well-mixed ices in the same fixed ratio, alternatively, the ratios of interior ices could be different in Uranus

and Neptune due to different formation conditions. On the other hand, as Figure 4.5 shows, varying the hydrogen content of the mantle by a factor of two relative to water makes little difference to the gravitational harmonics in our models, even at significant hydrogen mole fractions of $\chi'_{\mathrm{man}} \sim 20\%$. This invariance of the gravitational harmonics to χ'_{man} appears to suggest that the specific relative ratios of ammonia, water, and methane in the mantle would not affect the result that Neptune requires a substantial ($\gtrsim 10\%$) mole fraction of metals in its envelope (in this work presumed to be water) and that Uranus requires a considerably smaller fraction ($\lesssim 1\%$).

Furthermore, as mentioned earlier, the assumption of a fully adiabatic interior may not hold for Uranus and Neptune, especially as inhibited convection has often been invoked to possibly explain the low heat flux of Uranus (e.g. Podolak, Hubbard, and Stevenson 1991; Nettelmann et al. 2016; Leconte and Chabrier 2012; Podolak, Helled, and Schubert 2019). For the purposes of this work, the temperature gradient primarily affects the density distributions inferred from the equations of state. However, the presence of a dynamo in both Uranus and Neptune is thought to require convection in at least the outer ~ 20 percent of these planets (Stanley and Bloxham 2004, 2006). Below these depths, the thermal pressure correction is of minimal consequence to the equations of state.

4.5 Conclusions

It is standard practice to model the interiors of Uranus and Neptune as consisting of discrete, compositionally homogeneous layers. However, as discussed in Section 4.1, the choice of specific layer compositions–and the assumption of a discrete boundary between these layers–have not previously received rigorous physical justification. Accordingly, this work presents the first thermodynamically justified models of ice giant interiors, in which the layers and their compositions are based on the inference of hydrogen-water immiscibility in these planets. While the true mixing properties of hydrogen and water remain to be resolved at conditions relevant to the interiors of these planets, the presence of immiscible hydrogen and water in Uranus and Neptune would offer physical justification for a sharp compositional transition from the outer hydrogen-rich envelope to the deeper region of heavier constituents, a transition that is known from the gravity data to be necessary. If this transition is not discontinuous and a substantial density gradient instead exists in the outer ~ 30 percent of these planets, it is then challenging for models to produce convective flows sufficient to generate the observed magnetic fields.

Having produced models with the novel thermodynamic constraints applied, we have found that to satisfy the mean planet density and measured gravitational field, it seems that Neptune may require a substantial portion of water in its hydrogen-dominated envelope, $\chi'_{\rm env} \gtrsim 0.10$. In contrast, models capable of satisfying these constraints for Uranus must contain a much smaller metallicity in the outer shell, $\chi'_{\rm env} \lesssim 0.01$. As discussed in section 4.4, the inferred continued demixing of hydrogen and water in Neptune but not Uranus could possibly account for the disparity in heatflow between the planets. This disparity has long been a challenge to explain, and most of the focus has been on Uranus' unexpected lack of heatflow, rather than Neptune's significant heatflow. However, if the lack of intrinsic heatflow from Uranus is due to inhibited convection in the deep interior, it then becomes a challenge to explain why Neptune is different from Uranus in its heat output. Hence, the mechanism proposed in this work–of gravitational potential energy release due to present-day hydrogen-water demixing in Neptune but not Uranus–may offer a potential means to explain how Neptune could produce the observed heat flow, if its deep interior convection is indeed inhibited in a manner similar to Uranus.

Importantly to the understanding of these planets' interior dynamics, if further experimental and/or theoretical work ultimately were to confirm that hydrogen and water are immiscible at conditions of ice giant interiors beyond $\sim$ 3 GPa, the hydrogen-water coexistence curve could then provide a novel means to inform the compositions of the deep, intermediate-mass mantles. Accordingly, the thermodynamic rationale presented in this work provides a tentative approach to potentially infer the internal compositions of Uranus and Neptune. As gravity and magnetic field data cannot provide unique solutions to the deep interior compositions of these planets, it may ultimately be necessary to turn to chemical reasoning to resolve their bulk compositional degeneracies–and accordingly, to guide our understanding of their place in solar system formation.

Acknowledgements. We thank Mike Brown and his research group, Konstantin Batygin, Steve Markham, Jonathan Fortney, Nadine Nettlemann, Ravit Helled, and the attendees of the 2020 Bern ISSI Ice Giants meeting, for thoughtful and insightful discussions which guided the direction of this work.

Chapter 5

SOLAR OBLIQUITY INDUCED BY PLANET NINE

ABSTRACT

The six-degree obliquity of the sun suggests that either an asymmetry was present in the solar system's formation environment, or an external torque has misaligned the angular momentum vectors of the sun and the planets. However, the exact origin of this obliquity remains an open question. Batygin and Brown (2016a) have recently shown that the physical alignment of distant Kuiper Belt orbits can be explained by a $5 - 20\,m_\oplus$ planet on a distant, eccentric, and inclined orbit, with an approximate perihelion distance of ~ 250 AU. Using an analytic model for secular interactions between Planet Nine and the remaining giant planets, here we show that a planet with similar parameters can naturally generate the observed obliquity as well as the specific pole position of the sun's spin axis, from a nearly aligned initial state. Thus, Planet Nine offers a testable explanation for the otherwise mysterious spin-orbit misalignment of the solar system.

5.1 Introduction

The axis of rotation of the sun is offset by six degrees from the invariable plane of the solar system (Souami and Souchay 2012). In contrast, planetary orbits have an RMS inclination slightly smaller than one degree[1], rendering the solar obliquity a considerable outlier. The origin of this misalignment between the sun's rotation axis and the angular momentum vector of the solar system has been recognized as a a longstanding question (Kuiper 1951; Tremaine 1991; Heller 1993), and remains elusive to this day.

With the advent of extensive exoplanetary observations, it has become apparent that significant spin-orbit misalignments are common, at least among transiting systems for which the stellar obliquity can be determined using the Rossiter-McLaughlin effect (Rossiter 1924; McLaughlin 1924). Numerous such observations of planetary systems hosting hot Jupiters have revealed spin-orbit misalignments spanning tens of degrees (Hébrard et al. 2008; Winn et al. 2010; Albrecht et al. 2012), even including observations of retrograde planets (Narita et al. 2009; Winn et al. 2009; Bayliss et al. 2010; Winn et al. 2011). Thus, when viewed in the extrasolar context, the solar system seems hardly misaligned. However, within the framework of the nebular hypothesis, the expectation for the offset between the angular momentum vectors of the planets and sun is to be negligible, unless a specific physical mechanism induces a misalignment. Furthermore, the significance of the solar obliquity is supported by the contrasting relative coplanarity of the planets.

Because there is no directly observed stellar companion to the sun (or any other known gravitational influence capable of providing an external torque on the solar system sufficient to produce a six-degree misalignment over its multi-billion-year lifetime Heller 1993), virtually all explanations for the solar obliquity thus far have invoked mechanisms inherent to the nebular stage of evolution. In particular, interactions between the magnetosphere of a young star and its protostellar disk can potentially lead to a wide range of stellar obliquities while leaving the coplanarity of the tilted disk intact (Lai, Foucart, and Lin 2011). Yet another possible mechanism by which the solar obliquity could be attained in the absence of external torque is an initial asymmetry in the mass distribution of the protostellar core. Accordingly, asymmetric infall of turbulent protosolar material has been proposed as a mechanism for the sun to have acquired an axial tilt upon formation (Bate, Lodato, and

[1] An exception to the observed orbital coplanarity of the planets is Mercury, whose inclination is subject to chaotic evolution (Laskar 1994; Batygin, Morbidelli, and Holman 2015)

Pringle 2010b; Fielding et al. 2015). However, the capacity of these mechanisms to overcome the re-aligning effects of accretion, as well as gravitational and magnetic coupling, remains an open question (Lai, Foucart, and Lin 2011; Spalding and Batygin 2014b, 2015b).

In principle, solar obliquity could have been excited through a temporary, extrinsic gravitational torque early in the solar system's lifetime. That is, an encounter with a passing star or molecular cloud could have tilted the disc or planets with respect to the sun (Heller 1993; Adams 2010). Alternatively, the sun may have had a primordial stellar companion, capable of early star-disc misalignment (Batygin 2012; Spalding and Batygin 2014b; Lai 2014). To this end, ALMA observations of misaligned disks in stellar binaries (Jensen and Akeson 2014; Williams et al. 2014) have provided evidence for the feasibility of this effect. Although individually sensible, a general qualitative drawback of all of the above mechanisms is that they are only testable when applied to the extrasolar population of planets, and it is difficult to discern which (if any) of the aforementioned processes operated in our solar system.

Recently, Batygin and Brown (2016a) determined that the spatial clustering of the orbits of Kuiper Belt objects with semi-major axis $a \gtrsim 250\,\mathrm{AU}$ can be understood if the solar system hosts an additional $m_9 = 5 - 20\,m_\oplus$ planet on a distant, eccentric orbit. Here, we refer to this object as Planet Nine. The orbital parameters of this planet reside somewhere along a swath of parameter space spanning hundreds of AU in semi-major axis, significant eccentricity, and tens of degrees of inclination, with a perihelion distance of roughly $q_9 \sim 250\,\mathrm{AU}$ (Brown and Batygin 2016). In this work, we explore the possibility that this distant, planetary-mass body is fully or partially responsible for the peculiar spin axis of the sun.

Induction of solar obliquity of some magnitude is an inescapable consequence of the existence of Planet Nine. That is, the effect of a distant perturber residing on an inclined orbit is to exert a mean-field torque on the remaining planets of the solar system, over a timespan of ~ 4.5 Gyr. In this manner, the gravitational influence of Planet Nine induces precession of the angular momentum vectors of the sun and planets about the total angular momentum vector of the solar system. Provided that angular momentum exchange between the solar spin axis and the planetary orbits occurs on a much longer timescale, this process leads to a differential misalignment of the sun and planets. Below, we quantify this mechanism with an eye towards explaining the tilt of the solar spin axis with respect to the orbital angular momentum vector of the planets.

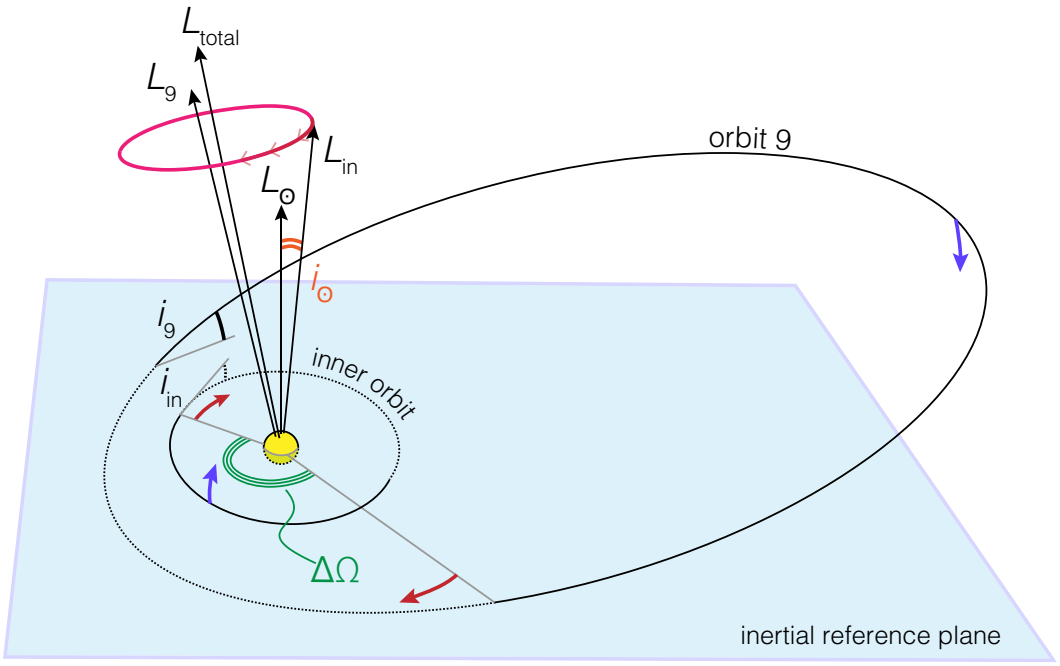

Figure 5.1: Geometric setup of the dynamical model. The orbits of the planets are treated as gravitationally interacting rings. All planets except Planet Nine are assumed to have circular, mutually coplanar orbits, and are represented as a single inner massive wire. The sun is shown as a yellow sphere, and elements are not to scale. Black, grey, and dotted lines are respectively above, on, and below the inertial reference plane. The pink arrows demonstrate the precession direction of the angular momentum vector of the inner orbit, L_{in}, around the total angular momentum vector of the solar system L_{total}. Red and blue arrows represent the differential change in longitudes of ascending node of the orbits and inclination, respectively. Although not shown in the figure, the tilting of the oblate sun is modeled as the tilting of an inner test ring. Over the course of 4.5 billion years, differential precession of the orbits induces a several-degree solar obliquity with respect to the final plane of the planets.

The chapter is organized as follows. Section 6.2 describes the dynamical model. We report our findings in section 6.3. We conclude and discuss our results in section 5.4. Throughout the manuscript, we adopt the following notation. Similarly named quantities (e.g. a, e, i) related to Planet Nine are denoted with a subscript "9", whereas those corresponding to the Sun's angular momentum vector in the inertial frame are denoted with a tilde. Solar quantities measured with respect to the solar system's invariable plane are given the subscript $\odot$.

5.2 Dynamical Model

To model the long-term angular momentum exchange between the known giant planets and Planet Nine, we employ secular perturbation theory. Within the framework of this approach, Keplerian motion is averaged out, yielding semi-major axes that are frozen in time. Correspondingly, the standard $N-$planet problem is replaced with a picture in which N massive wires (whose line densities are inversely proportional to the instantaneous orbital velocities) interact gravitationally (Murray and Dermott 1999a). Provided that no low-order commensurabilities exist among the planets, this method is well known to reproduce the correct dynamical evolution on timescales that greatly exceed the orbital period (Mardling 2007; Li et al. 2014a).

In choosing which flavor of secular theory to use, we must identify small parameters inherent to the problem. Constraints based upon the critical semi-major axis beyond which orbital alignment ensues in the distant Kuiper belt, suggest that Planet Nine has an approximate perihelion distance of $q_9 \sim 250\,\mathrm{AU}$ and an appreciable eccentricity $e_9 \gtrsim 0.3$ (Batygin and Brown 2016a; Brown and Batygin 2016). Therefore, the semi-major axis ratio (a/a_9) can safely be assumed to be small. Additionally, because solar obliquity itself is small and the orbits of the giant planets are nearly circular, here we take $e = 0$ and $\sin(i) \ll 1$. Under these approximations, we can expand the averaged planet-planet gravitational potential in small powers of (a/a_9), and only retain terms of leading order in $\sin(i)$.

In principle, we could self-consistently compute the interactions among all of the planets, including Planet Nine. However, because the fundamental secular frequencies that characterize angular momentum exchange among the known giant planets are much higher than that associated with Planet Nine, the adiabatic principle (Henrard 1982; Neishtadt 1984) ensures that Jupiter, Saturn, Uranus and Neptune will remain co-planar with each-other throughout the evolutionary sequence (see e.g. Batygin, Brown, and Fraser 2011; Batygin 2012 for a related discussion on perturbed self-gravitating disks). As a result, rather than modeling four massive rings individually, we may collectively replace them with a single circular wire having semi-major axis a and mass m, and possessing equivalent total angular momentum and moment of inertia:

$$\begin{aligned} m\sqrt{a} &= \sum_j m_j \sqrt{a_j} \\ m\,a^2 &= \sum_j m_j\, a_j^2, \end{aligned} \tag{5.1}$$

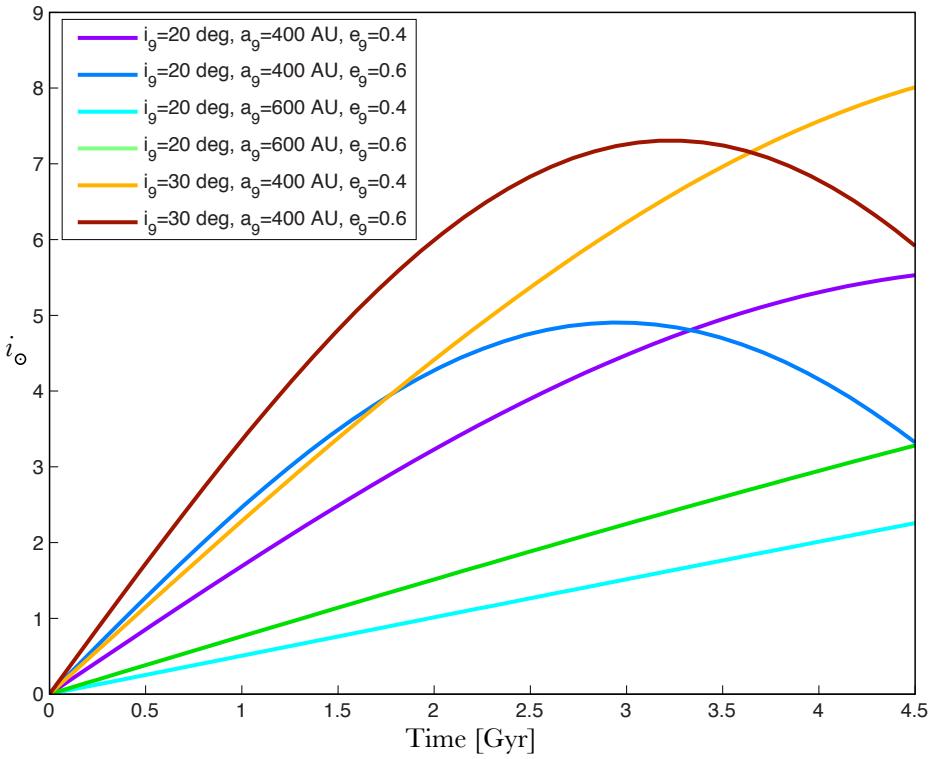

Figure 5.2: Time evolution of the solar obliquity $i_\odot$ in the frame of the solar system, starting with an aligned configuration of the solar system, and a $10m_\oplus$ Planet Nine with starting parameters in the exemplary range $a_9 \in [400, 600]$ AU, $e_9 \in [0.4, 0.6]$, and $i_9 \in [20, 30]$ deg, demonstrating gradual differential precession of the sun and planets over 4.5 Gyr.

where the index j runs over all planets. The geometric setup of the problem is shown in Figure (5.1).

To quadrupole order, the secular Hamiltonian governing the evolution of two interacting wires is (Kaula 1962; Mardling 2010):

$$\mathcal{H} = \frac{1}{4}\frac{m\,m_9}{a_9}\left(\frac{a}{a_9}\right)^2 \frac{1}{\varepsilon_9^3}\left[\frac{1}{4}\left(3\cos^2(i)-1\right)\left(3\cos^2(i_9)-1\right) + \frac{3}{4}\sin(2\,i)\,\sin(2\,i_9)\,\cos(\Omega-\Omega_9)\right], \tag{5.2}$$

where Ω is the longitude of ascending node and $\varepsilon_9 = \sqrt{1-e_9^2}$. Note that while the eccentricities and inclinations of the known giant planets are assumed to be small, no limit is placed on the orbital parameters of Planet Nine. Moreover, at this level of expansion, the planetary eccentricities remain unmodulated, consistent

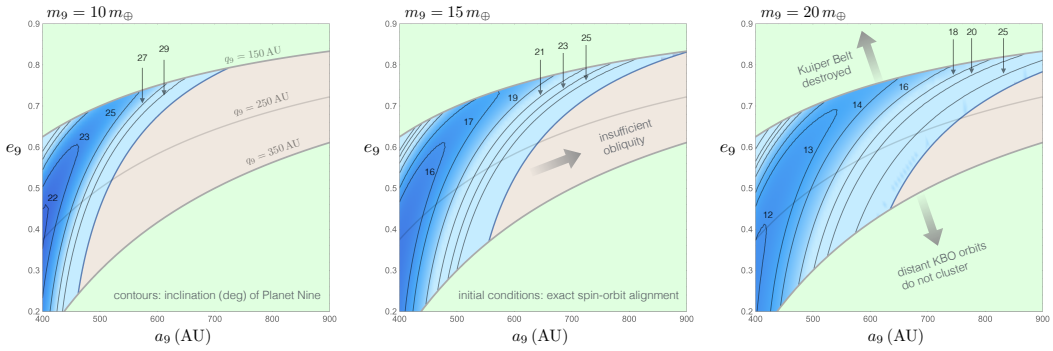

Figure 5.3: Parameters of Planet Nine required to excite a spin-orbit misalignment of $i_\odot = 6$ deg over the lifetime of the solar system, from an initially aligned state. Contours in a_9-e_9 space denote i_9, required to match the present-day solar obliquity. Contour labels are quoted in degrees. The left, middle, and right panels correspond to $m_9 = 10$, 15, and $20\,m_\oplus$ respectively. Due to independent constraints stemming from the dynamical state of the distant Kuiper belt, only orbits that fall in the $150 < q_9 < 350$ AU range are considered. The portion of parameter space where a solar obliquity of $i_\odot = 6$ deg cannot be attained are obscured with a light-brown shade.

with the numerical simulations of Batygin and Brown 2016a; Brown and Batygin 2016, where the giant planets and Planet Nine are observed to behave in a decoupled manner.

Although readily interpretable, Keplerian orbital elements do not constitute a canonically conjugated set of coordinates. Therefore, to proceed, we introduce action-angle coordinates:

$$\begin{aligned} \Gamma &= m\sqrt{M_\odot\, a} \\ \Gamma_9 &= m_9\sqrt{M_\odot\, a_9}\,\varepsilon_9 \\ Z &= \Gamma\big(1-\cos(i)\big) & z &= -\Omega \\ Z_9 &= \Gamma_9\big(1-\cos(i_9)\big) & z &= -\Omega_9. \end{aligned} \tag{5.3}$$

Generally, the action Z represents the deficit of angular momentum along the $\hat{k}-$axis, and to leading order, $i \approx \sqrt{2Z/\Gamma}$. Accordingly, dropping higher-order corrections in i, expression (5.2) takes the form:

$$\mathcal{H} = -\frac{m\,m_9}{a_9}\left(\frac{a}{a_9}\right)^2 \frac{1}{\epsilon_9^3}\left[\frac{1}{4}\left(2-\frac{6Z}{\Gamma}\right)\left(3\left(1-\frac{Z_9}{\Gamma_9}\right)^2-1\right)\right.$$
$$\left. + 3\left(1-\frac{Z_9}{\Gamma_9}\right)\sqrt{1-\frac{Z_9}{2\Gamma_9}}\sqrt{\frac{2Z}{\Gamma}\frac{2Z_9}{\Gamma_9}}\cos(z-z_9)\right]. \tag{5.4}$$

Application of Hamilton's equations to this expression yields the equations of motion governing the evolution of the two-ring system. However, we note that action-angle variables (5.3) are singular at the origin, so an additional, trivial change to Cartesian counterparts of coordinates is required to formulate a practically useful set of equations (Morbidelli 2002). This transformation is shown explicitly in the Appendix.

To complete the specification of the problem, we also consider the torque exerted on the sun's spin axis by a tilting solar system. Because the sun's angular momentum budget is negligible compared to that of the planets, its back-reaction on the orbits can be safely ignored. Then, the dynamical evolution of its angular momentum vector can be treated within the same framework of secular theory, by considering the response of a test ring with semi-major axis (Spalding and Batygin 2014b, 2015b):

$$\tilde{a} = \left[\frac{16\,\omega^2\,k_2^2\,R^6}{9\,I^2\,M_\odot} \right]^{1/3}, \tag{5.5}$$

where ω is the rotation frequency, k_2 is the Love number, R is the solar radius, and I is the moment of inertia.

Because we are primarily concerned with main-sequence evolution, here we adopt $R = R_\odot$ and model the interior structure of the sun as a $n = 3$ polytrope, appropriate for a fully radiative body (Chandrasekhar 1939). Corresponding values of moment of inertia and Love number are $I = 0.08$ and $k_2 = 0.01$ respectively (Batygin and Adams 2013b). The initial rotation frequency is assumed to correspond to a period of $2\pi/\omega = 10$ days and is taken to decrease as $\omega \propto 1/\sqrt{t}$, in accord with the Skumanich relation (Gallet and Bouvier 2013).

Defining scaled actions $\tilde{\Gamma} = \sqrt{M_\odot\,\tilde{a}}$ and $\tilde{Z} = \tilde{\Gamma}(1 - \cos(\tilde{i}))$ and scaling the Hamiltonian itself in the same way, we can write down a Hamiltonian that is essentially analogous to Equation (5.4), which governs the long-term spin axis evolution of the Sun:

$$\tilde{\mathcal{H}} = \sum_j \left(\frac{m_j}{4\,a_j^3} \right) \tilde{a}^2 \left[\frac{3\tilde{Z}}{\tilde{\Gamma}} + \frac{3}{4} \sqrt{\frac{2\tilde{Z}}{\tilde{\Gamma}} \frac{2Z}{\Gamma}} \cos(\tilde{z} - z) \right]. \tag{5.6}$$

Note that contrary to Equation (5.4), here we have assumed small inclinations for both the solar spin axis and the planetary orbits. This assumption transforms the Hamiltonian into a form equivalent to the Lagrange-Laplace theory, where the interaction coefficients have been expanded as hypergeometric series, to leading order

in semi-major axis ratio (Murray and Dermott 1999a). Although not particularly significant in magnitude, we follow the evolution of the solar spin axis for completeness.

Quantitatively speaking, there are two primary sources of uncertainty in our model. The first is the integration timescale. Although the origin of Planet Nine is not well understood, its early evolution was likely affected by the presence of the solar system's birth cluster (Izidoro et al. 2015; Li and Adams 2016), meaning that Planet Nine probably attained its final orbit within the first ~ 100 Myr of the solar system's lifetime. Although we recognize the $\sim 2\%$ error associated with this ambiguity, we adopt an integration timescale of 4.5 Gyr for definitiveness.

A second source of error stems from the fact that the solar system's orbital architecture almost certainly underwent a instability-driven transformation sometime early in its history (Tsiganis et al. 2005; Nesvorný and Morbidelli 2012). Although the timing of the onset of instability remains an open question (Levison et al. 2011; Kaib and Chambers 2016), we recognize that failure of our model to reflect this change in a and m (through equation 5.1) introduces a small degree of inaccuracy into our calculations. Nevertheless, it is unlikely that these detailed complications constitute a significant drawback to our results.

5.3 Results

As shown in Figure (5.2), the effect of Planet Nine is to induce a gradual differential precession of the sun and the solar system's invariable plane [2], resulting in a solar obliquity of several degrees over the lifetime of the solar system. The Sun's present-day inclination with respect to the solar system's invariable plane (Souami and Souchay 2012) is almost exactly $i_\odot = 6$ deg. Using this number as a constraint, we have calculated the possible combinations of a_9, e_9 and i_9 for a given m_9, that yield the correct spin-orbit misalignment after 4.5 Gyr of evolution. For this set of calculations, we adopted an initial condition in which the sun's spin axis and the solar system's total angular momentum vector were aligned.

The results are shown in Figure (5.3). For three choices of $m_9 = 10$, 15, and 20 $m_\oplus$, the Figure depicts contours of the required i_9 in $a_9 - e_9$ space. Because Planet Nine's perihelion distance is approximately $q_9 \sim 250$ AU, we have only considered orbital configurations with $150 < q_9 < 350$ AU. Moreover, within the considered

[2] Although we refer to the instantaneous plane occupied by the wire with parameters a and m as the invariable plane, in our calculations, this plane is not actually invariable. Instead, it slowly precesses in the inertial frame.

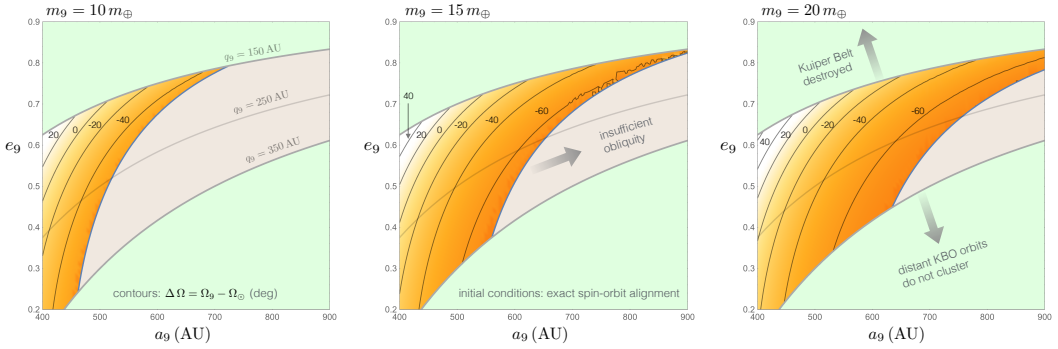

Figure 5.4: This set of plots depict the same parameter space as in Figure (5.3), but the contours represent the longitude of ascending node of Planet Nine, relative to that of the Sun, $\Delta\,\Omega$. As before the values are quoted in degrees.

locus of solutions, we neglect the region of parameter space where the required solar obliquity cannot be achieved within the lifetime of the solar system. This section of the graph is shown with a light brown shade in Figure (5.3). For the considered range of m_9, a_9 and e_9, characteristic inclinations of $i_9 \sim 15 - 30$ deg are required to produce the observed spin-orbit misalignment. This compares favorably with the results of Brown and Batygin 2016, where a similar inclination range for Planet Nine is obtained from entirely different grounds. However, we note that the constraints on a_9 and e_9 seen in Figure (5.3) are somewhat more restrictive than those in previous works. In particular, the illustrative $m_9 = 10\,m_\oplus$, $a_9 = 700$ AU, $e_9 = 0.6$ perturber considered by Batygin and Brown (2016a), as well as virtually all of the "high-probability" orbits computed by Brown and Batygin 2016 fall short of exciting 6 degrees of obliquity from a strictly coplanar initial configuration. Instead, slightly smaller spin-orbit misalignments of $i_\odot \sim 3 - 5$ deg are typically obtained. At the same time, we note that the lower bound on the semi-major axis of Planet Nine quoted in Brown and Batygin 2016 is based primarily on the comparatively low perihelia of the unaligned objects, rather than the alignment of distant Kuiper belt objects, constituting a weaker constraint.

An equally important quantity as the solar obliquity itself, is the solar longitude of ascending node[3] $\Omega_\odot \simeq 68$ deg. This quantity represents the azimuthal orientation of the spin axis and informs the direction of angular momentum transfer within the system. While the angle itself is measured from an arbitrary reference point, the difference in longitudes of ascending node $\Delta\,\Omega = \Omega_9 - \Omega_\odot$ is physically meaningful, and warrants examination.

[3]The quoted value is measured with respect to the invariable plane, rather than the ecliptic.

Figure (5.4) shows contours of $\Delta\,\Omega$ within the same parameter space as Figure (5.3). Evidently, the representative range of the relative longitude of ascending node is $\Delta\,\Omega \sim -60$ to 40 deg, with the positive values coinciding with high eccentricities and low semi-major axes. Therefore, observational discovery of Planet Nine with a correspondent combination of parameters a_9, e_9, i_9, and $\Delta\Omega$ depicted anywhere on an analog of Figures (5.3) and (5.4) constructed for the specific value of m_9, would constitute formidable evidence that Planet Nine is solely responsible for the peculiar spin axis of the sun. On the contrary, a mismatch of these parameters relative to the expected values, would imply that Planet Nine has merely modified the sun's spin axis by a significant amount.

Although Ω_9 is not known, Planet Nine's orbit is theoretically inferred to reside in approximately the same plane as the distant Kuiper belt objects, whose longitudes of ascending node cluster around $\langle\Omega\rangle = 113 \pm 13$ deg (Batygin and Brown 2016a). Therefore, it is likely that $\Omega_9 \simeq \langle\Omega\rangle$, implying that $\Delta\,\Omega \simeq 45$ deg. Furthermore, the simulation suite of Brown and Batygin 2016 approximately constrains Planet Nine's longitude of ascending node to the range $\Omega_9 \simeq 80 - 120$ deg, yielding $12 < \Delta\,\Omega < 52$ deg as an expected range of solar spin axis orientations.

If we impose the aforementioned range of $\Delta\,\Omega$ as a constraint on our calculations, Figure (5.4) suggests that $a_9 \lesssim 500\,\mathrm{AU}$ and $e_9 \gtrsim 0.4$. Although not strictly ruled out, orbits that fall in this range are likely to be incompatible with the observed orbital architecture of the distant Kuiper belt. As a result, we speculate that either (I) Planet Nine does not reside in the same plane as the distant Kuiper belt objects it shepherds, or (II) our adopted initial condition where the sun's primordial angular momentum vector coincides exactly with that of the solar system is too restrictive. Of these two possibilities, the latter is somewhat more likely.

While a null primordial obliquity is a sensible starting assumption, various theoretical studies have demonstrated that that substantial spin-orbit misalignments can be excited in young planetary systems (Lai, Foucart, and Lin 2011; Batygin 2012; Lai 2014; Spalding and Batygin 2014b, 2015b; Fielding et al. 2015), with substantial support coming from existing exoplanet data (Huber et al. 2013; Winn and Fabrycky 2015b). At the same time, the recent study of Spalding and Batygin 2016 has suggested that a fraction of multi-transiting exoplanet systems would be rendered unstable if their host stars had obliquities as large as that of the Sun, and instead inclinations as small as $1 - 2$ deg are more typical. Accordingly, it is sensible to suppose that the initial obliquity of the sun was not too different from the RMS

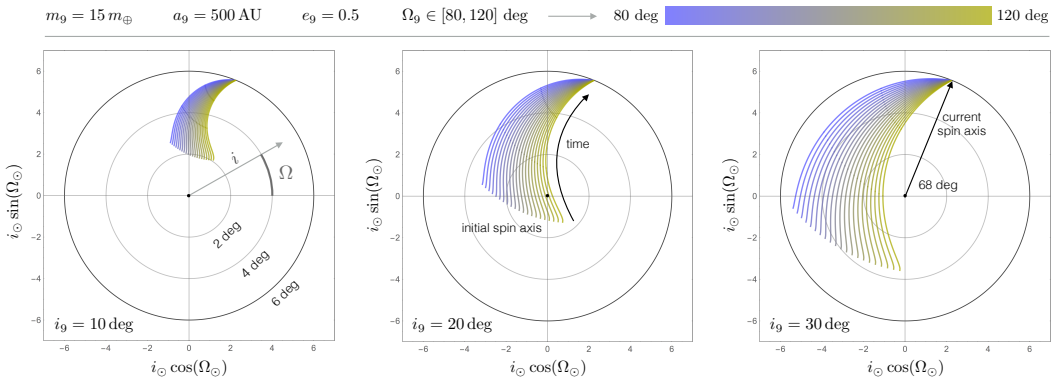

Figure 5.5: Illustrative evolution tracks of the solar spin axis, measured with respect to the instantaneous invariable plane. The graphs are shown in polar coordinates, where $i_\odot$ and $\Omega_\odot$ represent the radial and angular variables respectively. The integrations are initialized with the Sun's present-day configuration ($i_\odot = 6$ deg, $\Omega_\odot = 68$ deg), and are performed backwards in time. For Planet Nine, parameters of $m_9 = 15\,m_\oplus$, $a_9 = 500\,\mathrm{AU}$, $e_9 = 0.5$ are adopted throughout. Meanwhile, the left, middle, and right panels show results corresponding to $i_9 = 10$, 20, and 30 deg respectively. The present-day longitude of ascending node of Planet Nine is assumed to lie in the range $80 < \Omega_9 < 120$ deg and is represented by the color of the individual evolution tracks.

inclination of the planets $i_{RMS} \sim 1$ deg.

To examine this possibility, we considered whether a Planet Nine with $q_9 = 250\,\mathrm{AU}$ and $\Delta\,\Omega$ within the quoted range is consistent with a primordial solar obliquity of order $\sim 1 - 2$ deg. As an illustrative example, we adopted $a_9 = 500\,\mathrm{AU}$, $e_9 = 0.5$, $m_9 = 15\,m_\odot$, and evolved the system backwards in time. Because Hamiltonian (5.4) is integrable, a present-day combination of parameters maps onto a unique primordial state vector.

The calculations were performed for $i_9 = 10$, 20, and 30 deg, and the results are shown in Figure (5.5). Specifically, the panels depict a polar representation of the sun's spin axis evolution tracks measured from the instantaneous invariable plane, such that the origin represents an exactly aligned configuration. The color of each curve corresponds to a current value of Ω_9. Evidently, for the employed set of parameters, the calculations yield a primordial inclination range of $i_\odot \simeq 1 - 6$ deg. Intriguingly, the specific choice of $i_9 = 20\,\mathrm{deg}$, and $\Omega_9 \simeq \langle\Omega\rangle$ yields the lowest spin-orbit misalignment, that is consistent with i_{RMS}. Therefore, we conclude that the notion of Planet Nine as a dominant driver of solar obliquity is plausible.

5.4 Discussion

Applying the well-established analytic methods of secular theory, we have demonstrated that a solar obliquity of order several degrees is an expected observable effect of Planet Nine. Moreover, for a range of masses and orbits of Planet Nine that are broadly consistent with those predicted by Batygin and Brown 2016a; Brown and Batygin 2016, Planet Nine is capable of reproducing the observed solar obliquity of 6 degrees, from a nearly coplanar configuration. The existence of Planet Nine therefore provides a tangible explanation for the spin-orbit misalignment of the solar system.

Within the context of the Planet Nine hypothesis, a strictly null tilt of the solar spin-axis is disallowed. However, as already mentioned above, in addition to the long-term gravitational torques exerted by Planet Nine, numerous other physical processes are thought to generate stellar obliquities (see e.g. Crida and Batygin 2014 and the references therein). A related question then, concerns the role of Planet Nine with respect to every other plausible misalignment mechanism. Within the context of our model, this question is informed by the present-day offset between the longitudes of ascending node of Planet Nine and the Sun, $\Delta\,\Omega$. Particularly, if we assume that the solar system formed in a configuration that was strictly co-planar with the sun's equator, the observable combination of the parameters m_9, a_9, e_9, i_9 maps onto a unique value of the observable parameter $\Delta\,\Omega$.

Importantly, our calculations suggest that if the orbit of Planet Nine resides in approximately the same plane as the orbits of the $a \gtrsim 250\,\mathrm{AU}$ Kuiper belt objects (which inform the existence of Planet Nine in the first place), then the inferred range of $\Delta\,\Omega$ and Planet Nine's expected orbital elements are incompatible with an exactly co-linear initial state of the solar spin axis. Instead, backwards integrations of the equations of motion suggest that a primordial spin-orbit misalignment of the same order as the RMS spread of the planetary inclination ($i \sim 1$ deg) is consistent with the likely orbital configuration of Planet Nine. In either case, our results contextualize the primordial solar obliquity within the emerging extrasolar trend of small spin-orbit misalignments in flat planetary systems (Morton and Winn 2014), and bring the computed value closer to the expectations of the nebular hypothesis. However, we note that at present, the range of unconstrained parameters also allows for evolutionary sequences in which Planet Nine's contribution does not play a dominant role in exciting the solar obliquity.

Moreover, we find the result of Gomes, Deienno, and Morbidelli 2016 is compatible

with this work, the primary differences being the specific choice of methodology and the preference of Gomes, Deienno, and Morbidelli 2016 to consider select inclinations of Planet Nine which are significantly higher than the ~ 20 degree inclination of the distant aligned objects that first engendered the Planet Nine hypothesis (Batygin and Brown 2016a).

The integrable nature of the calculations performed in this work imply that observational characterization of Planet Nine's orbit will not only verify the expansion of the solar system's planetary album, but will yield remarkable new insights into the state of the solar system, at the time of its formation. That is, if Planet Nine is discovered in a configuration that contradicts a strictly aligned initial condition of the solar spin axis and planetary angular momentum, calculations of the type performed herein can be used to deduce the true primordial obliquity of the sun. In turn, this information can potentially constrain the mode of magnetospheric interactions between the young sun and the solar nebula (Koenigl 1991b; Lai, Foucart, and Lin 2011; Spalding and Batygin 2015b), as well as place meaningful limits on the existence of a putative primordial stellar companion of the sun (Batygin 2012; Xiang-Gruess and Papaloizou 2014).

Finally, this work provides not only a crude test of the likely parameters of Planet Nine, but also a test of the viability of the Planet Nine hypothesis. By definition, Planet Nine is hypothesized to be a planet having parameters sufficient to induce the observed orbital clustering of Kuiper belt objects with semi-major axis $a > 250$ AU (Batygin and Brown 2016a). According to this definition, Planet Nine must occupy a narrow swath in $a - e$ space such that $q_9 \sim 250\,\mathrm{AU}$, and its mass must reside in the approximate range $m_9 = 5 - 20\,m_\oplus$. If Planet Nine were found to induce a solar obliquity significantly higher than the observed value, the Planet Nine hypothesis could be readily rejected. Instead, here we have demonstrated that, over the lifetime of the solar system, Planet Nine typically excites a solar obliquity that is similar to what is observed, giving additional credence to the Planet Nine hypothesis.

Acknowledgments. We are grateful to Chris Spalding and Roger Fu for useful discussions, and to the anonymous reviewer for insightful comments.

5.5 Appendix

To octupole order in (a/a_9), the full Hamiltonian governing the secular evolution of a hierarchical triple is (Kaula 1962; Mardling 2010):

$$\begin{aligned}\mathcal{H} = -\frac{1}{4}\frac{\mu\, m_9}{a_9}\left(\frac{a}{a_9}\right)^2 \frac{1}{\varepsilon_9^3}\Bigg[&\left(1+\frac{3}{2}e^2\right)\frac{1}{4}\Big(3\cos(i)-1\Big)\Big(3\cos(i_9)-1\Big)\\ &+\frac{15}{14}e^2\sin^2(i)\cos(2\omega)+\frac{3}{4}\sin(2i)\sin(2i_9)\cos(\Omega-\Omega_9)\\ &+\frac{3}{4}\sin^2(i)\sin^2(i_9)\cos(2\Omega-2\Omega_9)\Bigg],\end{aligned}$$

where elements without a subscript refer to the inner body, and elements with subscript 9 refer to the outer body, in this case Planet Nine. Here $\mu = (M_\odot m)/(M_\odot + m) \approx m$, and ε_9 is equal to $\sqrt{1-e_9^2}$.

To attain integrability, we drop the Kozai harmonic because comparatively rapid perihelion precession of the known giant planets' orbits ensures that libration of ω is not possible (Batygin, Morbidelli, and Tsiganis 2011). Because the eccentricities of the known giant planets are small, we adopt $e = 0$ for the inner orbit. Additionally, because the inclination of the inner orbit is presumed to be small throughout the evolutionary sequence, we neglect the higher-order $\cos(2\Omega - 2\Omega_9)$ harmonic, because it is proportional to $\sin^2(i) \ll \sin(2i) \ll 1$.

Keeping in mind the trigonometric relationship $\sin i = \sqrt{1-\cos^2 i}$, and adopting canonical action-angle variables given by equation (5.3), the Hamiltonian takes the approximate form

$$\begin{aligned}\mathcal{H} = -\frac{1}{4}\frac{m\, m_9}{a_9}\left(\frac{a}{a_9}\right)^2 \frac{1}{\varepsilon^3}\Bigg[&\frac{1}{4}\left(3\left(1-\frac{Z}{\Gamma}\right)^2-1\right)\left(3\left(1-\frac{Z_9}{\Gamma_9}\right)^2-1\right)\\ &+\frac{3}{4}\left(2\left(1-\frac{Z}{\Gamma}\right)\sqrt{1-\left(1-\frac{Z}{\Gamma}\right)^2}\right)\left(2\left(1-\frac{Z_9}{\Gamma_9}\right)\sqrt{1-\left(1-\frac{Z_9}{\Gamma_9}\right)^2}\right)\cos\left(z-z_9\right)\Bigg].\end{aligned}$$

Because the inner orbit has small inclination, it is suitable to expand $\mathcal{H}$ to leading order in Z. This yields the Hamiltonian given in equation (5.4).

Since Hamiltonian (5.4) possesses only a single degree of freedom, the Arnold-Liouville theorem (Arnold 2009) ensures that by application of the Hamilton-Jacobi equation, $\mathcal{H}$ can be cast into a form that only depends on the actions. Then, the entirety of the system's dynamics is encapsulated in the linear advance of cyclic angles along contours defined by the constants of motion (Morbidelli 2002). Here,

rather than carrying out this extra step, we take the more practically simple approach of numerically integrating the equations of motion, while keeping in mind that the resulting evolution is strictly regular.

The numerical evaluation of the system's evolution can be robustly carried out after transforming the Hamiltonian to nonsingular Poincaré Cartesian coordinates

$$x = \sqrt{2Z}\cos(z) \qquad y = \sqrt{2Z}\sin(z)$$
$$x_9 = \sqrt{2Z_9}\cos(z_9) \qquad y_9 = \sqrt{2Z_9}\sin(z_9).$$

Then, the truncated and expanded Hamiltonian (5.4) becomes

$$\mathcal{H} = -\frac{1}{4}\frac{m\,m_9}{a_9}\left(\frac{a}{a_9}\right)^2\frac{1}{\varepsilon_9^3}\left[\frac{1}{4}\left(2-\frac{6}{\Gamma}\left(\frac{x^2+y^2}{2}\right)\right)\left(3\left(1-\frac{1}{\Gamma_9}\left(\frac{x_9^2+y_9^2}{2}\right)\right)^2-1\right)\right.$$
$$\left.+\,3\left(1-\frac{1}{\Gamma_9}\left(\frac{x_9^2+y_9^2}{2}\right)\right)\sqrt{1-\frac{1}{2\Gamma_9}\left(\frac{x_9^2+y_9^2}{2}\right)}\sqrt{\frac{1}{\Gamma\Gamma_9}}\left(xx_9+yy_9\right)\right].$$

Explicitly, Hamilton's equations $dx/dt = -\partial\mathcal{H}/\partial y$, $dy/dt = \partial\mathcal{H}/\partial x$ take the form:

$$\frac{dx}{dt} = \frac{a^2\,m\,m_9}{4\,a_9^3\,\epsilon_9^3}\left(\frac{3y_9\left(2\Gamma_9-x_9^2-y_9^2\right)}{4\Gamma_9}\sqrt{\frac{4\Gamma_9-x_9^2-y_9^2}{\Gamma\Gamma_9^2}}+\frac{3y}{2\Gamma}\left(1-\frac{3\left(2\Gamma_9-x_9^2-y_9^2\right)^2}{4\Gamma_9^2}\right)\right)$$

$$\frac{\partial y}{\partial t} = \frac{3\,a^2\;m\,m_9}{32\,a_9^3\,\Gamma\,\Gamma_9^2\,\epsilon_9^3}\left(2x_9\sqrt{\Gamma\left(4\Gamma_9-x_9^2-y_9^2\right)}\left(x_9^2+y_9^2-2\Gamma_9\right)\right.$$
$$\left.+\,x\left(8\Gamma_9^2+3x_9^4-12\Gamma_9y_9^2+3y_9^4+6x_9^2\left(y_9^2-2\Gamma_9\right)\right)\right)$$

$$\frac{\partial x_9}{\partial t} = \frac{3\,a^2\;m\,m_9}{16\,a_9^3\,\Gamma_9^2\,\epsilon_9^3}\left(-2y_9\left(xx_9+yy_9\right)\sqrt{\frac{4\Gamma_9-x_9^2-y_9^2}{\Gamma}}+y\left(2\Gamma_9-x_9^2-y_9^2\right)\sqrt{\frac{4\Gamma_9-x_9^2-y_9^2}{\Gamma}}\right.$$
$$\left.+\,\frac{1}{\Gamma}y_9\left(2\Gamma-3x^2-3y^2\right)\left(x_9^2+y_9^2-2\Gamma_9\right)-y_9\left(xx_9+yy_9\right)\frac{2\Gamma_9-x_9^2-y_9^2}{\sqrt{\Gamma\left(4\Gamma_9-x_9^2-y_9^2\right)}}\right)$$

$$\frac{\partial y_9}{\partial t} = -\frac{3\,a^2\;m\,m_9}{16\,a_9^3\,\Gamma_9^2\,\epsilon_9^3}\left(-2x_9\left(xx_9+yy_9\right)\sqrt{\frac{4\Gamma_9-x_9^2-y_9^2}{\Gamma}}+x\left(2\Gamma_9-x_9^2-y_9^2\right)\sqrt{\frac{4\Gamma_9-x_9^2-y_9^2}{\Gamma}}\right.$$
$$\left.+\,\frac{1}{\Gamma}x_9\left(2\Gamma-3x^2-3y^2\right)\left(x_9^2+y_9^2-2\Gamma_9\right)-x_9\left(xx_9+yy_9\right)\frac{2\Gamma_9-x_9^2-y_9^2}{\sqrt{\Gamma\left(4\Gamma_9-x_9^2-y_9^2\right)}}\right)$$

The evolution of the sun's axial tilt is computed in the same manner. The Hamiltonian describing the cumulative effect of the planetary torques exerted onto the solar spin-

axis is given by Equation (5.6). Defining scaled Cartesian coordinates

$$\tilde{x} = \sqrt{2\,\tilde{Z}}\cos(\tilde{z}) \qquad\qquad \tilde{y} = \sqrt{2\,\tilde{Z}}\sin(\tilde{z}),$$

we have:

$$\tilde{\mathcal{H}} = \sum_j \left(\frac{m_j}{4a_j^3}\right)\tilde{a}^2\left[\frac{3}{\tilde{\Gamma}}\left(\frac{\tilde{x}^2+\tilde{y}^2}{2}\right) + \frac{3}{4}\sqrt{\frac{1}{\tilde{\Gamma}\Gamma}}(\tilde{x}x+\tilde{y}y)\right].$$

Accordingly, Hamilton's equations are evaluated to characterize the dynamics of the sun's spin pole, under the influence of the planets:

$$\frac{d\tilde{x}}{dt} = -\sum_j \left(\frac{m_j}{4a_j^3}\right)\tilde{a}^2\left(\frac{3}{4}y\sqrt{\frac{1}{\Gamma\tilde{\Gamma}}} + \frac{3\tilde{y}}{\tilde{\Gamma}}\right)$$

$$\frac{d\tilde{y}}{dt} = \sum_j \left(\frac{m_j}{4a_j^3}\right)\tilde{a}^2\left(\frac{3}{4}x\sqrt{\frac{1}{\Gamma\tilde{\Gamma}}} + \frac{3\tilde{x}}{\tilde{\Gamma}}\right)$$

Note that unlike Γ and Γ_9, which are conserved, $\tilde{\Gamma}$ is an explicit function of time, and evolves according to the Skumanich relation. The above set of equations fully specifies the long-term evolution of the dynamical system.

Chapter 6

FEASIBILITY OF A RESONANCE-BASED PLANET NINE SEARCH

ABSTRACT

It has been proposed that mean motion resonances (MMRs) between Planet Nine and distant objects of the scattered disk might inform the semimajor axis and instantaneous position of Planet Nine. Within the context of this hypothesis, the specific distribution of occupied MMRs largely determines the available constraints. Here we characterize the behavior of scattered Kuiper Belt objects arising in the presence of an eccentric Planet Nine ($e_9 \in 0.1, 0.7$), focusing on relative sizes of populations occupying particular commensurabilities. Highlighting the challenge of predicting the exact MMR of a given object, we find that the majority of resonant test particles have period ratios with Planet Nine other than those of the form $P_9/P = N/1, N/2$ ($N \in \mathbb{Z}^+$). Taking into account the updated prior distribution of MMRs outlined in this work, we find that the close spacing of high-order resonances, as well as chaotic transport, preclude resonance-based Planet Nine constraints from current observational data.

6.1 Introduction

The primary line of evidence for the existence of "Planet Nine," a distant, massive planet in the solar system, stems from the physical confinement of KBO orbits with semimajor axis in excess of $a \sim 250$ AU and perihelion distance beyond Neptune. While the dominant mode of dynamical coupling between Planet Nine and KBO orbits remains a subject of active investigation, it has been suggested that mean-motion resonances (MMRs) may widely occur in the distant, eccentric confined population of the Kuiper Belt. In particular, Batygin and Brown 2016a were the first to recognize that synthetic particles exhibiting anti-alignment with Planet Nine exhibit temporary capture into MMRs with Planet Nine persisting over hundred-Myr time intervals. Although Beust 2016; Malhotra, Volk, and Wang 2016 have suggested that even non-resonant bodies might survive in a detached, anti-aligned state for the lifetime of the solar system, Batygin and Morbidelli 2017 have found that, while secular effects are responsible for orbital clustering and perihelion detachment of KBOs in the confined population, MMRs are implicated in their long-term survival.

Explicit behavioral dependence on the period and phase of resonantly interacting bodies suggests that MMRs between Planet Nine and distant members of the scattered disk might encode information about the present-day semimajor axis and current position of Planet Nine, a possibility explored quantitatively by Millholland and Laughlin 2017. To this end, we note that the likelihood for a given object to occupy a specific resonance is fundamental to constraining the semimajor axis a_9 and subsequently the mean anomaly M_9 of Planet Nine. Therefore, one aim of this work is to produce a characterization of relative population sizes expected to occupy specific MMRs in the high-eccentricity case of Planet Nine.

While high-order mean-motion resonances[1] have negligible capture probability in the well-studied case of the circular restricted three-body problem, this tendency degrades in the high-eccentricity scenario of Planet Nine and, by extension, the population of KBOs sculpted by its gravity (Batygin and Brown 2016a). In other words, the typical ordering of terms found in the low-eccentricity expansion of the disturbing function (Murray and Dermott 1999b) breaks down for the problem at hand, warranting a numerical evaluation of capture probabilities for specific resonances. Finally, in light of the prior distribution of MMRs derived in this work, we explore the feasibility of updated resonant constraints on Planet Nine's

[1] For m/n resonance, the order is typically defined as $|m - n|$.

present-day orbit and location.

The first potential resonance-based constraint is that on the semimajor axis of Planet Nine. Ideally, given the observed population of confined KBOs, it would be desirable to deduce likely period ratios with Planet Nine, thereby deriving the associated value of a_9. Using this brand of logic, Malhotra, Volk, and Wang 2016 reported an a_9 prediction of ~ 665 au, produced by supposing that the six confined objects known at the time reside in $P_9/P_{\rm KBO} = N/1$ and $N/2$ period ratios with Planet Nine. Subsequently, Millholland and Laughlin 2017 presented a more comprehensive analysis of the possibility of resonant constraints. Specifically, they constructed a a_9 distribution by assuming small integer ratio mean-motion resonances with 11 known KBOs, followed by a Monte Carlo test to confirm the significance of the highest peak in their distribution. Enticingly, the highest peak in their a_9 distribution occurs around 660 au, in apparent agreement with Malhotra, Volk, and Wang 2016. The second potential resonance-based constraint on the present-day, instantaneous position of the planet in its orbit requires knowledge of the resonant angles themselves. Crucially, such a constraint would be highly valuable in the observational search for Planet Nine.

This chapter is organized as follows. Section 6.2 describes our suite of semi-averaged n-body simulations. Section 6.3 describes the manner in which these simplified simulations capture the essence of the outer Kuiper belt's interactions with Planet Nine, and delineates the resulting numerically derived prior distribution of MMRs. The feasibility of resonance-based determination of Planet Nine's current location is further discussed in Section 6.4. Concluding remarks are provided in Section 6.5.

6.2 Two-Dimensional Numerical Simulations

By now, a considerable number of studies, employing variable levels of approximation aimed at simulating the dynamical evolution induced by Planet Nine, have been published in the literature (Batygin and Brown 2016a, 2016b; Brown and Batygin 2016; Bailey, Batygin, and Brown 2016; Fuente Marcos, Fuente Marcos, and Aarseth 2016; Shankman et al. 2016; Millholland and Laughlin 2017; Lawler et al. 2017; Becker et al. 2017; Batygin and Morbidelli 2017; Hadden et al. 2018). It has been found, in n-body simulations accounting for the observed inclinations of distant KBOs and the $\sim 20-30$ degree inclination of Planet Nine, that objects tend to chaotically skip among commensurabilities. The primary aim of this work is to

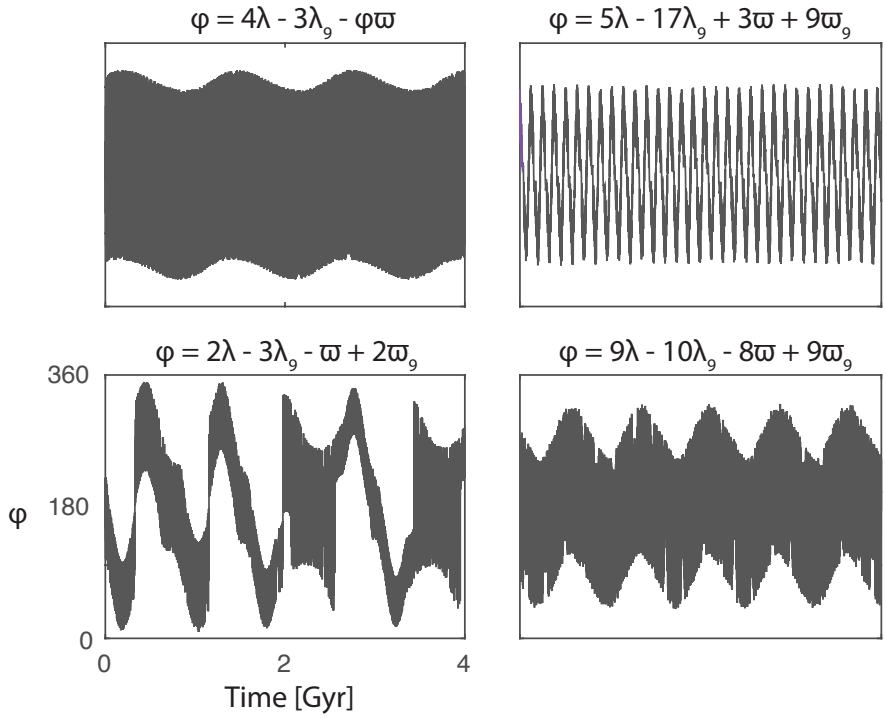

Figure 6.1: Four examples of resonant angles $\varphi = j_1\lambda + F\lambda_9 + j_3\varpi + j_4\varpi_9$, for a variety of resonances.

characterize a prior distribution of mean motion resonances in order to ascertain the feasibility of resonance-based constraints on Planet Nine, and such transitional behavior obfuscates the classification of specific MMRs. Thus, we employ a simplified, two-dimensional model of the solar system to understand the degree of resonance-based constraints that can be made. If significant resonance-based Planet Nine constraints can be obtained from present observational data, this capability should be best reflected in this highly idealized two-dimensional model.

Within the framework of this two-dimensional model, we confine all objects to the plane and average over the Keplerian motion of the known giant planets. Accordingly, the solar system interior to 30 au is treated as a central mass with a J_2 gravitational moment having magnitude equivalent to the mean-field contribution of the canonical giant planets to the secular evolution of exterior bodies (Burns 1976; Batygin and Brown 2016a). Hence, Planet Nine is the only massive perturber in these simulations. This model omits various realistic details. Notably, modulations in the eccentricity and inclination of KBOs due to close-range interactions with Neptune, as well as dynamics induced by the mutual inclination of the KBOs

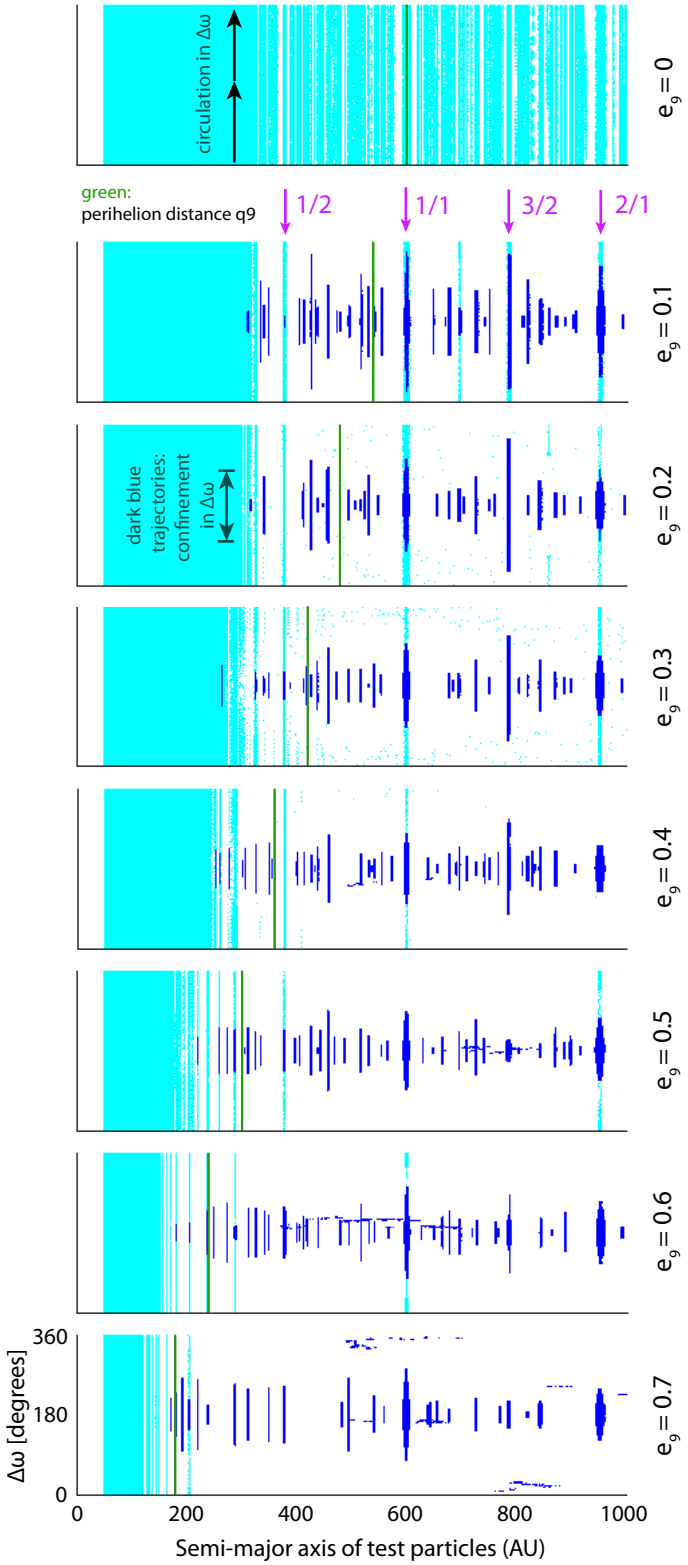

Figure 6.2: Trajectories in semimajor axis and longitude of perihelion offset $\Delta\varpi$ for all bodies surviving the entire 4-Gyr duration of simulations including a $10M$ Planet Nine with a_9 = 600 au. The anti-aligned population (dark blue) is distinguished from other bodies (light blue) by libration in $\Delta\varpi$. Furthermore, the approximate radius below which confinement does not occur is typically lower than the perihelion distance q_9 of Planet Nine (green). Each plot corresponds to the result for a specific eccentricity e_9 of Planet Nine. Among simulations having an eccentric Planet Nine, several low-order resonances are preferentially occupied, including the 1/2, 1/1, 3/2, and 2/1 resonances. However, predominantly occupied are a variety of high-order resonances.

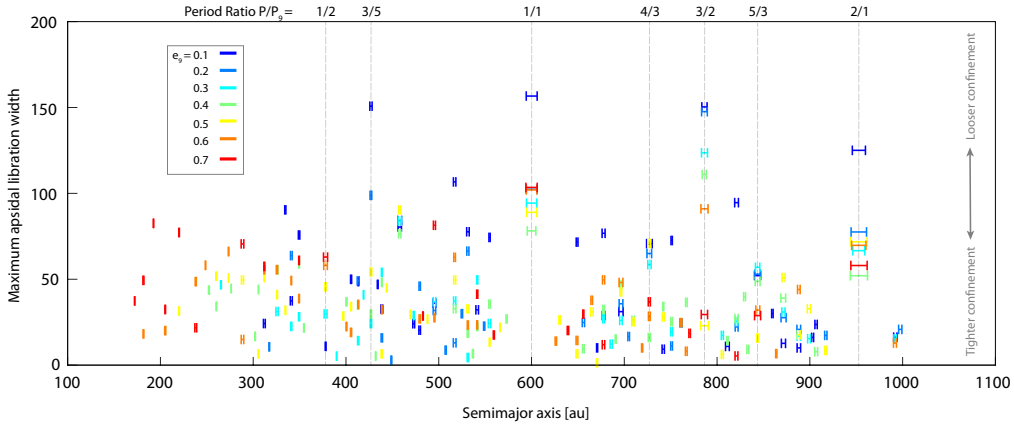

Figure 6.3: The range of semimajor axis and maximum apsidal libration width exhibited in simulations by apsidally confined objects in specific resonances, across simulations featuring a range of Planet Nine eccentricities e_9.

with Planet Nine, are absent from our calculations. Crucially, however, due to the lack of repeated transitions between resonances induced among surviving objects, these simplified simulations allow rigorous identification of the resonances in which objects reside, and their capacity to reveal Planet Nine's parameters.

We implemented direct n-body simulations using the mercury6 integration package (Chambers 1999), employing the built-in Hybrid symplectic/Bulirsch-Stoer integrator (Wisdom and Holman 1992; Press et al. 1992), with time step chosen to be $1/8$ the orbital period of Neptune. In the simulations, we evolve an initially axisymmetric disk of eccentric test particles having uniformly random angular distribution and perihelion distance and semi-major axis randomly drawn from the $q \in [30, 50]$ au and $a \in [50, 1000]$ au range, respectively. While the initial distribution of test particles does not reflect the complete evolution of KBOs into resonance with Planet Nine, it serves as a probe of relative strengths of resonances. For each of the eight values of e_9 tested, 6000 such test particles were randomly initialized and simulated. Particles attaining radial distances $r < 10,000$ au or $r < 30$ au were removed.

In principle, the relative strengths of resonances are not expected to vary significantly with a_9, as the relative strengths of individual terms associated with specific resonances in the usual expansion of the disturbing function only depend on the semimajor axis ratio of the interacting bodies (Murray and Dermott 1999b). Therefore, Planet Nine was assigned a single, nominal semimajor axis, $a_9 = 600$ au. However, we note that different semimajor axes of a_9 would, in reality, subject the innermost

resonances to variable levels of secular coupling with the canonical giant planets, altering the resonant widths slightly. Still, $a_9 = 600$ au is roughly in keeping with the semimajor axis predictions of Millholland and Laughlin 2017; Malhotra, Volk, and Wang 2016; thus, we choose this value of a_9. Moreover, eccentricities e_9 were tested ranging from 0 to 0.7 in increments of 0.1. The simulations in this work span 4 Gyr in approximate accordance with the solar system's lifetime.

Because this work addresses the distribution of closely-spaced, high-order mean motion resonances, which have finite width in semimajor axis, the period ratio alone is insufficient to confirm a specific resonance. Instead, we confirmed specific mean-motion resonances with Planet Nine among the surviving objects by searching for a librating resonant argument (Figure 6.1). The general form of such a resonant argument can be stated as $\varphi = j_1\lambda + j_2\lambda_9 + j_3\varpi + j_4\varpi_9$, where the d'Alembert relation, following from rotational symmetry, restricts the integer coefficients j to satisfy $\sum_{i=1}^{4} j_i = 0$ (Murray and Dermott 1999b). (For the 2-dimensional case, we adopt the standard convention that longitude of ascending node $\Omega = 0$, thus $\varpi = \omega$.) Based on the values found for coefficients j_1 and j_2, identification of a critical argument informs the individual resonance in which a particle resides. Specifically, for an object in p/q resonance with Planet Nine, the resonant argument takes the form $\varphi = q\lambda - p\lambda_9 + j_3\varpi + j_4\varpi_9$.

6.3 Behavioral regimes of surviving KBOs

For the range $e_9 \in [0, 0.7]$ of Planet Nine eccentricities examined, the range of longitude of perihelion explored by test particles surviving for the full length of the 4-Gyr simulations is shown in Figure (6.2). For all cases of nonzero perturber eccentricity, the surviving bodies occupy several specific regimes. Below a critical semimajor axis a_{crit}, the vast majority of surviving bodies exist in a circulating regime, in which $\Delta\varpi$ covers all angular values. Notably, the value of a_{crit} depends the semimajor axis, eccentricity, and mass of Planet Nine, and does not simply correspond to the perihelion distance of Planet Nine.

Objects with $a > a_{\text{crit}}$ exhibit orbital confinement, with the longitude of perihelion of the object relative to that of Planet Nine, $\Delta\varpi$, librating about 180 degrees over the course of the simulation (i.e. in an anti-aligned configuration with respect to Planet Nine's orbit). This population is taken to be analogous to the clustered population of the observed distant Kuiper belt objects (Batygin and Brown 2016a), and will be the focus of the following sections of this paper.

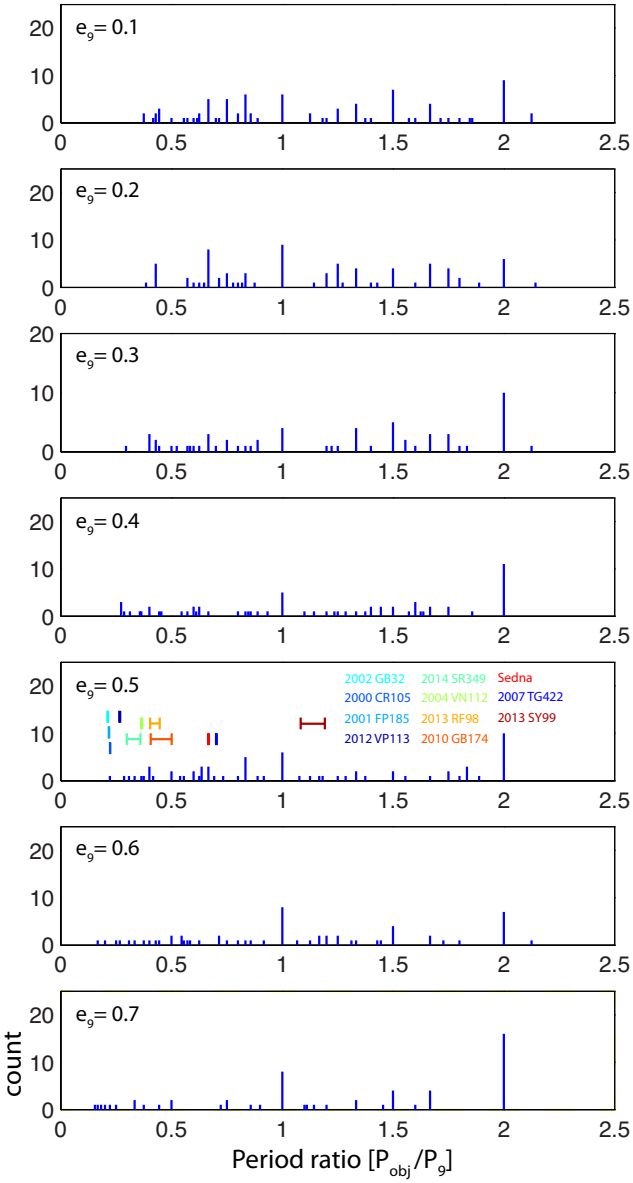

Figure 6.4: Histogram with discrete bins showing the number of objects in each occupied resonance, for a range of Planet Nine eccentricities. Each bin is located at the exact commensurability ascertained by identification of resonant angles for objects. Note the close spacing of occupied high-order resonances. Beyond the axis bound, single objects at the $10/1$, $11/1$, $13/3$, $13/4$, $20/1$, and $22/7$ commensurabilities were also identified. The colored lines in the lower plot delineate the locations of commensurabilities predicted by Malhotra, Volk, and Wang 2016 (i.e. with Sedna at the interior $3/2$ resonance), with $1-\sigma$ observational error bars. Due to observational error in the KBO semimajor axes and the close spacing of occupied high-order resonances, we find there is no clear preference for this as opposed to many other resonant configurations.

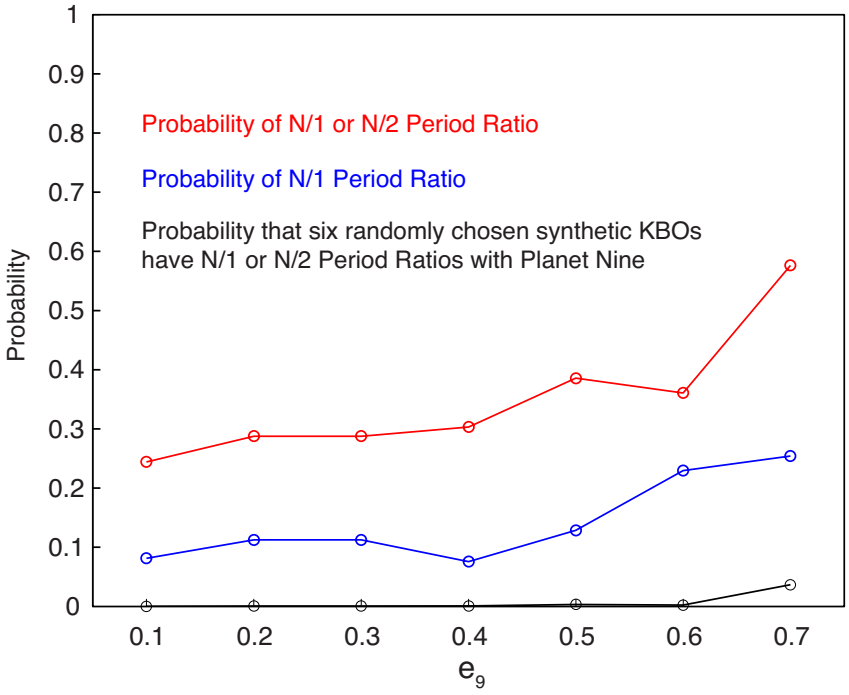

Figure 6.5: Probability that a chosen synthetic particle has a period ratio $P_9/P = N/1$ ($N \in \mathbb{Z}^+$) (blue), or a period ratio $N/1$ or $N/2$ (red). In particular, the probability that any six independently chosen objects will all have such period ratios is $\mathbb{P}(P_9/P \in \{N/1, N/2\})^6 < 0.05$, highlighting the prevalence of high-order resonances expected in the high-eccentricity case of Planet Nine.

While the majority of surviving bodies found in our two-dimensional simulations occupy the two aforementioned regimes, there are some exceptions. In particular, circulating objects are also found at distances significantly beyond a_{crit}–specifically, within a neighborhood of the $1/2$, $1/1$, $3/2$, and $2/1$ resonances with Planet Nine. Another class of objects observed is those that migrate stochastically through a variety of semimajor axes and values of $\Delta\varpi$ while avoiding ejection. Although fewer than 1 in 600 bodies exhibit this behavior in our two-dimensional simulations, such migratory evolution bears resemblance to the stochastic transport between commensurabilities observed among objects in full three-dimensional simulations.

The dynamical regimes occupied by test particles show broad-ranging consistency across all nonzero Planet Nine eccentricities examined. For example, Figure (6.3) shows the maximum width in a and widest apsidal excursion $|\omega - 180°|$ exhibited among objects in identified resonances. Notably, the width in a is similar across the e_9 tested, and there appears not to be a strict relation between e_9 and confinement in $\Delta\varpi$. Instead, the primary indicators of e_9 in these simulations are the location

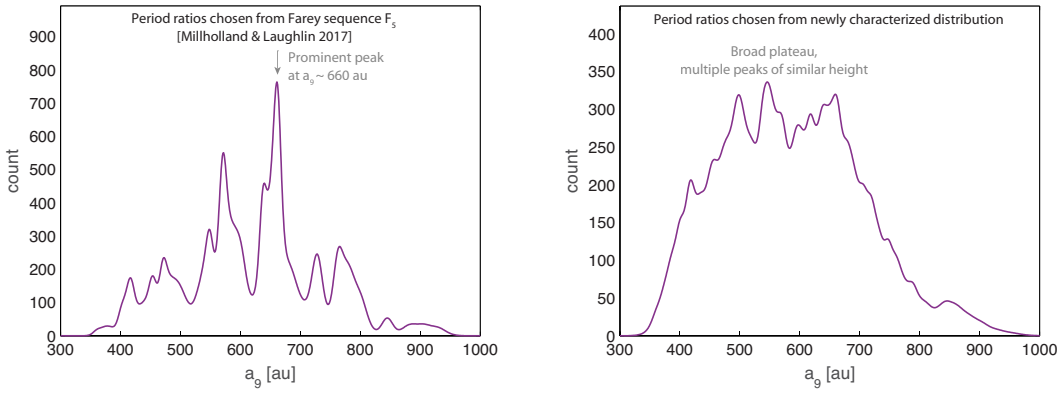

Figure 6.6: Two distributions of the semimajor axis a_9, illustrating the difference invoked by considering the prior distribution of period ratios developed from the two-dimensional simulations in this work. *Left:* Distribution developed by Millholland and Laughlin 2017. In constructing this distribution, the period ratios of observed objects were assumed to follow the distribution of the Farey sequence F_5 of period ratios having denominator ≤ 5, with all such period ratios assumed equally likely. *Right:* Distribution developed assuming the updated period ratio distribution. For details about the procedure invoked to produce these distributions, see Millholland and Laughlin 2017.

of a_{crit} and, in the two-dimensional case, the prevalence of circulating objects at the $1/2$, $1/1$, $3/2$, and $2/1$ resonances for lower-e_9 cases (Figure 6.2).

Numerically derived period ratio distribution

All confined objects in the simulation are in confirmed mean-motion resonance with Planet Nine. Moreover, the identified resonant angles persist over the full 4-Gyr simulation. This stable behavior can be attributed to the lack of interference from close encounters with Neptune occurring in unaveraged three-dimensional simulations. Figure (6.4) shows the number of bodies found in individual resonances across the seven simulations with e_9 ranging from 0.1 to 0.7. In all simulations with $e_9 > 0$, the individual resonances with the greatest number of occupied objects were the $1/1$ and exterior $2/1$ resonances. However, as the next section will discuss, most objects do not occupy these particular commensurabilities.

6.4 Feasibility of resonant constraints on Planet Nine

As Planet Nine's semimajor axis defines its period ratio with resonant KBOs, it is natural to attempt to predict a_9 through commensurabilities. Such predictions have been produced by Malhotra, Volk, and Wang 2016; Millholland and Laughlin 2017, in rough agreement at $a_9 \sim 665$ and $a_9 \sim 654$ au respectively. In particular,

Malhotra, Volk, and Wang 2016 postulated that $a_9 \sim 665$ au, placing Sedna at interior $3/2$ resonance and five other objects at $N/1$ and $N/2$ interior resonances with Planet Nine. However, the prior distribution of MMRs derived in this work appears to suggest that the majority of objects do not have period ratios with Planet Nine of the form $N/1$ or $N/2$ (Figure 6.4). Furthermore, the probability that any six independently chosen objects all have $N/1$ or $N/2$ period ratios is less than 0.05 (Figure 6.5). We therefore conclude the assumption that distant KBOs are likely to reside in $N/1$ and $N/2$ resonances with Planet Nine is not supported by these numerical simulations.

We now turn to our numerically derived resonance distribution from our two-dimensional simulations and consider what information can be gathered about Planet Nine's whereabouts, following the statistical approach developed by Millholland and Laughlin 2017. Each iteration of their method proceeds as follows: First, they draw a sample m_i from a truncated Gaussian mass distribution for Planet Nine, with mean $10M$ and bounds $5 - 20M$. Then, they randomly select one of the known distant KBO semimajor axes, together with one orbital period ratio from a chosen period ratio distribution. The implied Planet Nine semimajor axis is then calculated. If the implied semimajor axis lies in the range $[200 \text{ au} + 30m_i/M_\odot, 600 \text{ au} + 20m_i/M_\odot]$ (derived based on Brown and Batygin 2016), a Gaussian centered at the implied semimajor axis, with σ equal to the approximate resonance width, is added to the a_9 distribution being constructed. These steps are repeated until the resulting a_9 distribution is converged upon. In this way, Millholland and Laughlin 2017 have provided a rigorous means of estimating a_9 by inferring mean motion resonances with the observed Kuiper belt objects. However, the period ratio distribution from which they drew their sample was simplified; they considered period ratios in the Farey sequence F_N, which includes all fractions with denominators up to N (for example, $F_4 = \{\frac{1}{2}, \frac{1}{3}, \frac{1}{4}, \frac{2}{3}, \frac{3}{4}\}$). Critically, Millholland and Laughlin 2017 made the assumption that period ratios in F_N are equally occupied.

In contrast, Figure (6.6) illustrates the difference between the a_9 distribution reported by Millholland and Laughlin 2017 using the Farey sequence F_5 distribution, versus the distribution obtained using the identical methodology and set of observed objects, but employing the period ratio distribution obtained in this work. We note that, because Planet Nine's eccentricity is poorly constrained, and because the period ratio distributions for varied e_9 resemble each other across the board, we have considered the sum distribution of period ratios found for all cases $e_9 > 0$. Due to

the close spacing of many occupied high-order resonances, the prominent peak of the distribution of Millholland and Laughlin 2017 is replaced in our a_9 distribution by a broad plateau. We note that reduction of peak prominence also occurs when the resonance distribution is taken to be an equally-weighted Farey sequence of higher order, although such treatment neglects the relative population occupying each resonance.

Indeed, our resulting plateau-shaped distribution for a_9 demonstrates that when the prevalence of high-order MMRs is considered, hopes of a resonance-based constraint on a_9 all but vanish, at least given current observations. Furthermore, compared to the simulations of a simplified Planet Nine system described in this work, additional behavior arises in fully inclined simulations which include the canonical giant planets (especially Neptune). Because the behavior exhibited by eccentric test particles in these more comprehensive simulations includes repeated transitions between resonances, fully rigorous determination of the distribution of objects among mean motion resonances is challenged. Moreover, a running average of period ratios with Planet Nine among objects in full simulations shows no obvious prevalence of objects occupying particular resonances (Figure 6.7). Without constraints on the period ratios between observed objects and Planet Nine, constraints on Planet Nine's present-day location along its orbit remain elusive.

6.5 Conclusion

Using two- and three-dimensional direct n-body simulations, we have highlighted several features inherent to the resonant dynamics of distant KBOs. Overall, we have illustrated that the resonance-based search for Planet Nine is frustrated by the increased strength of high-order resonances that follows from the high eccentricity of Planet Nine and the test particles. Existing work aiming to predict a_9 by considering possible period ratios between Planet Nine and observed objects (Malhotra, Volk, and Wang 2016; Millholland and Laughlin 2017) unfortunately neglects the prevalence of high-order resonances and chaotic transport—traits of the system which, in practice, challenge characterization of the specific resonances occupied.

A constraint on a_9, to a degree allowing inference of the specific resonances in which observed objects reside, appears crucial for constraining the true anomaly of Planet Nine through resonant means. The degeneracy between mass and semimajor axis in simulations further complicates such efforts. Moreover, because knowledge of the specific period ratios between objects and Planet Nine are necessary to rule out

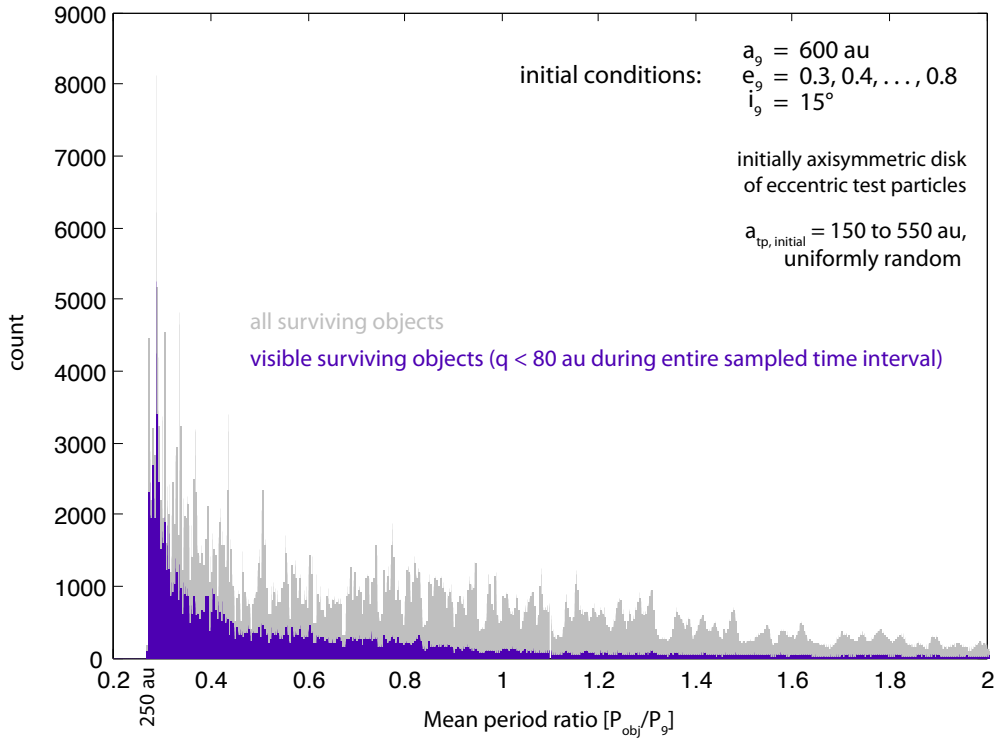

Figure 6.7: Mean period ratio with Planet Nine of objects in full three-dimensional simulations, sampled in 1-Myr intervals. Objects surviving the 4 Gyr simulation, with perihelion distance $q > 30$ and semimajor axis $a > 250$ au, were considered. These simulations included all canonical giant planets of the solar system, in addition to Planet Nine. In order to avoid sampling the mean semimajor axis $\|a_{t.p.}\|$ of a test particle during scattering events, time intervals having $\max(a_{t.p.}) > \|a_{t.p.}\| + 30$ au were excluded. A predominance of objects occupying any particular resonance is evidently lacking. This example suggests that the lessened predominance of low-order resonances in the high-eccentricity case of Planet Nine, demonstrated in the two-dimensional simulations of this work, continues to hold relevance in the realistic fully inclined case.

Planet Nine's instantaneous position from specific regions of its orbit, resonance-based constraints on the current orbital position of Planet Nine do not appear feasible at this time.

The prevalence of high-order resonances in our simulations, brought about by the high eccentricity of the system, serves as a reminder that care should be taken before assuming the dynamics of circular orbits will hold for an eccentric case, such as Planet Nine's interaction with the confined population. For example, the lack of orbital angle clustering found by Lawler et al. 2017 in n-body simulations can be explained in part as resulting from their condition that $e_9 = 0$. It has already been established (Batygin and Brown 2016a; Brown and Batygin 2016) that Planet Nine's orbit must be eccentric to produce the confinement of distant, eccentric Kuiper Belt objects. Although it follows from symmetry, the results of our direct n-body simulations provide additional illustration of this fact (Figure 6.2). Because confinement occurs at the lowest nonzero Planet Nine eccentricity tested, $e_9 = 0.1$, the lowest eccentricity necessary to produce confinement in the planar eccentric three-body system is a possible subject of interest for future work.

In summary, the expected phase-protected mean-motion resonances between observed distant KBOs and Planet Nine offer a tantalizing connection to the semimajor axis and current position of Planet Nine. Due to the high eccentricities involved, the underlying resonant dynamics are fundamentally different from the circular case, and high-order resonances with Planet Nine appear to dominate in the anti-aligned population. Considering this and taking the updated MMR distribution into account, the obtainable constraints on a_9 appear far less useful than suggested by Malhotra, Volk, and Wang 2016; Millholland and Laughlin 2017. A resonance-based constraint on the mean anomaly M_9 appears to require a constraint on a_9, so that correct resonant angles of observed objects can be deduced and specific regions of the orbit excluded. Thus, in addition to its unprecedented nature among planets in the solar system, the large eccentricity of Planet Nine currently postpones precise prediction of its position.

Chapter 7

CONCLUSIONS AND FUTURE DIRECTIONS

This thesis has addressed a range of topics related to the interior and orbital dynamics of several, varied classes of planets, both within our own solar system and orbiting other stars. In recent decades, some of these worlds—including hot Jupiters on extremely close-in, several-day orbits, as well as the hypothesized distant Planet Nine at an orbital distance of hundreds of au—have challenged traditional, pre-existing notions, based on the canonical eight planets of our solar system, of the planetary arrangements that can occur around sunlike stars. Accordingly, the chapters presented in this work have addressed several critical questions associated with the orbital and interior dynamics of planets residing at the extreme inner and outer fringes of planetary systems.

Chapters II and III have discussed the multiple proposed formation pathways of hot Jupiters, and the orbital and tidal dynamics of these extremely close-in giant planets. In Chapter II, it is specified how the mechanism of high-eccentricity inward migration, known to be responsible for the formation of some hot Jupiters, can, in principle, be harnessed to inform tidal dissipation in ecccentric, short-period giant planets with characterized exterior perturbers. A case study of the hot Jupiter HAT-P-2b has been carried out, demonstrating that, in addition to the simple tidal constraints that can be achieved based solely on the close-in planet's orbital state, detailed constraints on dissipation rates are attainable based on the hot Jupiter's observed semimajor axis and eccentricity, when combined with orbital and mass constraints on the exterior perturber (Lewis et al. 2013) expected to be implicated in the inner planet's attainment of a high-eccentricity, tidally dissipative state. Although it should be noted that short-period giant planets such as HAT-P-2b might potentially represent an intrinsically different population from other giant planets such as Jupiter and Saturn which have not undergone circumstances to convert them into hot Jupiters, the limited number of examples of giant planets in our own solar system means that any attainable tidal constraints on giant exoplanets should be intrinsically valuable for developing an understanding of planetary tidal processes.

Moreover, although observations of high-eccentricity hot Jupiters such as HAT-

P-2b offer a clear indication that the process of high-eccentricity migration is a viable generating mechanism for close-in giant planets, Chapter III puts forth novel evidence in apparent support of the in situ formation pathway as a possible major source of these enigmatic short-period giants. Following from relatively simple, generally accepted relationships between the viscous accretion rate of protoplanetary disks and the voids magnetically carved out in the centers of disks by rotating T-tauri stars, the -2/7 power-law relationship derived in Chapter III offers an explanation for how in situ formation could potentially account for inner edge of the period-mass distribution of the hot Jupiters. Accordingly, the potential for the mechanism of in situ hot Jupiter formation to offer an explanation for the characteristic boundary between the hot Jupiter population and the relatively unpopulated "desert" in the period-mass plane represents apparent evidence in support of the hypothesis that in situ formation is a dominant driver of hot Jupiter production.

However, if in situ formation is indeed the dominating mechanism by which hot Jupiters arise, numerous critical questions must then be addressed. In particular, if it is the case that hot Jupiters generally form in situ and do not typically form via disk-driven (Type-II) migration, it must then be established why long-range inward migration is less active process than classically expected. Moreover, a major issue with the picture of disk-driven migration as the dominant formation mode is that it becomes a serious challenge to explain how the observed mass-period distribution of hot Jupiters could then arise. Moreover, if hot Jupiters predominantly do form in situ rather than migrating inward from more distant orbits of tens of au, another major outstanding issue is then the question of why hot Jupiters are not found to orbit greater proportion of sunlike stars. Given that Batygin, Bodenheimer, and Laughlin 2016a have demonstrated the feasibility of in situ core accretion when a suitable core is available, and given that Kepler-like, close-in planets massive enough to serve as suitable cores for nucleating hot Jupiters are now understood to be a standard outcome of planet formation, occurring around $\sim 30\%$ of sunlike stars (Zhu et al. 2018), *why*, then, are hot Jupiters only found to occur around a mere $\sim 1\%$ of such stars (Howard et al. 2010; Gould et al. 2006; Wright et al. 2012)? What processes are limiting the formation of these planets? The absence of massive planets on short-period orbits in our own solar system remains a related mystery, especially considering that sufficient material was available to form the gas giants Jupiter and Saturn at greater orbital distances. Some existing work has sought to explain how the existence of "cold" Jupiters, including Jupiter in our own system, might inhibit formation of close-in, massive planets (Batygin and Laughlin 2015),

as well as investigating the role of tilted host star rotational bulges (Spalding, Marx, and Batygin 2018) and planetary mass excesses (Johansen et al. 2012) in destroying sets of close-in, Kepler-like planets. However, the question of why some planetary systems around sunlike stars have relatively empty inner regions, while others host close-in super-Earths, or even hot Jupiters, remains far from settled. Any complete theory of planet formation must account for the existence of our own solar system's architecture, as well as the other, varied planetary architectures surrounding sunlike stars.

At the long-period orbital extreme, Chapters V and VI have addressed the orbital dynamics and search for the hypothesized Planet Nine. While the view of Planet Nine as potentially being the primary driver of the six-degree solar obliquity has, in view of updated constraints on its orbit and mass, become outdated since the writing and publication of the work in Chapter V, the dynamical effect of a distant, inclined, massive object on an inner planetary system remains entirely relevant to the general understanding of planetary system dynamics. With evidence emerging for the existence of planetary- or brown-dwarf-class objects residing on gravitationally bound orbits potentially as wide as hundreds to thousands of au (e.g. Fomalhaut b; Liu et al. 2019, 2MASS J21265040-8140293; Deacon, Schlieder, and Murphy 2016), the dynamical effects of Planet Nine on the solar obliquity, as discussed in Chapter V, have not lost their general pertinence to planetary system dynamics, nor is such a distant, massive object in our own system lacking in apparent exoplanetary precedent. While the analysis presented in Chapter VI unfortunately presents a pessimistic outlook on the feasiblility of rapid direct detection of this elusive, proposed distant planet in our system, it simultaneously does not constitute evidence against Planet Nine's existence. Rather, Chapter VI merely demonstrates that the eccentric dynamics preclude the use of mean-motion resonances in carrying out the search. As the scientific community continues to await Planet Nine's direct detection, observations of long-period exoplanetary analogues may potentially shed light for inferring the possible nature and formation of our own putative distant planet.

In addition to planets at the most extreme inner and outer orbital regimes of planetary systems, in Chapter IV, this work has addressed the interiors of the so-called *ice giants* Uranus and Neptune, the furthest directly observed solar system planets. While the existence of these planets in our solar system has been known for well over a century, the compositions and interior dynamics of Uranus and Neptune remain poorly known relative to the gas giants Jupiter and Saturn. The obstacle to

Earth-based observations posed by their greater orbital distances, as well as a general lack of spacecraft coverage compared to all other planets[1], have been major factors implicated in the continuation of several major unsolved questions related to Uranus and Neptune. In particular, the order-of-magnitude difference in observed heat flows between the two planets, despite their distinctively similar masses, radii, and quadrupolar-dominant magnetic fields, has represented a longstanding paradox, as addressed in Chapter IV. Moreover, as discussed in that chapter, basic constraints on the interior compositions of Uranus and Neptune are inherently much more difficult to attain compared to Jupiter and Saturn, due to the compositional degeneracy posed by their intermediate densities. As gravitational and magnetic data cannot uniquely inform the interior compositions of the ice giants, in Chapter IV, we have turned to thermodynamic arguments about the mixing of likely major constituents, which, combined with observations of the gravitational and magnetic fields, might ultimately be used to constrain the interior compositions. While further laboratory and theoretical work remains necessary to better understand the mixing properties of hydrogen, water, and other plausible constituents at the conditions of these planets' interiors, the thermodynamically governed modeling approach described in Chapter IV already presents a possible natural explanation not only for the different observed heat flows of Uranus and Neptune, but also their different atmospheric ammonia contents, while maintaining consistency with the gravity and magnetic field data of these planets. While this finding is certainly intriguing, it still remains necessary, as highlighted by the recent collision-focused work of Reinhardt et al. 2020, to account for the processes which could have led to the inferred present-day difference in mixing states between Uranus and Neptune.

It is the author's intention that the work presented in this thesis will serve to motivate continued investigation into the dynamics of planets both residing in our own system, and orbiting other stars. Notably, calls for further spacecraft exploration of the ice giants have become loud and widespread across the scientific community in recent years. For many planetary scientists, an ice giant orbiter mission seems to represent a logical next step in our understanding of the solar system's content. Moreover, in light of the discussion of extreme short- and long-period planets detailed in this work, and given the increase over recent decades in extensive exoplanetary observations, it is of utmost importance that a self-consistent theory be developed

[1] Although the valuable data provided by the Voyager 2 flybys of Uranus and Neptune must not be discounted, this contribution to our knowledge about Uranus and Neptune cannot match the information attainable from an orbiter and entry probe.

to explain how our own solar system fits within the exoplanetary context. Notably, this type of gestalt understanding is necessary if we wish to understand how our own life-bearing planet formed, and hence to identify which other systems might represent true habitable analogues to our own.

BIBLIOGRAPHY

Abe, Y., and T. Matsui. 1988. "Evolution of an impact-generated H_2O-CO_2 atmosphere and formation of a hot proto-ocean on Earth." *Journal of Atmospheric Sciences* 45 (21): 3081–3101.

Adams, F. C. 2010. "The birth environment of the solar system". *Annual Review of Astronomy and Astrophysics* 48:47–85.

– . 2011. "Magnetically controlled outflows from hot Jupiters". *The Astrophysical Journal* 730 (1): 27.

Adams, F. C., and A. M. Bloch. 2015. "On the stability of extrasolar planetary systems and other closely orbiting pairs". *Monthly Notices of the Royal Astronomical Society* 446 (4): 3676–3686.

Albrecht, S., et al. 2012. "Obliquities of hot Jupiter host stars: Evidence for tidal interactions and primordial misalignments". *The Astrophysical Journal* 757 (1): 18.

Arnold, V. I. 2009. "On a theorem of Liouville concerning integrable problems of dynamics". *Collected Works: Representations of Functions, Celestial Mechanics and KAM Theory, 1957–1965*: 418–422.

Atreya, S. K. 1986. *Atmospheres and Ionospheres of the Outer Planets and their Satellites*.

Bailey, E., K. Batygin, and M. E. Brown. 2016. "Solar obliquity induced by planet nine". *The Astronomical Journal* 152 (5): 126.

Baines, K. H., et al. 1993. "The Abundances of CH4 and Ortho/Para H2 in Neptune and Uranus: Implications of New H2 4-0 Linestrength Measurements". In *Bulletin of the American Astronomical Society*, 25:1079.

Bakos, G. Á., et al. 2007. "HD 147506b: a supermassive planet in an eccentric orbit transiting a bright star". *The Astrophysical Journal* 670 (1): 826.

Bakos, G. Á., et al. 2002. "System description and first light curves of the Hungarian automated telescope, an autonomous observatory for variability search". *Publications of the Astronomical Society of the Pacific* 114 (799): 974.

Bakos, G. Á., et al. 2004. "Wide-Field Millimagnitude Photometry with the HAT: A Tool for Extrasolar Planet Detection". *Publications of the Astronomical Society of the Pacific* 116 (817): 266.

Bali, E., A. Audétat, and H. Keppler. 2013. "Water and hydrogen are immiscible in Earth's mantle". 495 (7440): 220–222. doi:10.1038/nature11908.

Baraffe, I., G. Chabrier, and T. Barman. 2008. "Structure and evolution of super-Earth to super-Jupiter exoplanets-I. Heavy element enrichment in the interior". *Astronomy & Astrophysics* 482 (1): 315–332.

Batalha, N. M., et al. 2013a. “Planetary candidates observed by Kepler. III. Analysis of the first 16 months of data”. *The Astrophysical Journal Supplement Series* 204 (2): 24.

Batalha, N. M., et al. 2013b. “Planetary Candidates Observed by Kepler. III. Analysis of the First 16 Months of Data”. 204, 24 (2): 24. doi:10.1088/0067-0049/204/2/24. arXiv: 1202.5852 [astro-ph.EP].

Bate, M. R., G. Lodato, and J. E. Pringle. 2010a. “Chaotic star formation and the alignment of stellar rotation with disc and planetary orbital axes”. *Monthly Notices of the Royal Astronomical Society* 401 (3): 1505–1513.

– . 2010b. “Chaotic star formation and the alignment of stellar rotation with disc and planetary orbital axes”. *Monthly Notices of the Royal Astronomical Society* 401 (3): 1505–1513.

Batygin, K. 2012. “A primordial origin for misalignments between stellar spin axes and planetary orbits”. *Nature* 491 (7424): 418–420.

Batygin, K., and F. C. Adams. 2013a. “Magnetic and gravitational disk-star interactions: An interdependence of PMS stellar rotation rates and spin-orbit misalignments”. *The Astrophysical Journal* 778 (2): 169.

– . 2013b. “Magnetic and gravitational disk-star interactions: An interdependence of PMS stellar rotation rates and spin-orbit misalignments”. *The Astrophysical Journal* 778 (2): 169.

Batygin, K., P. H. Bodenheimer, and G. P. Laughlin. 2016a. “In situ formation and dynamical evolution of hot Jupiter systems”. *The Astrophysical Journal* 829 (2): 114.

– . 2016b. “In situ formation and dynamical evolution of hot Jupiter systems”. *The Astrophysical Journal* 829 (2): 114.

Batygin, K., and M. E. Brown. 2016a. “Evidence for a distant giant planet in the solar system”. *The Astronomical Journal* 151 (2): 22.

– . 2016b. “Generation of highly inclined trans-Neptunian objects by planet nine”. *The Astrophysical Journal Letters* 833 (1): L3.

Batygin, K., M. E. Brown, and W. C. Fraser. 2011. “Retention of a primordial cold classical Kuiper belt in an instability-driven model of solar system formation”. *The Astrophysical Journal* 738 (1): 13.

Batygin, K., and G. Laughlin. 2015. “Jupiter’s decisive role in the inner Solar System’s early evolution”. *Proceedings of the National Academy of Sciences* 112 (14): 4214–4217.

Batygin, K., and A. Morbidelli. 2017. “Dynamical Evolution Induced by Planet Nine”. *The Astronomical Journal* 154 (6): 229.

Batygin, K., A. Morbidelli, and M. J. Holman. 2015. “Chaotic disintegration of the inner solar system”. *The Astrophysical Journal* 799 (2): 120.

Batygin, K., A. Morbidelli, and K. Tsiganis. 2011. "Formation and evolution of planetary systems in presence of highly inclined stellar perturbers". *Astronomy & Astrophysics* 533:A7.

Batygin, K., et al. 2019. "The Planet Nine Hypothesis". *Physics Reports*.

Bayliss, D., et al. 2010. "Confirmation of a retrograde orbit for exoplanet WASP-17b". *The Astrophysical Journal Letters* 722 (2): L224.

Beaugé, C., and D. Nesvorn. 2012. "Multiple-planet scattering and the origin of hot Jupiters". *The Astrophysical Journal* 751 (2): 119.

Becker, J. C., et al. 2017. "Evaluating the dynamical stability of outer solar system objects in the presence of planet nine". *The Astronomical Journal* 154 (2): 61.

Becker, J. C., et al. 2015. "WASP-47: A hot Jupiter system with two additional planets discovered by K2". *The Astrophysical Journal Letters* 812 (2): L18.

Bernabe, D., A. Romero-Martinez, and A. Trejo. 1988. "Liquid—liquid coexistence curves for binary systems". *Fluid phase equilibria* 40 (3): 279–288.

Bernardinelli, P. H., et al. 2020. "Testing the isotropy of the Dark Energy Survey's extreme trans-Neptunian objects". *arXiv preprint arXiv:2003.08901*.

Bethkenhagen, M., et al. 2017. "Planetary ices and the linear mixing approximation". *The Astrophysical Journal* 848 (1): 67.

Bethkenhagen, M., et al. 2015. "Superionic phases of the 1: 1 water–ammonia mixture". *The Journal of Physical Chemistry A* 119 (42): 10582–10588.

Beust, H. 2016. "Orbital clustering of distant Kuiper belt objects by hypothetical Planet 9. Secular or resonant?" *Astronomy & Astrophysics* 590:L2.

Bodenheimer, P., O. Hubickyj, and J. J. Lissauer. 2000a. "Models of the in situ formation of detected extrasolar giant planets". *Icarus* 143 (1): 2–14.

– . 2000b. "Models of the in situ formation of detected extrasolar giant planets". *Icarus* 143 (1): 2–14.

Bodenheimer, P., and J. B. Pollack. 1986. "Calculations of the accretion and evolution of giant planets: The effects of solid cores". *Icarus* 67 (3): 391–408.

Boley, A. C., A. P. G. Contreras, and B. Gladman. 2016. "The in situ formation of giant planets at short orbital periods". *The Astrophysical Journal Letters* 817 (2): L17.

Boué, G., and J. Laskar. 2010. "A Collisionless Scenario for Uranus Tilting". 712 (1): L44–L47. doi:10.1088/2041-8205/712/1/L44. arXiv: 0912.0181 [astro-ph.EP].

Bouvier, J., et al. 2007. "Protostars and Planets V". *Univ. Arizona, Tucson, AZ*: 479.

Brown, M. E. 2017. "Observational bias and the clustering of distant eccentric Kuiper belt objects". *The Astronomical Journal* 154 (2): 65.

Brown, M. E., and K. Batygin. 2016. “Observational constraints on the orbit and location of Planet Nine in the outer solar system”. *The Astrophysical Journal Letters* 824 (2): L23.

Burns, J. A. 1976. “Elementary derivation of the perturbation equations of celestial mechanics”. *American Journal of Physics* 44 (10): 944–949.

Cameron, A. G. W. 1988. “Origin of the solar system”. *Annual Review of Astronomy and Astrophysics* 26 (1): 441–472.

Carrington, R. C. 1853-61. “Observations made at Redhill”.

Chambers, J. E. 1999. “A hybrid symplectic integrator that permits close encounters between massive bodies”. *Monthly Notices of the Royal Astronomical Society* 304 (4): 793–799.

Chandrasekhar, S. 1939. *Book Review: An Introduction to the Study of Stellar Structure, by S. Chandrasekhar*.

Chen, J., and D. Kipping. 2016. “Probabilistic forecasting of the masses and radii of other worlds”. *The Astrophysical Journal* 834 (1): 17.

Chiang, E., and G. Laughlin. 2013. “The minimum-mass extrasolar nebula: In situ formation of close-in super-Earths”. *Monthly Notices of the Royal Astronomical Society* 431 (4): 3444–3455.

Connerney, J. E. P., M. H. Acuna, and N. F. Ness. 1991. “The magnetic field of Neptune”. *Journal of Geophysical Research: Space Physics* 96 (S01): 19023–19042.

– . 1987. “The magnetic field of Uranus”. *Journal of Geophysical Research: Space Physics* 92 (A13): 15329–15336. doi:10.1029/JA092iA13p15329.

Conrath, B. J., et al. 1984. “The helium abundance of Saturn from Voyager measurements”. *The Astrophysical Journal* 282:807–815.

Conrath, B., et al. 1989. “Infrared observations of the Neptunian system”. *Science* 246 (4936): 1454–1459.

Crida, A., and K. Batygin. 2014. “Spin-orbit angle distribution and the origin of (mis) aligned hot Jupiters”. *Astronomy & Astrophysics* 567:A42.

Damay, P., and F. Leclercq. 1991. “Asymmetry of the coexistence curve in binary systems. Size effect”. *The Journal of chemical physics* 95 (1): 590–599.

Dawson, R. I., R. A. Murray-Clay, and J. A. Johnson. 2014a. “The Photoeccentric Effect and Proto-hot Jupiters. III. A Paucity of Proto-hot Jupiters on Super-eccentric Orbits”. *The Astrophysical Journal* 798 (2): 66.

– . 2014b. “The Photoeccentric Effect and Proto-hot Jupiters. III. A Paucity of Proto-hot Jupiters on Super-eccentric Orbits”. *The Astrophysical Journal* 798 (2): 66.

de Pater, I., P. N. Romani, and S. K. Atreya. 1991. “Possible microwave absorption by H_2S gas in Uranus’ and Neptune’s atmospheres”.

Deacon, N. R., J. E. Schlieder, and S. J. Murphy. 2016. “A nearby young M dwarf with a wide, possibly planetary-mass companion”. *Monthly Notices of the Royal Astronomical Society* 457 (3): 3191–3199.

Debras, F., and G. Chabrier. 2019. “New models of Jupiter in the context of Juno and Galileo”. *The Astrophysical Journal* 872 (1): 100.

Demarcus, W. C. 1958. “The constitution of Jupiter and Saturn”. *The Astronomical Journal* 63:2.

Dressing, C. D., and D. Charbonneau. 2015. “The occurrence of potentially habitable planets orbiting M dwarfs estimated from the full Kepler dataset and an empirical measurement of the detection sensitivity”. *The Astrophysical Journal* 807 (1): 45.

– . 2013. “The occurrence rate of small planets around small stars”. *The Astrophysical Journal* 767 (1): 95.

Fabrycky, D. 2008. “Radiative thrusters on close-in extrasolar planets”. *The Astrophysical Journal Letters* 677 (2): L117.

Fabrycky, D., and S. Tremaine. 2007a. “Shrinking binary and planetary orbits by Kozai cycles with tidal friction”. *The Astrophysical Journal* 669 (2): 1298.

– . 2007b. “Shrinking binary and planetary orbits by Kozai cycles with tidal friction”. *The Astrophysical Journal* 669 (2): 1298.

Fazio, G. G., et al. 1976. “The effective temperature of Uranus.” 209 (): 633–637. doi:10.1086/154760.

Fegley, B., and R. G. Prinn. 1986. “Chemical models of the deep atmosphere of Uranus”. *The Astrophysical Journal* 307:852–865.

Fegley, B., et al. 1991. “Spectroscopy and chemistry of the atmosphere of Uranus”.

Fielding, D. B., et al. 2015. “The turbulent origin of spin–orbit misalignment in planetary systems”. *Monthly Notices of the Royal Astronomical Society* 450 (3): 3306–3318.

Fogg, M. J., and R. P. Nelson. 2007. “The effect of type I migration on the formation of terrestrial planets in hot-Jupiter systems”. *Astronomy & Astrophysics* 472 (3): 1003–1015.

Fressin, F., et al. 2013. “The false positive rate of Kepler and the occurrence of planets”. *The Astrophysical Journal* 766 (2): 81.

Fuente Marcos, C. de la, R. de la Fuente Marcos, and S. J. Aarseth. 2016. “Dynamical impact of the Planet Nine scenario: N-body experiments”. *Monthly Notices of the Royal Astronomical Society: Letters* 460 (1): L123–L127.

Fulton, B. J., et al. 2017a. “The California-Kepler survey. III. A gap in the radius distribution of small planets”. *The Astronomical Journal* 154 (3): 109.

Fulton, B. J., et al. 2017b. “The California-Kepler survey. III. A gap in the radius distribution of small planets”. *The Astronomical Journal* 154 (3): 109.

Gallet, F., and J. Bouvier. 2013. “Improved angular momentum evolution model for solar-like stars”. *Astronomy & Astrophysics* 556:A36.

Gao, P., and D. J. Stevenson. 2013. “Nonhydrostatic effects and the determination of icy satellites’ moment of inertia”. 226 (2): 1185–1191. doi:10.1016/j.icarus.2013.07.034.

Gavrilov, S. V., and V. N. Zharkov. 1977. “Love numbers of the giant planets”. *Icarus* 32 (4): 443–449.

Ghosh, P., and F. K. Lamb. 1979. “Accretion by rotating magnetic neutron stars. II-Radial and vertical structure of the transition zone in disk accretion”. *The Astrophysical Journal* 232:259–276.

Goldreich, P., and S. Soter. 1966. “Q in the Solar System”. *icarus* 5 (1-6): 375–389.

Gomes, R., R. Deienno, and A. Morbidelli. 2016. “The inclination of the planetary system relative to the solar equator may be explained by the presence of Planet 9”. *The Astronomical Journal* 153 (1): 27.

Gould, A., et al. 2006. “Frequency of hot Jupiters and very hot Jupiters from the OGLE-III transit surveys toward the Galactic Bulge and Carina”. *arXiv preprint astro-ph/0601001*.

Greenberg, R. 2009. “Frequency dependence of tidal Q”. *The Astrophysical Journal Letters* 698 (1): L42.

Guillot, T. 1995. “Condensation of methane, ammonia, and water and the inhibition of convection in giant planets”. *Science* 269 (5231): 1697–1699.

Gulkis, S., M. A. Janssen, and E. T. Olsen. 1978. “Evidence for the depletion of ammonia in the Uranus atmosphere”. *Icarus* 34 (1): 10–19.

Gupta, A., and H. E. Schlichting. 2019. “Sculpting the valley in the radius distribution of small exoplanets as a by-product of planet formation: the core-powered mass-loss mechanism”. *Monthly Notices of the Royal Astronomical Society* 487 (1): 24–33.

Hadden, S., et al. 2018. “Chaotic Dynamics of Trans-Neptunian Objects Perturbed by Planet Nine”. *The Astronomical Journal* 155 (6): 249.

Hanel, R., et al. 1986. “Infrared Observations of the Uranian System”. *Science* 233 (4759): 70–74. doi:10.1126/science.233.4759.70.

Hansen, B. M. S. 2010. “Calibration of equilibrium tide theory for extrasolar planet systems”. *The Astrophysical Journal* 723 (1): 285.

Hartmann, L., et al. 1998. “Accretion and the evolution of T Tauri disks”. *The Astrophysical Journal* 495 (1): 385.

Hayashi, C. 1981. “Structure of the solar nebula, growth and decay of magnetic fields and effects of magnetic and turbulent viscosities on the nebula”. *Progress of Theoretical Physics Supplement* 70:35–53.

Hébrard, G., et al. 2008. “Misaligned spin-orbit in the XO-3 planetary system?” *Astronomy & Astrophysics* 488 (2): 763–770.

Helled, R., J. D. Anderson, and G. Schubert. 2010. “Uranus and Neptune: Shape and rotation”. 210 (1): 446–454. doi:10.1016/j.icarus.2010.06.037.

Heller, C. H. 1993. “Encounters with protostellar disks. I-Disk tilt and the nonzero solar obliquity”. *The Astrophysical Journal* 408:337–346.

Henrard, J. 1982. “Capture into resonance-an extension of the use of adiabatic invariants”. *Celestial mechanics* 27:3–22.

Howard, A. W., et al. 2010. “The occurrence and mass distribution of close-in super-Earths, Neptunes, and Jupiters”. *Science* 330 (6004): 653–655.

Huang, C., Y. Wu, and A. H. M. J. Triaud. 2016. “Warm Jupiters are less lonely than hot Jupiters: Close neighbors”. *The Astrophysical Journal* 825 (2): 98.

Hubbard, W. B. 2013. “Concentric Maclaurin Spheroid Models of Rotating Liquid Planets”. *The Astrophysical Journal* 768, 43 (1): 43.

Hubbard, W. B., and J. J. Macfarlane. 1980. “Structure and evolution of Uranus and Neptune.” 85 (B1): 225–234. doi:10.1029/JB085iB01p00225.

Hubbard, W. B., M. Podolak, and D. J. Stevenson. 1995. “The interior of Neptune.” In *Neptune and Triton*, 109–138.

Huber, D., et al. 2013. “Stellar spin-orbit misalignment in a multiplanet system”. *Science* 342 (6156): 331–334.

Hut, P. 1981. “Tidal evolution in close binary systems”. *Astronomy and Astrophysics* 99:126–140.

Ikoma, Masahiro, Hiroyuki Emori, and Kiyoshi Nakazawa. 2001. “Formation of giant planets in dense nebulae: critical core mass revisited”. *The Astrophysical Journal* 553 (2): 999.

Ingersoll, A. P. 1969. “The Runaway Greenhouse: A History of Water on Venus.” *Journal of Atmospheric Sciences* 26 (6): 1191–1198. doi:10.1175/1520-0469(1969)026<1191:TRGAHO>2.0.CO;2.

Izidoro, A., et al. 2015. “Gas giant planets as dynamical barriers to inward-migrating super-Earths”. *The Astrophysical Journal Letters* 800 (2): L22.

Jackson, B., R. Greenberg, and R. Barnes. 2008. “Tidal evolution of close-in extrasolar planets”. *The Astrophysical Journal* 678 (2): 1396.

Jacobson, R. A. 2009. “The Orbits of the Neptunian Satellites and the Orientation of the Pole of Neptune”. 137 (5): 4322–4329. doi:10.1088/0004-6256/137/5/4322.

– . 2014. “The Orbits of the Uranian Satellites and Rings, the Gravity Field of the Uranian System, and the Orientation of the Pole of Uranus”. 148, 76 (5): 76. doi:10.1088/0004-6256/148/5/76.

Jensen, E., and R. Akeson. 2014. “Misaligned protoplanetary disks in a young binary star system”. *Nature* 511 (7511): 567–569.

Johansen, A., et al. 2012. “Can planetary instability explain the Kepler dichotomy?” *The Astrophysical Journal* 758 (1): 39.

Johnson, K. S. 1914. *Unpublished notes*.

Kaib, N. A., and J. E. Chambers. 2016. “The fragility of the terrestrial planets during a giant-planet instability”. *Monthly Notices of the Royal Astronomical Society* 455 (4): 3561–3569.

Kaspi, Y., et al. 2013. “Atmospheric confinement of jet streams on Uranus and Neptune”. 497 (7449): 344–347. doi:10.1038/nature12131.

Kaula, W. M. 1962. “Development of the lunar and solar disturbing functions for a close satellite”. *The Astronomical Journal* 67:300.

Kley, W., and R. P. Nelson. 2012. “Planet-disk interaction and orbital evolution”. *Annual Review of Astronomy and Astrophysics* 50:211–249.

Knutson, H. A., et al. 2014. “Friends of hot Jupiters. I. A radial velocity search for massive, long-period companions to close-in gas giant planets”. *The Astrophysical Journal* 785 (2): 126.

Koenigl, A. 1991a. “Disk accretion onto magnetic T Tauri stars”. *The Astrophysical Journal* 370:L39–L43.

– . 1991b. “Disk accretion onto magnetic T Tauri stars”. *The Astrophysical Journal* 370:L39–L43.

Kuiper, G. P. 1951. “On the origin of the solar system”. *Proceedings of the National Academy of Sciences of the United States of America* 37 (1): 1.

Kurosaki, K., and M. Ikoma. 2017. “Acceleration of Cooling of Ice Giants by Condensation in Early Atmospheres”. 153, 260 (6): 260. doi:10.3847/1538-3881/aa6faf.

Lai, D. 1999. “Magnetically driven warping, precession, and resonances in accretion disks”. *The Astrophysical Journal* 524 (2): 1030.

– . 2014. “Star–disc–binary interactions in protoplanetary disc systems and primordial spin–orbit misalignments”. *Monthly Notices of the Royal Astronomical Society* 440 (4): 3532–3544.

Lai, D., F. Foucart, and D. N. C. Lin. 2011. “Evolution of spin direction of accreting magnetic protostars and spin–orbit misalignment in exoplanetary systems”. *Monthly Notices of the Royal Astronomical Society* 412 (4): 2790–2798.

Lainey, V., et al. 2009. “Strong tidal dissipation in Io and Jupiter from astrometric observations”. *Nature* 459 (7249): 957–959.

Lambrechts, M., and E. Lega. 2017. “Reduced gas accretion on super-Earths and ice giants”. *Astronomy & Astrophysics* 606:A146.

Laskar, J. 1994. *Astronomy & Astrophysics, 287*.

Laughlin, G., and J. J. Lissauer. 2015. “Exoplanetary Geophysics–An Emerging Discipline”. *arXiv preprint arXiv:1501.05685*.

Laughlin, G., et al. 2009. “Rapid heating of the atmosphere of an extrasolar planet”. *Nature* 457 (7229): 562–564.

Lawler, S. M., et al. 2017. “Observational Signatures of a massive distant planet on the scattering disk”. 153, 33 (1): 33. doi:10.3847/1538-3881/153/1/33. arXiv: 1605.06575 [astro-ph.EP].

Leconte, J., and G. Chabrier. 2012. “A new vision of giant planet interiors: Impact of double diffusive convection”. 540 (A20): A20. doi:10.1051/0004-6361/201117595.

Leconte, J., et al. 2017. “Condensation-inhibited convection in hydrogen-rich atmospheres-Stability against double-diffusive processes and thermal profiles for Jupiter, Saturn, Uranus, and Neptune”. *Astronomy & Astrophysics* 598:A98.

Leconte, J., et al. 2010. “Is tidal heating sufficient to explain bloated exoplanets? Consistent calculations accounting for finite initial eccentricity”. *Astronomy & Astrophysics* 516:A64.

Lee, E. J., and E. Chiang. 2016. “Breeding super-Earths and birthing super-puffs in transitional disks”. *The Astrophysical Journal* 817 (2): 90.

– . 2015. “To cool is to accrete: analytic scalings for nebular accretion of planetary atmospheres”. *The Astrophysical Journal* 811 (1): 41.

Lee, Man Hoi, and S. J. Peale. 2002. “Dynamics and origin of the 2: 1 orbital resonances of the GJ 876 planets”. *The Astrophysical Journal* 567 (1): 596.

Levison, H. F., et al. 2011. “Late orbital instabilities in the outer planets induced by interaction with a self-gravitating planetesimal disk”. *The Astronomical Journal* 142 (5): 152.

Levrard, B., C. Winisdoerffer, and G. Chabrier. 2009. “Falling transiting extrasolar giant planets”. *The Astrophysical Journal Letters* 692 (1): L9.

Lewis, N. K., et al. 2013. “Orbital phase variations of the eccentric giant planet HAT-P-2b”. *The Astrophysical Journal* 766 (2): 95.

Li, C., et al. 2020. “The water abundance in Jupiter’s equatorial zone”. *Nature Astronomy*: 1–8.

Li, G., and F. C. Adams. 2016. “Interaction cross sections and survival rates for proposed solar system member planet nine”. *The Astrophysical Journal Letters* 823 (1): L3.

Li, G., et al. 2014a. “Chaos in the test particle eccentric Kozai-Lidov mechanism”. *The Astrophysical Journal* 791 (2): 86.

Li, G., et al. 2014b. “Eccentricity growth and orbit flip in near-coplanar hierarchical three-body systems”. *The Astrophysical Journal* 785 (2): 116.

Lin, D. N. C., P. Bodenheimer, and D. C. Richardson. 1996. “Orbital migration of the planetary companion of 51 Pegasi to its present location”. *Nature* 380 (6575): 606–607.

Lindal, G. F. 1992. “The Atmosphere of Neptune: an Analysis of Radio Occultation Data Acquired with Voyager 2”. 103 (): 967. doi:10.1086/116119.

Lindal, G. F., et al. 1990. “The atmosphere of Neptune: Results of radio occultation measurements with the Voyager 2 spacecraft”. *Geophysical Research Letters* 17 (10): 1733–1736.

– . 1987. “The atmosphere of Uranus: Results of radio occultation measurements with Voyager 2”. 92 (A13): 14987–15001. doi:10.1029/JA092iA13p14987.

Liu, L., et al. 2019. “American Astronomical Society logo American Astronomical Society logo iop-2016. png iop-2016. png A publishing partnership Formation of a Magnetic Flux Rope in the Early Emergence Phase of NOAA Active Region 12673”. *The Astrophysical Journal* 884 (1).

Lodders, K. 2010. “Solar System Abundances of the Elements”. *Astrophysics and Space Science Proceedings* 16 (): 379. doi:10.1007/978-3-642-10352-0_8.

Lodders, K., and B. Fegley. 1994. “The Origin of Carbon Monoxide in Neptune’s Atmosphere”. 112 (2): 368–375. doi:10.1006/icar.1994.1190.

Loeillet, B., et al. 2008. “Refined parameters and spectroscopic transit of the super-massive planet HD 147506b”. *Astronomy & Astrophysics* 481 (2): 529–533.

Loewenstein, R. F., D. A. Harper, and H. Moseley. 1977. “The effective temperature of Neptune.” 218 (): L145. doi:10.1086/182594.

Loewenstein, R. F., et al. 1977. “Far-Infrared and Submillimeter Observations of the Planets.” 31 (3): 315–324. doi:10.1016/0019-1035(77)90025-2.

Lopez, E. D., and J. J. Fortney. 2014. “Understanding the mass-radius relation for sub-Neptunes: Radius as a proxy for composition”. *The Astrophysical Journal* 792 (1): 1.

Lundkvist, M. S., et al. 2016. “Hot super-Earths stripped by their host stars”. *Nature Communications* 7 (1): 1–8.

Madigan, A., and M. McCourt. 2016. “A new inclination instability reshapes Keplerian discs into cones: application to the outer Solar system”. *Monthly Notices of the Royal Astronomical Society: Letters* 457 (1): L89–L93.

Malhotra, R., K. Volk, and X. Wang. 2016. “Corralling a distant planet with extreme resonant Kuiper belt objects”. *The Astrophysical Journal Letters* 824 (2): L22.

Mao, H. K., et al. 1988. “Synchrotron X-ray diffraction measurements of single-crystal hydrogen to 26.5 gigapascals”. *Science* 239 (): 1131–1134. doi:10.1126/science.239.4844.1131.

Marcy, G. W., et al. 2001. “A pair of resonant planets orbiting GJ 876”. *The Astrophysical Journal* 556 (1): 296.

Mardling, R. A. 2007. “Long-term tidal evolution of short-period planets with companions”. *Monthly Notices of the Royal Astronomical Society* 382 (4): 1768–1790.

– . 2010. “The determination of planetary structure in tidally relaxed inclined systems”. *Monthly Notices of the Royal Astronomical Society* 407 (2): 1048–1069.

Marley, M. S., P. Gómez, and M. Podolak. 1995. “Monte Carlo interior models for Uranus and Neptune”. 100 (E11): 23349–23354. doi:10.1029/95JE02362.

Matson, D. L., G. A. Ransford, and T. V. Johnson. 1981. “Heat flow from Io (JI)”. *Journal of Geophysical Research: Solid Earth* 86 (B3): 1664–1672.

Matsumura, Soko, Genya Takeda, and F. A. Rasio. 2008. “On the origins of eccentric close-in planets”. *Proceedings of the International Astronomical Union* 4 (S253): 189–195.

Mayor, M., et al. 2011. “The HARPS search for southern extra-solar planets XXXIV. Occurrence, mass distribution and orbital properties of super-Earths and Neptune-mass planets”. *arXiv preprint arXiv:1109.2497*.

Mayor, M., and D. Queloz. 1995. “A Jupiter-mass companion to a solar-type star”. *Nature* 378 (6555): 355–359.

Mazeh, T., T. Holczer, and S. Faigler. 2016. “Dearth of short-period Neptunian exoplanets: A desert in period-mass and period-radius planes”. *Astronomy & Astrophysics* 589:A75.

McLaughlin, D. B. 1924. “Some results of a spectrographic study of the Algol system.” 60 (): 22–31. doi:10.1086/142826.

McQuillan, A., T. Mazeh, and S. Aigrain. 2013. “Stellar rotation periods of the Kepler objects of interest: A dearth of close-in planets around fast rotators”. *The Astrophysical Journal Letters* 775 (1): L11.

Mestel, L. 1961. “A note on equatorial acceleration in a magnetic star”. *Monthly Notices of the Royal Astronomical Society* 122 (6): 473–478.

Miller, N., and J. J. Fortney. 2011. “The heavy-element masses of extrasolar giant planets, revealed”. *The Astrophysical Journal Letters* 736 (2): L29.

Millholland, S., and G. Laughlin. 2017. “Constraints on Planet Nine’s Orbit and Sky Position within a Framework of Mean-motion Resonances”. *The Astronomical Journal* 153 (3): 91.

Misner, C. W., K. S. Thorne, J. A. Wheeler, et al. 1973. *Gravitation*. Macmillan.

Morbidelli, A. 2002. "Modern celestial mechanics: aspects of solar system dynamics".

Morbidelli, A., et al. 2012. "Explaining why the Uranian satellites have equatorial prograde orbits despite the large planetary obliquity". *Icarus* 219 (2): 737–740. doi:10.1016/j.icarus.2012.03.025.

Morrison, D., and CM . T.elesco. 1980. "Io: Observational constraints on internal energy and thermophysics of the surface". *Icarus* 44 (2): 226–233.

Morton, T. D., and J. N. Winn. 2014. "Obliquities of Kepler stars: Comparison of single-and multiple-transit systems". *The Astrophysical Journal* 796 (1): 47.

Mulders, G. D., I. Pascucci, and D. Apai. 2015. "An increase in the mass of planetary systems around lower-mass stars". *The Astrophysical Journal* 814 (2): 130.

Murray-Clay, R. A., E. I. Chiang, and N. Murray. 2009. "Atmospheric escape from hot Jupiters". *The Astrophysical Journal* 693 (1): 23.

Murray, C. D., and S. F. Dermott. 1999a. *Solar System Dynamics*. Cambridge University pPress.

– . 1999b. *Solar system dynamics by Murray*.

Nakajima, S., Y. Hayashi, and Y. Abe. 1992. "A study on the "runaway greenhouse effect" with a one-dimensional radiative–convective equilibrium model". *Journal of the Atmospheric Sciences* 49 (23): 2256–2266.

Naoz, S. 2016. "The eccentric Kozai-Lidov effect and its applications". *Annual Review of Astronomy and Astrophysics* 54:441–489.

Naoz, S., and D. C. Fabrycky. 2014. "Mergers and obliquities in stellar triples". *The Astrophysical Journal* 793 (2): 137.

Naoz, S., et al. 2011a. "Hot Jupiters from secular planet–planet interactions". *Nature* 473 (7346): 187–189.

Naoz, S., et al. 2011b. "Hot Jupiters from secular planet–planet interactions". *Nature* 473 (7346): 187–189.

– . 2013. "Secular dynamics in hierarchical three-body systems". *Monthly Notices of the Royal Astronomical Society* 431 (3): 2155–2171.

Narita, N., et al. 2009. "First evidence of a retrograde orbit of a transiting exoplanet HAT-P-7b". *Publications of the Astronomical Society of Japan* 61 (5): L35–L40.

Neishtadt, A. I. 1984. "The separation of motions in systems with rapidly rotating phase". *Journal of Applied Mathematics and Mechanics* 48 (2): 133–139.

Nellis, W. J., et al. 1981. "Shock compression of liquid carbon monoxide and methane to 90 GPa (900 kbar)". 75 (6): 3055–3063. doi:10.1063/1.442401.

Ness, N. F., et al. 1986. “Magnetic Fields at Uranus”. *Science* 233 (4759): 85–89. doi:10.1126/science.233.4759.85.

Ness, Norman F., et al. 1989. “Magnetic Fields at Neptune”. *Science* 246 (4936): 1473–1478. doi:10.1126/science.246.4936.1473.

Nesvorný, D., and A. Morbidelli. 2012. “Statistical study of the early Solar System’s instability with four, five, and six giant planets”. *The Astronomical Journal* 144 (4): 117.

Nettelmann, N., et al. 2013. “New indication for a dichotomy in the interior structure of Uranus and Neptune from the application of modified shape and rotation data”. 77 (): 143–151. doi:10.1016/j.pss.2012.06.019.

Nettelmann, N., et al. 2016. “Uranus evolution models with simple thermal boundary layers”. 275 (): 107–116. doi:10.1016/j.icarus.2016.04.008.

Ngo, H., et al. 2016. “Friends of hot Jupiters. IV. Stellar companions beyond 50 au might facilitate giant planet formation, but most are unlikely to cause Kozai-Lidov migration.” *The Astrophysical Journal* 827 (1): 8.

Ngo, H., et al. 2015. “Friends of hot Jupiters. II. No correspondence between hot-Jupiter spin-orbit misalignment and the incidence of directly imaged stellar companions”. *The Astrophysical Journal* 800 (2): 138.

Niemann, H. B., et al. 1996. “The Galileo probe mass spectrometer: Composition of Jupiter’s atmosphere”. *Science* 272 (5263): 846–849.

Ogilvie, G. I. 2014. “Tidal dissipation in stars and giant planets”. *Annual Review of Astronomy and Astrophysics* 52:171–210.

Owen, J. E., and D. Lai. 2018. “Photoevaporation and high-eccentricity migration created the sub-Jovian desert”. *Monthly Notices of the Royal Astronomical Society* 479 (4): 5012–5021.

Owen, J. E., and Y. Wu. 2013. “Kepler planets: a tale of evaporation”. *The Astrophysical Journal* 775 (2): 105.

– . 2017. “The evaporation valley in the Kepler planets”. *The Astrophysical Journal* 847 (1): 29.

Pál, A., et al. 2010. “Refined stellar, orbital and planetary parameters of the eccentric HAT-P-2 planetary system”. *Monthly Notices of the Royal Astronomical Society* 401 (4): 2665–2674.

Pearl, J. C., and B. J. Conrath. 1991. “The albedo, effective temperature, and energy balance of Neptune, as determined from Voyager data”. *Journal of Geophysical Research: Space Physics* 96 (S01): 18921–18930.

Peebles, P. J. E. 1964. “The structure and composition of Jupiter and Saturn”. *The Astrophysical Journal* 140:328.

Penev, K., and D. Sasselov. 2011. “Tidal evolution of close-in extrasolar planets: high stellar Q from new theoretical models”. *The Astrophysical Journal* 731 (1): 67.

Petigura, E. A., A. W. Howard, and G. W. Marcy. 2013. “Prevalence of Earth-size planets orbiting Sun-like stars”. *Proceedings of the National Academy of Sciences* 110 (48): 19273–19278.

Petrovich, C. 2015. “Hot Jupiters from coplanar high-eccentricity migration”. *The Astrophysical Journal* 805 (1): 75.

Piskorz, D., et al. 2015. “Friends of hot Jupiters. III. an infrared spectroscopic search for low-mass stellar companions”. *The Astrophysical Journal* 814 (2): 148.

Podolak, M. 1976. “Methane Rich Models of Uranus”. 27 (4): 473–477. doi:10.1016/0019-1035(76)90163-9.

Podolak, M., R. Helled, and G. Schubert. 2019. “Effect of non-adiabatic thermal profiles on the inferred compositions of Uranus and Neptune”. 487 (2): 2653–2664. doi:10.1093/mnras/stz1467. arXiv: 1905.09099 [astro-ph.EP].

Podolak, M., W. B. Hubbard, and D. J. Stevenson. 1991. “Models of Uranus’ interior and magnetic field”. In *Uranus*, 29–61. University of Arizona Press; Space Science Series.

Podolak, M., J. I. Podolak, and M. S. Marley. 2000. “Further investigations of random models of Uranus and Neptune”. 48 (2-3): 143–151. doi:10.1016/S0032-0633(99)00088-4.

Podolak, M., A. Weizman, and M. Marley. 1995. “Comparative models of Uranus and Neptune”. 43 (12): 1517–1522. doi:10.1016/0032-0633(95)00061-5.

Podolak, M., R. Young, and R. Reynolds. 1985. “The internal structures and the relative rotation rates of Uranus and Neptune”. 63 (2): 266–271. doi:10.1016/0019-1035(85)90010-7.

Pollack, J. B., et al. 1996. “Formation of the giant planets by concurrent accretion of solids and gas”. *icarus* 124 (1): 62–85.

Press, W. H., et al. 1992. *Numerical recipes in Fortran 77: volume 1, volume 1 of Fortran numerical recipes: the art of scientific computing*. Cambridge university press.

Rafikov, R. R. 2006. “Atmospheres of protoplanetary cores: critical mass for nucleated instability”. *The Astrophysical Journal* 648 (1): 666.

Rasio, F. A., and E. B. Ford. 1996. “Dynamical instabilities and the formation of extrasolar planetary systems”. *Science* 274 (5289): 954–956.

Ree, F. H. 1976. “Lawrence Livermore Laboratory Technical Report No”. *UCRL-52190*.

Reinhardt, C., et al. 2020. "Bifurcation in the history of Uranus and Neptune: the role of giant impacts". *Monthly Notices of the Royal Astronomical Society* 492 (4): 5336–5353.

Rey, J., et al. 2018. "A 4.6-year period brown-dwarf companion interacting with the hot-Jupiter CoRoT-20 b". *arXiv preprint arXiv:1807.01229*.

Rossiter, R. A. 1924. "On the detection of an effect of rotation during eclipse in the velocity of the brigher component of beta Lyrae, and on the constancy of velocity of this system." *The Astrophysical Journal* 60.

Roulston, M. S., and D. J. Stevenson. 1995. "Prediction of neon depletion in Jupiter's atmosphere". *Eos* 76:343.

Safronov, V. S. 1966. *Sizes of the largest bodies falling onto the planets during their formation*.

Savvidou, S., B. Bitsch, and M. Lambrechts. 2020. "Influence of grain growth on the thermal structure of protoplanetary discs". *arXiv preprint arXiv:2005.14097*.

Scholtz, J., and J. Unwin. 2019. "What if Planet 9 is a Primordial Black Hole?" *arXiv preprint arXiv:1909.11090*.

Sefilian, A. A., and J. R. Touma. 2019. "Shepherding in a self-gravitating disk of Trans-Neptunian objects". *The Astronomical Journal* 157 (2): 59.

Seward, T. M., and E. U. Franck. 1981. "The system hydrogen-water up to 440° C and 2500 bar pressure". *Berichte der Bunsengesellschaft für physikalische Chemie* 85 (1): 2–7.

Shankman, C., et al. 2016. "OSSOS. II. A sharp transition in the absolute magnitude distribution of the Kuiper belt's scattering population". *The Astronomical Journal* 151 (2): 31.

Shu, F., et al. 1994. "Magnetocentrifugally driven flows from young stars and disks. 1: A generalized model". *The Astrophysical Journal* 429:781–796.

Sinton, W. M. 1981. "The thermal emission spectrum of Io and a determination of the heat flux from its hot spots". *Journal of Geophysical Research: Solid Earth* 86 (B4): 3122–3128.

Smith, K. L. 1986. "On the origins of the quality factor Q". *Quarterly Journal of the Royal Astronomical Society* 27:695.

Soderlund, K. M., et al. 2013. "Turbulent models of ice giant internal dynamics: Dynamos, heat transfer, and zonal flows". *Icarus* 224 (1): 97–113.

Souami, D., and J. Souchay. 2012. "The solar system's invariable plane". *Astronomy & Astrophysics* 543:A133.

Soubiran, F., and B. Militzer. 2015. "Miscibility calculations for water and hydrogen in giant planets". *The Astrophysical Journal* 806 (2): 228. doi:10.1016/j.hedp.2014.10.005.

Spalding, C., and K. Batygin. 2017. “A secular resonant origin for the loneliness of hot Jupiters”. *The Astronomical Journal* 154 (3): 93.

– . 2014a. “Early excitation of spin-orbit misalignments in close-in planetary systems”. *The Astrophysical Journal* 790 (1): 42.

– . 2014b. “Early excitation of spin-orbit misalignments in close-in planetary systems”. *The Astrophysical Journal* 790 (1): 42.

– . 2015a. “Magnetic Origins of the Stellar Mass-Obliquity Correlation in Planetary Systems”. *The Astrophysical Journal* 811 (2): 82.

– . 2015b. “Magnetic Origins of the Stellar Mass-Obliquity Correlation in Planetary Systems”. *The Astrophysical Journal* 811 (2): 82.

– . 2016. “Spin-orbit misalignment as a driver of the Kepler dichotomy”. *The Astrophysical Journal* 830 (1): 5.

Spalding, C., N. W. Marx, and K. Batygin. 2018. “The resilience of Kepler systems to stellar obliquity”. *The Astronomical Journal* 155 (4): 167.

Stanley, S., and J. Bloxham. 2004. “Convective-region geometry as the cause of Uranus’ and Neptune’s unusual magnetic fields”. 428 (6979): 151–153. doi:10.1038/nature02376.

– . 2006. “Numerical dynamo models of Uranus’ and Neptune’s magnetic fields”. 184 (2): 556–572. doi:10.1016/j.icarus.2006.05.005.

Stevenson, D. J. 1983. “Anomalous bulk viscosity of two-phase fluids and implications for planetary interiors”. *Journal of Geophysical Research: Solid Earth* 88 (B3): 2445–2455.

– . 1982a. “Formation of the giant planets”. *Planetary and Space Science* 30 (8): 755–764.

– . 1982b. “Interiors of the giant planets”. *Annual Review of Earth and Planetary Sciences* 10 (1): 257–295.

– . 2003. “Mission to Earth’s core—a modest proposal”. *Nature* 423 (6937): 239–240.

– . 1980. “Saturn’s luminosity and magnetism”.

Stevenson, D. J., and E. E. Salpeter. 1977a. “The dynamics and helium distribution in hydrogen-helium fluid planets”. *The Astrophysical Journal Supplement Series* 35:239–261.

– . 1977b. “The phase diagram and transport properties for hydrogen-helium fluid planets”. *The Astrophysical Journal Supplement Series* 35:221–237.

Struve, O. 1952. “Proposal for a project of high-precision stellar radial velocity work”. *The Observatory* 72:199–200.

Teyssandier, J., et al. 2013. “Extreme orbital evolution from hierarchical secular coupling of two giant planets”. *The Astrophysical Journal* 779 (2): 166.

Tremaine, S. 1991. “On the origin of the obliquities of the outer planets”. *Icarus* 89 (1): 85–92.

Tsiganis, K., et al. 2005. “Origin of the orbital architecture of the giant planets of the Solar System”. *Nature* 435 (7041): 459–461.

Vick, M., D. Lai, and K. R. Anderson. 2019. “Chaotic tides in migrating gas giants: forming hot and transient warm Jupiters via Lidov–Kozai migration”. *Monthly Notices of the Royal Astronomical Society* 484 (4): 5645–5668.

Wahl, S. M., et al. 2017. “Comparing Jupiter interior structure models to Juno gravity measurements and the role of a dilute core”. *Geophysical Research Letters* 44 (10): 4649–4659.

Walsh, K. J., et al. 2011. “A low mass for Mars from Jupiter’s early gas-driven migration”. *Nature* 475 (7355): 206–209.

Weidenschilling, S. J. 1977. “The distribution of mass in the planetary system and solar nebula”. *Astrophysics and Space Science* 51 (1): 153–158.

Williams, J. P., et al. 2014. “ALMA observations of a misaligned binary protoplanetary disk system in Orion”. *The Astrophysical Journal* 796 (2): 120.

Wilson, H. F., and B. Militzer. 2012a. “Rocky Core Solubility in Jupiter and Giant Exoplanets”. *Physical Review Letters* 108 (111101). doi:https://doi.org/10.1103/PhysRevLett.108.111101.

– . 2010. “Sequestration of noble gases in giant planet interiors”. *Physical review letters* 104 (12): 121101.

– . 2012b. “Solubility of Water Ice in Metallic Hydrogen: Consequences for Core Erosion in Gas Giant Planets”. 745 (1): 54. doi:10.1088/0004-637X/745/1/54.

– . 2011. “Solubility of water ice in metallic hydrogen: Consequences for core erosion in gas giant planets”. *The Astrophysical Journal* 745 (1): 54.

Wilson, H. F., M. L. Wong, and B. Militzer. 2013. “Superionic to Superionic Phase Change in Water: Consequences for the Interiors of Uranus and Neptune”. *Physical Review Letters* 110, 151102 (15): 151102. doi:10.1103/PhysRevLett.110.151102. arXiv: 1211.6482 [astro-ph.EP].

Winn, J. N., et al. 2011. “Orbital orientations of Exoplanets: HAT-P-4b is prograde and HAT-P-14b is retrograde”. *The Astronomical Journal* 141 (2): 63.

Winn, J. N., and D. C. Fabrycky. 2015a. “The occurrence and architecture of exoplanetary systems”. *Annual Review of Astronomy and Astrophysics* 53:409–447.

– . 2015b. “The occurrence and architecture of exoplanetary systems”. *Annual Review of Astronomy and Astrophysics* 53:409–447.

Winn, J. N., et al. 2009. “HAT-P-7: a retrograde or polar orbit, and a third body”. *The Astrophysical Journal Letters* 703 (2): L99.

Winn, J. N., et al. 2010. “Hot stars with hot Jupiters have high obliquities”. *The Astrophysical Journal Letters* 718 (2): L145.

Winn, J. N., et al. 2007. “Spin-orbit alignment for the eccentric exoplanet HD 147506b”. *The Astrophysical Journal Letters* 665 (2): L167.

Wisdom, J. 1980. “The resonance overlap criterion and the onset of stochastic behavior in the restricted three-body problem”. *The Astronomical Journal* 85:1122–1133.

Wisdom, J., and M. Holman. 1992. “Symplectic maps for the n-body problem-stability analysis”. *The Astronomical Journal* 104:2022–2029.

Wolszczan, A., and D. A. Frail. 1992. “A planetary system around the millisecond pulsar PSR1257+ 12”. *Nature* 355 (6356): 145–147.

Wright, J. T., et al. 2012. “The frequency of hot Jupiters orbiting nearby solar-type stars”. *The Astrophysical Journal* 753 (2): 160.

Wu, Y., and Y. Lithwick. 2011. “Secular chaos and the production of hot Jupiters”. *The Astrophysical Journal* 735 (2): 109.

Wu, Y., and N. Murray. 2003a. “Planet migration and binary companions: The case of HD 80606b”. *The Astrophysical Journal* 589 (1): 605.

– . 2003b. “Planet migration and binary companions: The case of HD 80606b”. *The Astrophysical Journal* 589 (1): 605.

Xiang-Gruess, M., and J. C. B. Papaloizou. 2014. “Evolution of a disc–planet system with a binary companion on an inclined orbit”. *Monthly Notices of the Royal Astronomical Society* 440 (2): 1179–1192.

Yoder, C. F., and S. J. Peale. 1981. “The tides of Io”. *Icarus* 47 (1): 1–35.

Zharkov, V. N., and V. P. Trubitsyn. 1978. *Physics of planetary interiors*.

Zharkov, V. N., I. A. Tsarevsky, and V. P. Trubitsyn. 1978. “Equations of state of hydrogen, hydrogen compounds, crystals of inert gases, oxides, iron and FeS”. *NASA TM* 75311.

Zhu, W., et al. 2018. “About 30% of Sun-like stars have Kepler-like planetary systems: a study of their intrinsic architecture”. *The Astrophysical Journal* 860 (101).